Performance Investigation of Spatial Modulation Systems Under Realistic Channel Models

by

Yu Fu

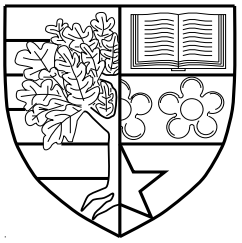

Submitted for the degree of Doctor of Philosophy
at
Heriot-Watt University
School of Engineering and Physical Sciences

September 2015

Abstract

In order to fulfil the explosive demand for convenient wireless data access, novel wireless technologies such as the multiple-input-multiple-output (MIMO) have widely been used to improve the link reliability and capacity of wireless communication systems. In recent years, a new MIMO technology named the spatial modulation (SM) has attracted significant research interest due to its reported enhancement on the system performance with the reasonable system complexity. Before a new technology comes into real use, it is necessary to comprehensively evaluate its performance under different scenarios. In this thesis, we investigate the performance of SM systems under some important realistic scenarios for future wireless communications, such as the vehicle-to-vehicle (V2V), the high-speed train (HST), and the massive MIMO scenarios.

Firstly, the bit error rate (BER) performance of SM systems under a novel three-dimensional (3D) geometry based stochastic model (GBSM) for V2V MIMO channels is investigated by both theoretical analysis and system simulations. The impacts of vehicle traffic density (VTD), Doppler effect, and 3D feature on the BER performance of SM systems are thoroughly studied. In addition, other MIMO technologies, such as the vertical Bell Labs layered space-time (V-BLAST), the Alamouti scheme are compared with SM under different simulation settings.

Secondly, the BER performance of SM systems is studied under a non-stationary wideband HST GBSM considering the non-ideal channel estimation case. The time-varying behaviour of the channel and its impact on the performance of SM systems are comprehensively investigated. The accurate theoretical BER expression of SM systems under a non-stationary wideband HST channels with non-ideal channel estimation is derived. A novel statistic property named stationary interval in terms of the space-time correlation function (STCF) is introduced in order to clearly explain all theoretical and simulation results.

Thirdly, the performance of SM systems is evaluated under a Kroneck-based massive MIMO channel model. As a massive MIMO system employs large numbers of antennas, antenna elements are distributed over a wide range. Thus, different antenna elements may observe different sets of clusters. How this phenomenon affects the performance of SM systems is investigated by considering a survival probability of clusters, which abstracts the birth-death process of each cluster in the channel model.

Moreover, the performance of SM systems is also compared with that of other MIMO technologies under the massive MIMO channel model.

In summary, all research works in this thesis have considered realistic MIMO channel models, which are meaningful for the test, performance evaluation, and implementation of SM technology for future advanced wireless communications systems.

To my families and colleagues

Acknowledgments

Without the help of my supervisors, colleagues, friends and families, this dissertation could not have been completed. I would like to take this opportunity to express my utmost gratitude to them.

First of all, my greatest appreciations to my primary supervisor Prof. Cheng-Xiang Wang for his excellent guidance and paternal encouragement. Besides his academic supervision, he is so considerate about my personal life as well. In addition, my heartfelt thanks must go to my second supervisor, Prof. David Wolfe Corne, for his kind help to my PhD research.

Secondly, I am extremely delighted to have the privilege of knowing my colleagues of past and present in the AWiTec Group, namely, Xuemin Hong, Xiang Cheng, Omar Salih, Zengmao Chen, Margaret Anyaegbu, Qi Yao, Ivan Ku, Pat Chambers, Ammar Ghazal, Yi Yuan, Fourat Haider, Shangbin Wu, Xianyue Wu, Piya Patcharamaneepakorn, Yan Zhang, Ahmed Al-Kinani, Liang Gong and Qianru Zhou. I really enjoy the time we spent together. I hope our friendship will last forever. Also, my greatest appreciations go to our visiting scholars, Jian Sun, Wuxiong Zhang, and Xiangyang Wang.

Thirdly, I want to gratefully acknowledge the kind help from Dr. Raed Mesleh from University of Tabuk, Saudi Arabia. As one of the most famous experts in the research on Spatial Modulation, his kind help and useful comments are important to my research.

My special gratitude goes to my families. My parents, Qingmin Fu & Donglan Zhang, thank you for your unconditional love and infinite support. I miss you every day and night during the past 5 years. Weihua, my dear wife, thank you for your love, understanding, patience, and support. I really appreciate your unshakable trust and wait. I love you so much!

Yu Fu
Edinburgh, August 2015.

Declaration of Authorship

I, Yu Fu, declare that this thesis titled, 'Performance Investigation of Spatial Modulation Systems Under Realistic Channel Models' and the work presented in it are my own. I confirm that:

- This work was done wholly while in candidature for a research degree at Heriot-Watt University.
- Where I have consulted the published work of others, this is always clearly attributed.
- Where I have quoted from the work of others, the source is always given. With the exception of such quotations, this thesis is entirely my own work.
- I have acknowledged all main sources of help.
- Where the thesis is based on work done by myself jointly with others, I have made clear exactly what was done by others and what I have contributed myself.

Signed: _____

Date: _____

Contents

List of Figures

List of Tables

Abbreviations

1G	First Generation
2D	Two Dimensional
2G	Second Generation
3D	Three Dimensional
3G	Third Generation
4G	Fourth Generation
5G	Fifth Generation
AoA	Angle of Arrival
AAoA	Azimuth Angle of Arrival
AoD	Angle of Departure
AAoD	Azimuth Angle of Departure
ABER	Average Bit Error Rate
ACF	Autocorrelation Function
A/EAoD	Azimuth/Elevation Angle of Departure
AWGN	Additive White Gaussian Noise
BANs	Body Area Networks
BD	Block Diagonalization
BER	Bit Error Rate
BICM	Bit Interleaved Coded Modulation
BS	Base Station
CA	Close Area
CCF	Cross Correlation Function

CEA	Closer Area
CRC	Cyclic Redundancy Checking
DB	double-bounced
D2D	Device-to-Device
DF	Demodulate-and-Forward
DAS	Distributed Antenna System
EAoA	Elevation Angle of Arrival
EAoD	Elevation Angle of Departure
F2M	Fix to Mobile
GBSM	Geometry-Based Stochastic Channel Model
GSM	Global System for Mobile communications
GPRS	General Packet Radio Service
HST	High-Speed Train
ICI	Inter-Channel-Interference
i.i.d.	Independent and Identically Distributed
IoT	Internet of Things
ISI	Inter-Symbol-Interference
IUI	inter-User-Interference
KBSM	Kroneck-Based Stochastic Model
LED	Light-Emitting Diode
LoS	Line-of-Sight
LRS	Local Region of Stationariness
LTE-A	Long Term Evolution Advanced
MC-CDMA	Multicarrier Code-Division Multiple Access
MEV	Method of Equal Volume
MF	Matched Filter
MGF	Moment Generation Function
MIMO	Multiple-Input Multiple-Output
ML	Maximum Likelihood
MMSE	Minimum Mean-squared Error
MRS	Mobile Relay Station

MS	Mobile Station
MU	Multiple Users
OFDM	Orthogonal Frequency Division Multiplexing
PDF	Probability Density Function
PEP	Pairwise Error Probability
PPM	Pulse Position Modulation
PSK	Phase-Shift Keying
QAM	Quadrature-Amplitude Modulation
RF	Radio Fequency
Rx	Receiver
SB	Single-Bounced
SIMO	Single-Input-Multiple-Output
SM	Spatial Modulation
SNR	Signal to Noise Ratio
SSK	Space Shift Keying
STSK	Space-Time Shift Keying
STBC	SpaceTime Block Code
STC	Space-Time-Coding
STCF	Space Time Correlation Function
SVD	Singular Value Decomposition
TDMA	Time-Division Multiple Access
Tx	Transmitter
V2V	Vehicle-to-Vehicle
V-BLAST	Vertical Bell Labs Layered Space-Time
VLC	Visible Light Communications
VMF	von Mises-Fisher
VTD	Vehicle Traffic Density
WSS	Wide-Sense Stationary
ZF	Zero-Forcing

Symbols

$(\cdot)^T$	transpose of a matrix/vector
$(\cdot)^H$	Hermitian transpose of a matrix/vector
$(\cdot)^*$	complex conjugate
$\lvert\cdot\rvert$	absolute value (amplitude) of a complex vector
$\mathbf{max}\{\cdot\}$	maximum value of a vector
$\mathbf{min}\{\cdot\}$	minimum value of a vector
$\mathbf{H}\{\cdot\}$	Hilbert transform
$\mathbf{E}[\cdot]$	statistical expectation
$\mathrm{I}_0(\cdot)$	zeroth-order modified Bessel function of the first kind
$\mathrm{J}_0(\cdot)$	zeroth-order Bessel function of first kind
$\mathbf{Q}\{\cdot,\cdot\}$	Marcum Q-function
$\bigotimes$	Convolutions operation
$\cup$	union of sets
$\sum$	summation
$\prod$	multiple product

α	azimuth angle of the VMF PDF
α_0	mean azimuth angle of the scatterers located on a sphere
α_{T0}	mean AAoD of the scatterers located on a sphere around the Tx
α_{R0}	mean AAoA of the scatterers located on a sphere around the Rx
α_m	ray offset angles of the mth sub-path

α_R^{LoS}	AAoA of the LoS paths
$\alpha_T^{(n_i)}$	AAoD of the waves that impinge on the effective scatterers $s^{(n_i)}$
$\alpha_R^{(n_i)}$	AAoA of the waves travelling from the effective scatterers $s^{(n_i)}$
$\alpha_T^{(n_{l,i})}$	AAoD of the waves that impinge on the effective scatterers $s^{(n_{l,i})}$
$\alpha_R^{(n_{l,i})}$	AAoA of the waves travelling from the effective scatterers $s^{(n_{l,i})}$
$\underset{\text{SM}}{\text{ABER}}$	The ABER of SM Systems
$\underset{\text{Signal}}{\text{ABER}}$	The ABER of SM that error only occurs in the digital modulation part
$\underset{\text{MOD}}{\text{APEB}}(n_t)$	The ABER of error of digital modulated symbols transmitted though n_t
β	elevation angle of the VMF PDF
β_0	mean elevation angle of the scatterers located on a sphere
β_{T0}	mean EAoD of the scatterers located on a sphere around the Tx
β_{R0}	mean EAoA of the scatterers located on a sphere around the Rx
β_R^{LoS}	EAoA of the LoS paths
$\beta_T^{(n_i)}$	EAoD of the waves that impinge on the effective scatterers $s^{(n_i)}$
$\beta_R^{(n_i)}$	EAoA of the waves travelling from the effective scatterers $s^{(n_i)}$
$\beta_T^{(n_{l,i})}$	EAoD of the waves that impinge on the effective scatterers $s^{(n_{l,i})}$
$\beta_R^{(n_{l,i})}$	EAoA of the waves travelling from the effective scatterers $s^{(n_{l,i})}$
γ_T	moving direction of the Tx in the x-y plane
γ_R	moving direction of the Rx in the x-y plane
γ	signal-to-noise ratio
δ_T	antenna elements spacing at the Tx
δ_R	antenna elements spacing at the Rx
Δd_s	antenna elements spacing at the BS
Δd_u	antenna elements spacing at the MS
$\Delta_{P,k}$	movement of the Tx and Rx
$\Delta_{T,k}$	movement of the Tx
$\Delta_{R,k}$	movement of the Rx
$\Delta_{x_{T/R}}$	Antenna spacing at the Tx/Rx
$\Delta\varphi_{n,m}$	AoA offset
ε_{pq}	distances between T_p and T_q
ε_{pn_i}	distances between T_p and $s^{(n_i)}$

$\varepsilon_{n_1 n_2}$	distances between $s^{(n_1)}$ and $s^{(n_2)}$
$\varepsilon_{n_i q}$	distances between $s^{(n_i)}$ and T_q
$\varepsilon_{p n_{l,i}}$	distances between T_p and $s^{(n_{l,i})}$
$\varepsilon_{n_{l,1} n_{l,2}}$	distances between $s^{(n_{l,1})}$ and $s^{(n_{l,2})}$
$\varepsilon_{n_{l,i} q}$	distances between $s^{(n_{l,i})}$ and T_q
η_{SB_i}	power-related parameter of ith single-bounced ray
η_{DB}	power-related parameter of the double-bounced ray
$\eta_{SB_{1,i}}$	power-related parameter of ith single-bounced ray in first tap
$\eta_{DB_{1,i}}$	power-related parameter of ith double-bounced ray in first tap
$\eta_{SB_{l,i}}$	power-related parameter of ith single-bounced ray in lth tap
$\eta_{DB_{l,i}}$	power-related parameter of ith double-bounced ray in lth tap
θ_T	orientation of the Tx antenna array in the x-y plane
θ_R	orientation of the Rx antenna array in the x-y plane
θ_c	moving direction of the MC at BS
θ_v	relative moving direction of MS relative to MC
θ_{MC}	moving direction of the MC at MS
θ_{MS}	moving direction of the MS
$\rho_{h_{pq} h_{p'q'}}(\tau)$	ST CF between $h_{pq}(t)$ and $h_{p'q'}(t)$
σ_0^2	mean power of $h_{pq}(t)$
τ	time separation
τ	time delay
τ_l	lth tap delay
τ_n	nth tap delay
$\tau_n(t)$	time-varying delay of the nth cluster
τ_{pq}	travel time of the wave through the link $T_p \rightarrow T_q$
τ_{pq,n_i}	travel time of the wave through the link $T_p \rightarrow S_{n_i} \rightarrow T_q$
τ_{pq,n_1,n_2}	travel time of the wave through the link $T_p \rightarrow S_{n_1} \rightarrow S_{n_2} \rightarrow T_q$
$\upsilon_{n,m}$	Doppler frequency of the MS related to $\varphi_{n,m}$
Υ	period
ψ_n	random phase of nth tap
ψ_{n_i}	random phase of the narrowband ith single-bounced rays

$\psi_{n1,n2}$	random phase of the narrowband double-bounced rays
$\Phi_{n,m}$	random phase
Ω_{pq}	total power of the $T_p \rightarrow R_q$ link
χ_p	total power of all taps
a	semi-major axis of the narrowband elliptic-cylinder model
b	semi-minor axis of the narrowband elliptic-cylinder model
c	speed of light
D	Tx-Rx distance
$D_{\min}$	Minimum distance between the BS and the track
$D_s\,(t)$	The time-varying distance between the BS and MRS
f	half distance between two focal points of the elliptic-cylinder
f_c	carrier frequency
f_{max}	maximum Doppler frequency
f_D	Doppler frequency
f_{Tmax}	maximum Doppler frequency due to the motion of the Tx
f_{Rmax}	maximum Doppler frequency due to the motion of the Rx
$f(\alpha, \beta)$	VMF PDF
$h_{u,s}(t, \tau)$	fading envelope between the sth and uth antenna elements
$h_{pq}(t)$	fading envelope between the pth and qth antenna elements
$h_{p'q'}(t)$	fading envelope between the p'th and q'th antenna elements
$h_{pq}^{LoS}(t)$	fading envelope of the LoS component
$h_{pq}^{SB_i}(t)$	fading envelope of the ith single-bounced rays
$h_{pq}^{DB}(t)$	fading envelope of the double-bounced rays
$\mathbf{H}(t)$	MIMO channel matrix
$\mathbf{H_est}(t)$	Estimated MIMO channel matrix
k	a parameter of VMF PDF that controls the angle spread
$k^{(1)}$	a parameter of VMF PDF at the Tx sphere
$k^{(2)}$	a parameter of VMF PDF at the Rx sphere
$k^{(3)}$	a parameter of VMF PDF at the elliptic-cylinder
K	Ricean factor

L	total number of taps (or virtual confocal elliptic-cylinders)
$M_r(.)$	the moment generation function (MGF)
n	nth effective scatterers
N	number of independent effective scatterers
N_2	number of effective scatterers around the Rx lying on a sphere
N_3	number of effective scatterers lying on the an elliptic-cylinder
$N_H(.)$	Hamming distance
$P(.)$	pairwise error probability
R_T	radius of a sphere around the Tx in the two-sphere model
R_R	radius of a sphere around the Rx in the two-sphere model
$\mathbf{R}_{BS}$	spatial correlation matrix of BS antennas
$\mathbf{R}_{MS}$	spatial correlation matrix of MS antennas
$s^{(n_1)}$	n_1th effective scatterer located on a sphere around the Tx
$s^{(n_2)}$	n_2th effective scatterer located on a sphere around the Rx
$s^{(n_3)}$	n_3th effective scatterer located on an elliptic-cylinder
t	time
v_T	Tx velocity
v_R	Rx velocity

Chapter 1

Introduction

1.1 Problem Statement

In 1896, Marconi made his first successful demonstration of transmitting radio signals over the English channel [1]–[3]. This time is recognised as the beginning of the history for modern wireless communications. Since that time, wireless communications have greatly changed lives of human beings. Nowadays, if we look around, wireless communications happen everywhere in our daily life. Our social manners and economical behaviours are changing along with the evolution of wireless communications technologies. At the same time, continuous emerging demands of human beings become the driving force behind the development of wireless communications.

Investigating the history of wireless communications, the first generation (1G) commercial wireless communication system was established in 1980s, which supports the voice communication service using the analogue cellular architecture. In 1991, the second generation (2G) wireless communication system started to depute all over the world, which is known as the Global System for Mobile communications (GSM). The 2G system is based on the digital cellular architecture, which can offer a better spectral efficiency than the analogue system. Until today, the GSM system is still in service all over the world. For the 1G and the early release of 2G systems, only voice communication service is supported. There is no data service offered (in the later

release of GSM system, very basic low-speed data service using general packet radio service (GPRS) is supported). In order to fulfil the demand of high-speed wireless data access, the third generation (3G) wireless communications system was launched in 2001, which can support data services at the speed up to 2Mbps [3], [4]. In 2011, the long term evolution advanced (LTE-A) standard was released as the fourth generation (4G) wireless communications standard [5]. Benefiting from using advanced wireless technologies such as the orthogonal frequency division multiplexing (OFDM) and multiple-input multiple-output (MIMO), the data rate for 4G systems can reach up to 1Gbps for low mobility scenarios and 100Mbps for high mobility scenarios [5], [6].

In recent years, caused by emerging mobile Internet based services [7], there is an explosive growth in the demand of wireless network access. Furthermore, with the development of devices networks which is also known as the Internet of things (IoT), it is predicted that by 2020 there will be over 50 billions mobile devices connected to the Internet [8]. The traffic of future wireless networks will be dramatically increasing, and the limit of current 4G systems will be approached quickly. Therefore, it is necessary to start the research on the fifth generation (5G) wireless communication system immediately.

In principle, the standardisation work of 5G systems is expected to be finished by 2020. Currently, there is no certain and accurate definition of 5G systems. But in academic and industry, there are wide agreements on the performance criterion of 5G systems [9], [10]. Compared with 4G systems, 5G systems should obtain 1000 times system capacity, 10 times spectral efficiency, energy efficiency and data rate, the average throughput should be the 25 times level of current 4G systems, and there should be a 5 times reduction in latency [9]–[11]. Besides, 5G systems should support more novel communication scenarios such as the high-speed train (HST) scenario with the operating speed up to 500 km/h [9].

In order to realise the miracle of 5G systems, some research projects on related topics have been started. For example, the UK-China science bridge project: RD on (B)4G wireless communications [12], which might be the first government-supported

research project on 5G technologies. In Europe, supported by the 7th Framework program (FP7), some research projects on 5G related research projects such as the METIS project [13], and the 5GNOW [14] are in process now. In China, a number of research projects on 5G wireless communications technologies are supported by the government funding such as the National 863 key project [9]. Besides research projects, there are also some predicted research on 5G technologies reported in [9]–[11], [15]–[20]. For example, in [9], the authors present the potential cellular architecture for the future 5G systems, in which different cellular architectures such as macrocells, microcells, small cells, relays, and femtocells, are existing heterogeneously. It is also pointed out that the indoor scenario and the outdoor scenario are completely isolated in future 5G wireless communications systems. Besides novel cellular architectures, various novel technologies will be employed to realise the performance criterion of 5G systems. These technologies include the massive MIMO technology, millimetre wave communications, visible light communications (VLC), cognitive radio networks, green communications, and the spatial modulation (SM) technology [9]–[11], [15].

In aforementioned literatures [9]–[11], [15], SM has been introduced as a potential technology for 5G wireless communications. Its basic idea is to activate single transmit antenna at each time instant and use the antenna index to carry information. The outstanding enhancement of SM in terms of system performance, spectral-energy efficiency trade-off, and system complexity reduction, have been introduced in [21]–[23]. In order to be used by the 5G systems, it is necessary to investigate the performance of SM under some important typical 5G scenarios. However, most research works of SM so far are mainly carried out under some unrealistic assumptions using simple channel models such as Rayleigh, Rician, Nakagami fading channels [24]–[28]. These researches are not sufficient to support the use of SM in the future 5G systems.

1.2 Motivation

The motivation of this PhD project is to study the bit error rate (BER) performance of the SM under some typical 5G scenarios using accurate channel models, and offer

the solid theoretical support of using SM in future 5G systems. Referring to the research statement of 5G systems, following typical 5G scenarios will be selected: 1) the vehicle-to-vehicle (V2V) scenario which reflects the research trend of device-to-device (D2D) communications in 5G systems; 2) the HST scenario, which reflects the research interest on wireless communications systems with high mobility; 3) the Multiple-users (MU) massive MIMO scenario, which reflects one of the most attractive potential 5G technologies, and the realistic challenges on the 5G wireless systems development.

1.3 Contributions

The key contributions of this thesis are summarised as follows:

Research on SM over 2D and 3D V2V channel models

- Studied the BER performance of SM systems under a three-dimensional (3D) narrowband V2V MIMO geometry-based stochastic channel model (GBSM). The impact of the vehicle traffic density (VTD), the Doppler effect, and the different impacts of 3D and two-dimensional (2D) V2V channel models were investigated.
- Derived a tight closed-form upper bound of the theoretical average bit error rate (ABER) of SM systems under a 3D narrowband V2V MIMO GBSM.
- Compared the BER performance of SM with other MIMO technologies include the vertical Bell Labs layered space-time (V-BLAST) and the Alamouti schemes under the realistic 3D V2V MIMO GBSM.

Research on SM over wideband HST MIMO channel models

- Studied the BER performance of SM systems under a non-stationary wideband HST channel model. Further specified scenarios and time-varying parameters

obtained from measurements are used. The non-ideal channel estimation was also considered to make simulation results more realistic.

- Derived a tight closed-form upper bound of the theoretical ABER for SM systems under the non-stationary wideband HST MIMO GBSM assumed the non-ideal channel estimation error.

- Proposed a novel statistic property named the stationary interval in terms of the space-time correlation function (STCF) to describe the channel model's time-varying behaviour and to investigate the time varying BER performance of the SM system.

Research on MU SM over massive MIMO channel models

- Studied the BER performance of MU-SM systems under a Kroneck-based stochastic model (KBSM) for massive MIMO systems which considered the evolution of clusters for each antennas.

- Derived a tight upper bound of the theoretical ABER of MU-SM systems using block diagonalisation (BD) precoding scheme under the KBSM for massive MIMO systems.

- Compared the performance of different massive MIMO system solutions, includes the time-division multiple access (TDMA) SM system, the BD SM system, the BD V-BLAST system, and the conventional channel inversion system.

1.4 Original Publications

The work presented in this thesis has led to the following publications:

Journals

1. **Y. Fu**, C.-X. Wang, Y. Yuan, R. Mesleh, H. M. Aggoune, M. M. Alwakeel, and H. Hass, "BER performance of spatial modulation systems under 2D and 3D

vehicle-to-vehicle channel models," *IEEE Trans. Veh. Technol.*, 2015, vol. , no. 99, pp. 1-7, July 2015. DOI: 10.1109/TVT.2015.2461638

2. **Y. Fu**, C.-X. Wang, A. Ghazal, e. H. M. Aggoune, and M. M. Alwakeel,"Performance investigation of spatial modulation systems under non-stationary wideband high-speed train channel models," *IEEE Trans. Wireless Commun.*, 2015, submitted for publication.

3. **Y. Fu**, C.-X. Wang, S. Wu, X. F. Fang, and M.Di Renzo, "Performance investigation of spatial modulation systems under a Kronecker-based massive MIMO channel model," *IEEE Trans. Veh. Technol.*, 2015, submitted for publication.

Conferences

1. **Y. Fu**, C.-X. Wang, R. M. Mesleh, X. Cheng, H. Haas, and Y. He, "A performance study of spatial modulation technology under vehicle-to-vehicle channel models", in *Proc. IEEE VTC'14-Spring*, Seoul, South Korea, May 2014, pp. 1–5.

Technical Reports

1. P. Chambers, X. Hong, N. Serafimovski, A. Younis, R. Mesleh, Z. Chen, **Y. Fu**, W. Thompson, C.-X. Wang, H Haas, and M. Beach, "NI wireless testbed solution for novel future generation communication systems," 2012.

   Graphical System Design Achievement Award (RF and Communications) presented by National Instruments in 2013.

1.5 Thesis Organisation

The remainder of this thesis is organised as follows:

Chapter 2 offers a literature review of the existing research on SM and channel modelling for selected typical 5G scenarios. This chapter starts with the background

information related to MIMO technologies. Following that, the principle, the research history, and the latest research statement of SM are introduced sequentially. In the second part of this chapter, some background knowledges regarding channel modelling on V2V, HST, and massive MIMO scenarios are reviewed.

Chapter 3 investigates the BER performance of SM systems under a 3D V2V channel model. This chapter starts with the introduction of the 3D V2V MIMO channel model and essential statistical properties that affect the system performance. Following that, the theoretical expression of the ABER for SM under the 3D V2V MIMO channel model is derived. Finally, different simulation results are presented and analysed.

Chapter 4 focuses on the study of the BER performance of SM systems under a non-stationary HST MIMO channel model. The non-stationary wideband HST MIMO channel model and related important statistical properties including the novel non-stationary statistic property are firstly introduced. Then, the error model to describe the condition of the non-ideal channel estimation is proposed. The theoretical BER expression for SM systems under the time-varying HST channel model assuming the non-ideal channel estimation is derived. Finally, different simulation results are presented and analysed.

Chapter 5 presents the investigation of the BER performance of SM systems under a KBSM of MU massive MIMO scenarios. It begins with an introduction of the system architecture of MU SM systems using both the TDMA scheme and the BD precoding scheme. The description of the KBSM for massive MIMO scenarios is given as the following section. Then theoretical BER expressions for both TDMA-MU-SM system and BD-MU-SM system under the massive MIMO channel model are derived. Finally, different simulation results are presented and analysed.

Finally, Chapter 6 summarise the thesis and addresses some potential future research direction on SM related topics.

Chapter 2

Background

2.1 Spatial Modulation: A Novel MIMO Technology

2.1.1 Overview

In past decades, in order to achieve the higher data rate and to increase the spectral and the energy efficiency for wireless communication systems, the multiple antennas technology which is also known as the MIMO technology has been widely used by advanced wireless communication systems [22], [29]–[31].

In general, existing MIMO technologies can be classified into the following two categories [22], [31]. In the first category, multiplexing gain is achieved through the spatial multiplexing, where multiple independent signal streams are transmitted through different antennas at the same time instant [22], [31]. The Bell labs layered space-time architecture (BLAST) [32] is a typical example of the spatial multiplexing. Spatial multiplexing systems can obtain an extremely high data rate under promising channel environments. However, its performance suffers significantly from severe channel conditions, such as the high spatial correlation, and also from the existence of the

inter-channel-interference (ICI) [22]. The second widely used category of MIMO technologies is the space-time-coding (STC) [22], [31], which improves the reliability of the system by maximising the spatial diversity. The Alamouti scheme [33] is a typical example of this category. For the STC technology, redundant data are transmitted through different antennas in order to improve the system's reliability. However, the major problem of STC technology is the limited spectral efficiency [34], where even for a full diversity STC system, the maximum spectral efficiency is only one symbol per time instant.

In order to solve these unpleasant issues of existing MIMO technologies, many new ideas of MIMO system have been investigated. In recent years, SM was treated as a novel MIMO technology and has attracted lots of research interest due to its enhancement on spectral efficiency and the reasonable system complexity. The basic idea for SM is that at each time instant, only one antenna is activated. The index of the active antenna becomes a resource to carry information. Benefiting from this extra resource, SM can obtain a relatively high spectral efficiency with low-order modulation schemes [22]. Besides, as only one antenna is used to transmit at each time instant, the ICI problem is entirely avoided and simple receiver algorithms can be employed [22]–[24].

2.1.2 The Principle of Spatial Modulation Technology

In Fig. 2.1, principles of these three MIMO technologies are illustrated. Compared with other MIMO technologies, the most unique characteristic of SM is that only one antenna is used to transmit data at each time instant, and at the same time, antenna indexes are used to carry information [22]. In order to implement this setting, the system should be designed as follows: let us assume a SM system with N_t transmit antennas and N_r receive antennas, and the M-quadrature-amplitude modulation (QAM)/phase-shift keying (PSK) modulation scheme is used as the digital modulator. The bits stream is divided into two parts, the first $\log_2(N_t)$ bits are carried by the antenna index, which are also used for antenna selection. The other $\log_2(M)$ bits are transmitted by the digital modulated symbol. Thus at each time instant,

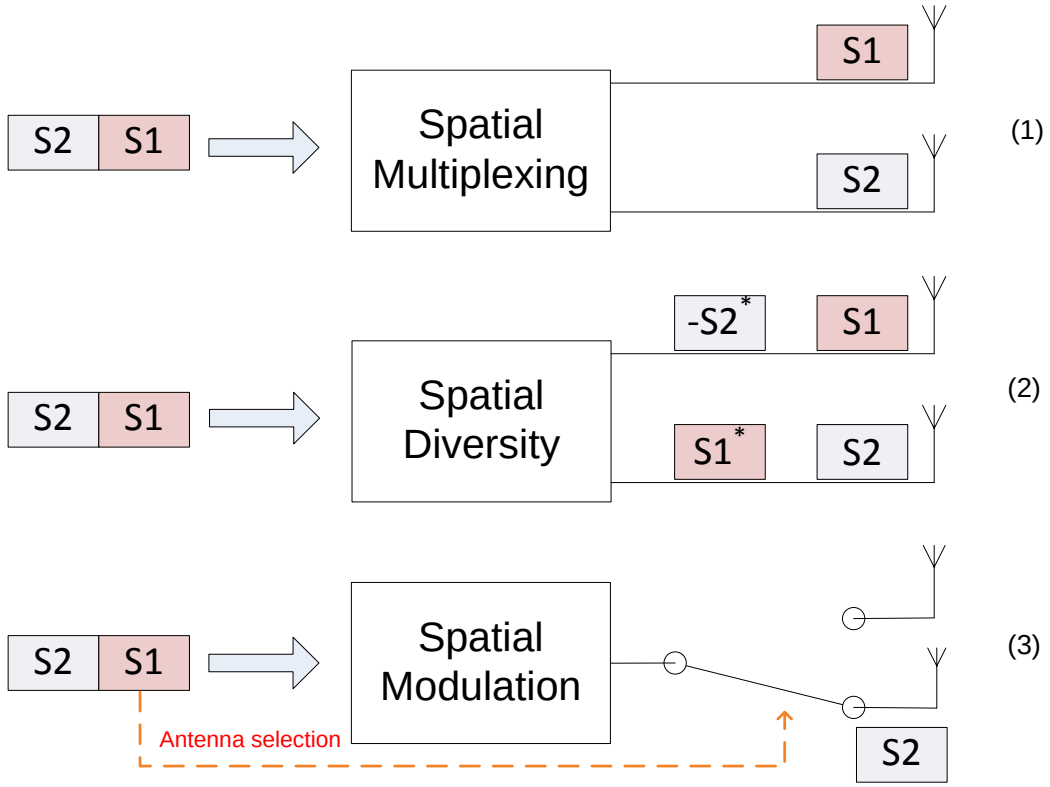

FIGURE 2.1: Principle diagrams of three MIMO technologies: (1) spatial multiplexing; (2) spatial diversity; (3) SM. [23]

$m = \log_2(N_t) + \log_2(M)$ bits are transmitted, where m is the spectral efficiency of the SM system in bits/symbol.

The block diagram of the SM system under wireless fading channels is shown in Fig. 2.2. A MIMO system using 4 transmit antennas and 4PSK/4QAM modulation scheme is considered in this figure. Let us assume the bits sequence 0001 is transmitted. At the transmitter (Tx) side, the first two bits 00 will be carried by the antenna index and also used to select Tx1 as the transmit antenna. The other two bits 01 are mapped to the modulated symbol S_2 based on the constellation diagram. In Tab. 2.1, the mapping rule for the system using 4 transmit antennas and 4PSK/4QAM modulation schemes are illustrated. Then, the symbol is radiated by the antenna Tx1 through the channel $\boldsymbol{H}$. At the Rx side, the active transmit antenna and the transmitted symbol S_2 are estimated and used to retrieve the binary message [24].

Let $\boldsymbol{S}$ denote the transmit vector at the Tx side, which is a vector with the dimension of $N_t \times 1$. At each time instant, as there is only one Tx antenna activated, $\boldsymbol{S}$ can be

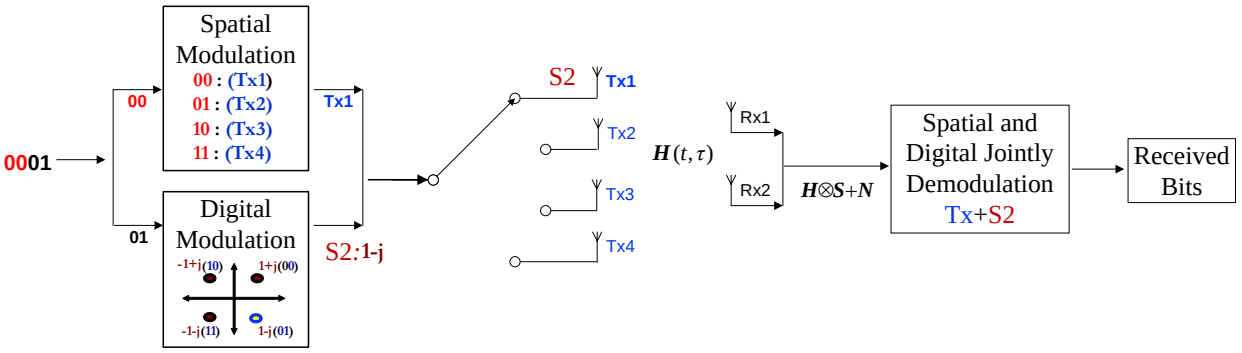

FIGURE 2.2: Block diagram of Spatial Modulation system under mobile fading channels.

TABLE 2.1: SM mapping table for $N_t = 4$ and $M = 4$.

Input Bits	Antenna Index	Transmit Symbol	Input Bits	Antenna Index	Transmit Symbol
0000	1	+1+j	1000	3	+1+j
0001	1	-1+j	1001	3	-1+j
0010	1	-1-j	1010	3	-1-j
0011	1	+1-j	1011	3	+1-j
0100	2	+1+j	1100	4	+1+j
0101	2	-1+j	1101	4	-1+j
0110	2	-1-j	1110	4	-1-j
0111	2	+1-j	1111	4	+1-j

further expressed as $\boldsymbol{S} = [0, 0, .., S, ..0, 0]^T_{N_t}$, where $[.]^T$ denotes transpose operation. At the Rx, the received $N_r \times 1$ vector $\boldsymbol{y}(t)$ can be written as:

$$\boldsymbol{y}(t) = \boldsymbol{H}(t, \tau) \otimes \boldsymbol{S}(t) + \boldsymbol{n} \tag{2.1}$$

where $\otimes$ denotes the convolution operation, $\boldsymbol{n}$ is the $N_r \times 1$ complex additive white Gaussian noise (AWGN) vector, with real and imaginary parts both having a double-sided power spectral density equal to $N_0/2$ [22]. In addition, $\boldsymbol{H}(t, \tau)$ is the $N_r \times N_t$ channel matrix, which is composed with the channel impulse response elements $h_{q,p}(t, \tau), q = 1...N_r, p = 1...N_t$.

In this system, the Tx and the Rx are assumed with the perfect synchronisation on time and frequency. At the Rx side, the index of the active transmit antenna and the modulation symbol at this particular time instant can be detected using

different receiver algorithms. Let us assume the optimum maximum likelihood (ML) detector proposed in [24] is employed to estimate the transmit antenna index $\hat{p}$ and the transmitted data symbol $\hat{s}$, using the estimated channel matrix $\boldsymbol{H_{est}}$. The receiver will compare all possible options with the received vector, and selected the one with the minimum Euclidean distance difference as the final results. This procedure is described in 2.2 as

$$\left[\hat{p}, \hat{k}\right] = \arg\min_{p,k} \left(\|y - \boldsymbol{H_{est}} \otimes S_k\|_F^2\right), p \in \{1 : N_T\} \text{ and } k \in \{1 : M\} \ , \tag{2.2}$$

where $\|\cdot\|_F$ denotes the Frobenius norm. M is the modulation order.

2.1.3 Advantages and Drawbacks of SM

Due to the special system structure, there are some potential advantages of SM compared with conventional MIMO technologies, which can be highlighted as follows [23]

1. Lower cost in the system construction. As at each time instant, a SM system only activates one transmit antenna, it only needs one radio frequency (RF) chain. In this case, a system can be established with single RF chain with multiple antenna elements. The cost of SM systems is much lower than that of conventional MIMO systems which should use multiple RF chains.

2. Simpler transmitter design. Due to only single antenna is active, it not necessary to consider the complex synchronisation algorithm.

3. Simpler receiver design. As only one antenna is activated for each time instant, the system is total ICI free. The ML -optimum performance can be achieved at the cost of single-stream decoding complexity [24].

4. Higher spectral efficiency than space-time block code (STBC) MIMO and single-input-multiple-output (SIMO) systems, as some data can be carried by the antenna index.

5. Better energy efficiency performance. SM uses only a single RF chain but multiple antennas to obtain the multiplex gain. As the consumed power only depends on the number of RF chains rather than the antenna number, the consumed energy of SM system is lower than conventional MIMO systems.

On the other hand, there are some drawbacks that SM suffers and some challenges should be carefully taken into account for the future widely use of SM.

1. Lower throughput than spatial multiplex systems. The throughput of spatial multiplexing systems is increased in the linear relation with the number of antennas (also the number of RF chains). While for SM, its throughput increases at the ratio of the logarithm of antenna numbers. Thus, when it uses the same number of antennas, the throughput of SM is lower than that of the spatial multiplexing system. However, this drawback can be solved by the combination of SM with massive MIMO technologies. For spatial multiplexing systems, considering the system complexity, it is hard to use extremely large number of antennas, while SM can establish massive MIMO systems using extremely large number of antenna elements with the acceptable complexity. In this case, SM can achieve comparable throughput as the spatial multiplexing, but with a better performance in the system complexity and the energy efficiency.

2. Fast switching of antenna elements. As SM uses multiple antennas with the single RF chain, a sufficiently quick switcher which can operate at least at the data symbol rate will be employed. Design and produce these high-speed switcher (frequency over 10 GHz) is the most critical part for the SM transmitter design, especially when combining SM with the massive MIMO and the millimetre wave technologies.

3. Sensitive to propagation environments. The performance of SM is highly determined by the propagation environments. As some data are encoded in the antenna index, the receiver will decoding this part of data rely on the difference of sub-channels. Thus, SM can achieve a good performance under low correlated channels, which are scenarios with weak line-of-sight (LoS) paths and rich

scattering. However, under 5G systems, this condition is hard to be fulfilled. As 5G systems will use some high frequency spectrum, lots of communications will occur in a short range, where there are strong LoS propagations and lack of scatterings, thus the channel are highly correlated. How to achieve a promising performance using SM in these scenarios is a big challenge.

2.1.4 The History of SM Research: A Survey

It is noticed that SM has attracted lots of research interest in recent years. However, SM is actually a technology with a more than 10 years history. Its history can be tracked back to 2001. In [35], a modulation concept called the space modulation was introduced. Its idea is to carry information through the difference of signals transmitted by different antennas, which is very similar to the conventional SM.

In 2004, the literature [36] was published, in which the SM was described as "a channel hopping technique". In the Fig. 1 of [36], the principle of SM was illustrated, the information to be transmitted is divided into two streams, the first stream is carried by the modulation symbol while the other is carried by activating a selective antenna.

In 2005, Mesleh et al. proposed a modulation scheme in [37]. The aim of this work was to propose a ICI free framework for MIMO systems. In the proposed framework, the ICI problem is solved by using a single antenna to transmit signals at each time instant, while some information are encoded to the antenna switch process. This is exactly what is known as SM for nowadays. In this paper, the author also pointed out that the proposed scheme can obtain a better BER performance compared with the V-BLAST systems. And the receiver complexity is lower than the V-BLAST system.

In 2006, the same authors further extended the work in [37] by combining SM with the OFDM technology in [38]–[41], and the word "spatial modulation" is used for the first time. From that time, spatial modulation is used to identify the new MIMO scheme.

In 2008, two years after the name of "spatial modulation" was given, the first remarkable key reference that comprehensively concluded existing researches on SM was published as [22]. In this paper, a two-step receiver algorithm with a low-complexity was proposed. It was also the first time that the performance of SM was compared with the spatial multiplexing and the Alamouti code scheme. The advantages of SM both in the system performance and the system complexity compared with conventional MIMO technologies were announced. At the same year, in [24], the authors presented a ML-optimum demodulator which can jointly estimate the active antenna index and the transmitted symbol using the maximum likelihood algorithm. Compared with the algorithm proposed in [22], the BER performance of the system in [24] was better with the cost of higher complexity.

From that time point, SM has become a well-know MIMO technology and attracted significant research interest. In December 2011, the first survey paper on SM was published as [21]. In [42], SM and the space shift keying (SSK) were surveyed as members of MIMO technologies family. The most comprehensive survey work was carried by Renzo et al. in [23], and there are corresponding tutorials presented on IEEE Wireless Communications and Networking Conference 2013 and IEEE Vehicular Technology Conference 2013.

Besides the aforementioned research on the theoretical knowledge of SM, following milestones should be highlighted. In [43], the performance of SM was firstly investigated under realistic channel models from measurements, and the concept of using SM for massive MIMO system (expressed as the large-scale MIMO) was introduced and investigated as a novel point of this paper .

In [44], for the first time in the world, SM was implemented in a hardware testbed at Heriot-Watt University (see Fig. 2.3). In order to realise this system in the testbed, some further developments are carried out in this work. For example, the frame structure must be redesigned which should consider the synchronisation, the signal-to-noise ratio calculation, the pilots for channel estimation and the zero paddings to avoid the inter frame interference.

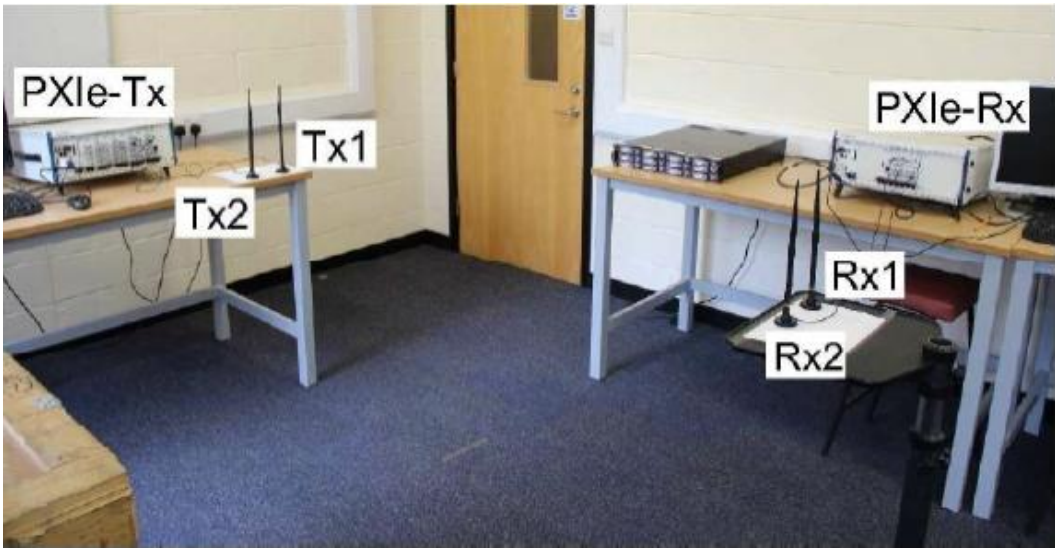

FIGURE 2.3: The hardware testbed of HWU for SM practical implementation [44].

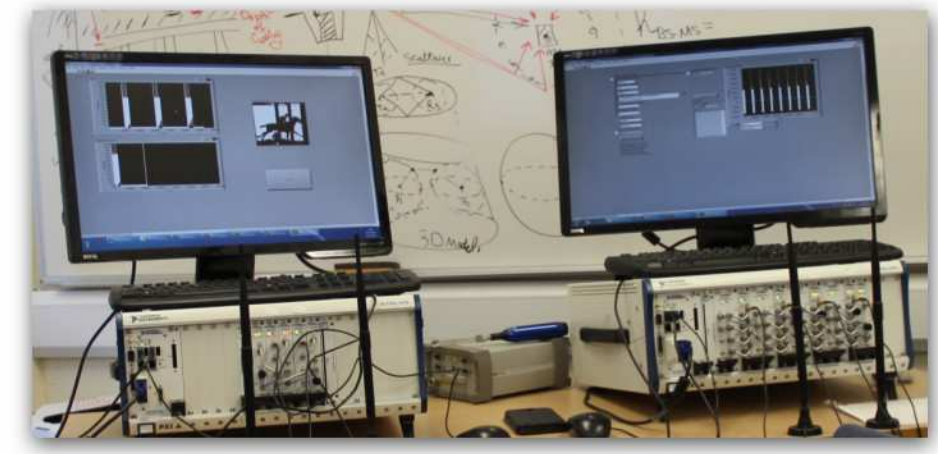

FIGURE 2.4: The real time demonstration of SM [12].

In 2012, a real-time demonstration of SM system related to this work was given in the UK-China science bridge [12] workshop, which is the first time in the world that SM is implemented in a real-time hardware testbed.

2.1.5 Investigation on the BER Performance of SM

As an important performance metric for wireless communication systems, the BER performance of SM system has been widely investigated in past years, related results

can be found in [22], [24]–[28], [45]–[57]. The main goal of these studies can be concluded as following aspects: 1) to investigate the impact of wireless fading channels on the system performance of SM technology; 2) to identify suitable channel environments that SM can be employed to improve the performance of wireless MIMO communication systems; 3) to find new ideas that can improve the performance of SM systems. In [45], the first attempt to investigate the BER performance of SM was introduced. In [22], the same author further extended this work to a OFDM SM system. In this two references, the framework to compute the theoretical BER expression of the two-step detector under Rayleigh fading channels was proposed. In [47], this framework was used to study the theoretical BER of SM systems under Nakagami-m channel models. In [24], [25], the theoretical framework to study the BER performance of SM systems under Rayleigh fading channels using the ML-optimum receiver algorithm was proposed. In this framework, it was pointed out that the error probability performance of SM systems is mainly determined by the Euclidean distance of pairs of channel impulse responses. In [46], the author investigated the BER performance for SM under correlated Rician fading channels. The theoretical error probability expression was derived using the union-bound-based method, and the random matrix theory was used to compute the pairwise error probability. The similar research was also reported in [50].

In [24], [55]–[57], coding works were involved to improve the performance of SM system. In [24], the bit interleaved coded modulation (BICM) aided scheme were investigated. And in [55]–[57], the Trellis-coded scheme was considered to improve the system performance under correlated channel models. In all of these literatures, theoretical BER expressions were derived correspondingly using the similar method, and this methodology was also applicable to other convolution coding frameworks.

For a SM system, when it only uses antenna index to carry information, the system becomes a SSK-MIMO system. The study on the BER performance of SSK systems is also meaningful to the SM system. In [27], [28], [51], [53], the BER performance of SSK-MIMO systems was investigated by both simulation and theoretical analysis under correlated Nakagami-m and Rician fading channels. From these studies, it can

be observed that the BER performance of SSK system was mainly affected by the difference between pairs of channel impulse responses, which can also be reflected by the correlation between sub channels. Under the correlated Rician fading channel, it can be found that the performance of SSK system became worse when the K factor increasing. This behaviour was opposite to conventional MIMO systems, whose performance were usually improved with the increase of the K factor. This fact clearly showed that SSK (and SM) and other MIMO technologies can be combining used under different propagation conditions to improve the system performance.

In [26], the BER framework of SSK systems proposed in [27], [28], [51], [53] was extended to SM systems under different generalised fading channels. In this work, the author pointed out that existing BER theoretical frame works were with some limitations such as: 1) neglect different roles played by the spatial and the signal modulation on the BER performance of SM systems, 2) not sufficiently accurate for cases of high order modulation scheme and small numbers of antennas. Thus, an improved theoretical BER upper bound was proposed in this literature that classified error conditions into three terms: 1) errors only occur in the signal modulation part; 2) errors only occur in the spatial modulation part; 3) errors occur in both parts. From the comparison between the theoretical and the simulation results, the high accuracy of this BER framework under wide ranges of mobile fading channels was announced. Besides, in this work, some novel conclusions were presented. 1) SM system can obtain better performance when using PSK modulation schemes compared with using QAM schemes, which was in contrast to the conventional understanding. This is an important finding as it gives a guideline to establish the system. This finding can highly benefit the latest research on using constant-envelope modulation schemes for massive MIMO systems, which aimed to decrease the system complexity and improve the energy efficiency. 2) Theoretical and simulation results indicates that under the same system data rate, different system settings of allocation of informations bits on to the signal constellation and the spatial constellation diagram can result in significantly different system performance. For each condition, there is an optimal point which is mainly determined by the fading characteristic of wireless channel.

2.1.6 Spatial Modulation: Towards 5G

In recent years, there are fruitful achievements in the research of SM that related to the 5G system development. In this section, we selected some of the most meaningful achievements that reflect the latest trend of the 5G research such as the relay network, VLC and green communications.

2.1.6.1 Generalised Spatial Modulation

For conventional SM systems, as only one antenna is activated at each time instant, the number of antennas should be limited to powers of two. This restriction limits the efficiency of antenna elements use and the flexibility of the system construction. In [58], [59], the concept of the generalised SM was proposed, its basic idea is to use antenna sets rather than single antenna index to carry information. By using this idea, more than one antenna can be activated at each time instant, the achievable spectral efficiency can be further improved, and the ICI free benefit can be still preserved at the same time. However, compared with the conventional SM, the system complexity of the generalised spatial modulation is higher as it needs more operations for the demodulation work at the Rx side.

For the generalised SM, as there are more than one antennas can be activated, some researchers tried to combine SM with other MIMO technologies in order to take advantages of both while avoiding their drawbacks. In [60], the authors attempted to combine the generalised SM with the spatial multiplexing in order to further improve the data rate of the system. The basic idea for this system is to transmit multiple different symbols from multiple selected antennas, and the set of selected antennas can also used to encode informations at the same time. The main advantage of this idea is a much higher system data rate, however, the cost of this improvement is the highly increased system complexity and the ICI. In [61], the idea of the generalised SM was combined with the STBC . The principle of this new combination is to transmit STBC streams from selected pairs of antennas. Besides data bits encoded in STBC streams, some data bits are encoded in antenna selection sets. Thus, the normalised

system data rate is more than one symbol per time slot. In order to obtain the maximum diversity gain, some optimisation were used to the STBC constellation scheme. For example, some rotation angles were involved to achieve the diversity gain. From simulation results proposed in this paper, the system performance of this generalised SM-STBC system are still comparable with the ML-optimum performance of conventional SM systems. And it can offer better performance compared with conventional STBC schemes with the cost of increasing RF elements but not RF chains.

Besides these aforementioned attempts of generalised SM, there were also some researchers tried to break the limitation of antenna numbers that should be in the powers of two by using flexible numbers of antennas and RF chains. One typical solution was reported in [62], in which an encode algorithm relies on the application of the module conversion to achieve a flexible data rate was reported. However, due to use module conversion based encode algorithm, there was a error propagation effort. This problem was solved in [63] by using the bits padding method to avoid the error propagation effect.

2.1.6.2 Spatial Modulation for Green Communications

For 5G systems, the green communications is an import issue. It is expected that the 5G systems can achieve 10 times higher spectral and energy efficiency compared with 4G systems. As a potential 5G wireless communication technology, the performance of SM in terms of spectral and energy efficiency has widely been investigated.

It was reported in [22] and [23] that by employing numbers of antennas but only a few RF chains, a SM system can benefit from the MIMO structure as other conventional MIMO technologies, but with other advantages such as the lower system complexity and the better spectral-energy efficiency. Thus, at the same time the energy consumption from RF chains and the amplifiers can be significantly decrease. On the other hand, when combined SM with other MIMO technologies, the spectral and energy efficiency of conventional MIMO can be improved by encoding information to antenna indexes and activating fewer antennas and RF chains.

In [64], [65], the potential energy-efficiency enhancement of SM was investigated. In this work, the consumption power model proposed by the Europe project Energy Aware Radio and neTwork tecHnologies (EARTH) [66] was considered. For this power model, it was assumed that the static power assumption of a MIMO system is increased linearly with the increase of the number of active RF chains. For this work, the energy efficiency of BSs using SM and conventional MIMO technologies were compared in different scenarios. From proposed simulation results, the advantage of SM in energy efficiency was highlighted, especially under medium throughput cases. Considering high throughput cases, the spatial multiplex can have superior performance due to SM in this work only used very small numbers of antennas. If the system equips with large numbers of antenna elements (not RF chains), the energy efficiency of SM system can be further improved.

In [67], the authors designed an energy-efficient transmission scheme using the SSK-MIMO principle. The basic idea of this work is to use the nonequiprobable signalling alphabet, which means low-power modulated symbols are used for transmitting more frequently. Besides, the authors investigated the optimisation of the system for minimum the achievable average symbol power consumption, some import practical issues were considered includes the spectral efficiency, the error performance and the system complexity. As the general-SSK scheme was also considered in this work, the number of active RF chains were investigated to optimise the system energy efficiency.

2.1.6.3 Spatial Modulation in Relay and Distributed Wireless Networks

For 5G systems, one of its basic ideas is to isolate indoor scenarios and outdoor scenarios [9]. In order realise this idea, different relays and distributed networks will be used. Indeed, the combination of these technologies with SM will further benefit the development of 5G wireless communication systems in terms of the energy efficiency and the spectrum efficiency [23]. On the research of SM combining with relays and distributed wireless networks, there are the following highlighted achievements.

In [68], a dual-hop relay system was considered. In this system, all devices were equipped with multiple antennas, and SM was considered as the MIMO scheme. Under the demodulate-and-forward (DF) protocol, the DF-SM relay system demonstrated a improvement on end-to-end error probability compared with conventional DF relay systems. The analytic study on this topic can also be found in [69], [70].

In [71], a distributed relay network was proposed, which also used the DF protocol. The communication between the source and relays were conventional wireless links. At the relay, the cyclic redundancy checking (CRC) was used to detect errors at the relay and determine whether the relay processing continue. Then the corrected data will be re-encoded and sent to the user using the space-time shift keying (STSK), which is similar to SM. Involved the CRC can eliminate the error that happened due to the relay. In [72], this work was further extended, where multi-carrier code-division multiple access (MC-CDMA) was used to avoid the interferences between different users.

In [73], the authors proposed a two-phase relay scheme in order to enhance the throughput of the system by achieving the diversity gain. In the first phase, which was named as the listening phase, the resource broadcasts data to both the destination and numbers of relays. On the second phase named the cooperative phase, the resource still transmits the same data, and relays will decode received data of phase one, and transmit to the destination using SM-MIMO principle. From simulation result in this paper, it can be observed that the proposed two-phase relay scheme can further improve the system throughput.

In [74], the concept of the distributed space shift keying (DSSK) was investigated under a relay network for the uplink scenario. The major contribution of this work is proposing an optimal demodulator for the receiver which was with the ability to correct decoding errors of the relay process. From simulation results, it can be found that this solution can offer the better diversity gain compared with other solutions. The similar work was carried out in [75], while the concept was used in a half-duplex relay system in order to improve the achievable bandwidth efficiency.

2.1.6.4 Spatial Modulation for Visible Light Communications

In order to solve the spectrum resource shortage problem, offer much wider available bandwidth for future wireless systems. Some unexplored spectrum resources have been considered in 5G systems. As a promising complementary for RF communications, the VLC has been widely investigated. For a VLC system, optical elements such as light-emitting diodes (LEDs) rather than antennas were used to transmit data, and an achievable data rate of 3.5 Gb/s using a single LED component has been reported in [9].

The idea of combining VLC with SM has attracted lot of research interest in recent years. In [76], the concept of combining SM with VLC was proposed. Similar to the RF SM, some data are carried by the index of LED components while some are represented by the intensity level of the light rather than modulated symbols. Simulation results were obtained using a ray-tracing based channel model for VLC. From these results, it can be observed that without optimising positions of transmit and receive elements, the system seriously suffered from highly correlated channels and resulted in the poor performance. By increasing the number of receive elements and applying channel coding, the system performance can be significantly improved. Compared with other VLC modulation schemes, the proposed optical SM scheme can offer a better trade-off in terms of the system performance, the system complexity and the energy efficiency. The similar research was carried out in [77], which further investigated the influence of the alignment of LED elements position. It can be observed that the aligned system shows a significant enhancement in terms of the bandwidth and the energy usage.

In [78], a combination of the SSK-MIMO scheme and the pulse position modulation (PPM) was proposed. From the Tx, PPM pulse patterns rather than the constant light power (for SSK) or light of modulated intensity levels (for conventional VLC) were transmitted. This combination can benefit from both the superior energy efficiency enhancement of PPM technology and the advantage of low system complexity for SSK systems. Simulation results indicate that compared with conventional SSK and other VLC schemes, the proposed system demonstrated the enhanced performance.

In [79], the authors comprehensively compared the performance of different MIMO schemes used in VLC systems. From these proposed results, it can be observed that SM can offer more robustness to the high correlation among sub paths. A significantly improved spectral efficiency can be achieved by SM especially at low SNR cases. Under conditions of highly correlated channels, the performance of SM can be improved by using the power imbalance technology as it can mitigate the correlation effect. Over all, this work demonstrated that the performance of VLC systems can be enhanced by using MIMO technologies such as SM.

2.2 Wireless channel modelling for 5G scenarios

Compared with conventional wired communication systems, wireless communication systems suffer more challenges due the propagate media, which is known as the wireless channel. In wireless channels, the signal suffers from the multipath effect as the result of reflection diffraction and scattering phenomena occur during its propagation [80]. For the Rx, in order to recover the data from received multiple copies of the original signal which also combined with the interference and noise, it should carefully consider the fading issue of wireless channels. Thus, for designing and testing wireless communication technologies, channel models that accurately represents the propagation environments of the real world is important.

For different scenarios, their channel characteristics are significantly different. Thus, their channel models should be designed considering different propagation issues. In future 5G systems, as more novel technologies will be used and more scenarios will be considered, there are more challenges on the development of channel models for 5G systems.

In this PhD project, as three typical 5G scenarios are considered, correspondingly, we will firstly give a review on channel modelling works on V2V, HST and MU-massive MIMO scenarios.

2.2.1 Channel modelling for V2V scenarios: from 2D to 3D

Compared with conventional fix-to-mobile (F2M) communications, the biggest challenge in V2V communications is the severe environment caused by the fast movement of both the Tx and the Rx. In order to design and test V2V communication technologies, channel models that can accurately represent the propagation characteristic of V2V communication environments should be developed.

Among various channel modelling methodologies, regular-shaped geometry-based stochastic models (RS-GBSMs) are widely used due to their flexibility and convenience for the theoretical analysis [81]– [82]. The first V2V RS-GBSM was proposed by Akki and Haber in [81], which is a two-dimensional (2D) two-ring narrowband single-input single-output (SISO) Rayleigh fading channel with the assumption of isotropic scattering and only double bounced rays. Since then, various V2V RS-GBSMs [83]–[86] have been developed.

In order to more accurately model the propagation characteristic of V2V scenarios, some researchers have tried to propose 3D V2V channel models [87], [82]. In the 3D channel model, the propagation of signals in the elevation plane is also considered. And compared with 2D channel models, 3D models are more accurate in representing the fading characteristic as they offer more flexibility due to the extended propagate dimension. One important 3D model has been proposed in [87] by Yuan et al. , it is a novel 3D V2V RS-GBSM which includes an elliptic-cylinder and two spheres combining the LoS component, single-bounced (SB), and double-bounced (DB) components for the non-isotropic scattering case. It is also the first 3D V2V channel model that can accurately capture the effect of VTD on statistic properties of the channel. In Chapter III, this channel model will be used to test the performance of SM technology.

2.2.2 Channel modelling for HST scenarios: from WSS to non-stationary

Research work for channel measurements and channel modelling on HST scenarios can be found in [88]–[93]. For most of these aforementioned channel modelling work, in order to reduce the complexity, these channel models are assumed to fulfil the wide-sense stationary (WSS) assumption. However, as the speed of nowadays HST can easily reach over 300 km/h, the WSS assumption is not sufficiently accurate for HST channel modelling. This viewpoint has been proved by the measurement data of [94]. It is necessary to propose non-stationary channel models for designing and testing wireless communication technologies applied for HST communication systems.

The first non-stationary RS-GBSM for HST scenarios was proposed by Ghazal et al. in [95], [96], which represents the non-stationary behaviour by considering the distance between the Tx and the Rx as time-varying. In [97], this model was further improved by involving more time-varying parameters such as angles of arrival (AoAs) and angles of departure (AoDs). Compared with conventional channel models for low mobility scenarios, it can be found that the proposed HST channel model in [97] is with significantly different fading features and can accurately represent the characteristic of HST channels. This channel model is used to investigate the BER performance of SM systems in Chapter IV of this PhD thesis.

2.2.3 Channel modelling for massive MIMO scenarios: from sharing the same set of clusters to clusters evolution

Been treated as a promising technology for 5G wireless communications systems, the massive MIMO technology has attracted lots of research interest in recent years [98]–[101]. For designing and testing massive MIMO technologies, channel models for massive MIMO scenarios is important. And this topic has attracted some research interest in recent years.

One nature manner to develop massive MIMO channel models is to extend conventional small scale MIMO channel models to massive MIMO. Related works have been reported in [102]–[106]. In these literatures, [102] and [103] are massive MIMO channel models extended from independent and identically distributed (i.i.d) channel models, [104] and [105] are optimised KBSM, [106] are proposed from conventional MIMO GBSM.

However, for a massive MIMO system, as large numbers of antennas are distributed over a wide range, different antenna elements may observe different sets of clusters. Measurement results in [107], [108] have proved this observation. Thus, aforementioned channel models are not accurate for massive MIMO scenarios.

The geometry-based stochastic models proposed in [109], [110] by Wu et al. are the first serial of channel models that considered the evolution of clusters, and therefore they can accurately capture the characteristics of massive MIMO channels. The drawbacks of these models are their high complexity which make it is not easy to use these channel models especially for further theoretical analysis. In [111], a KBSM for massive MIMO channel is presented by the same author. This channel model has considered the evolution of clusters for each antenna element using a survival probability matrix. This matrix is the abstraction of the birth-death process of clusters. This channel model is a KBSM, it is easy to be used for theoretical analysis. Due to its good balance in accuracy and complexity. It is used to test the performance of massive MIMO SM systems in Chapter V of this PhD thesis.

2.3 Summary

In this chapter, we have given a survey on the research of SM systems and channel modelling on some important 5G scenarios. From this survey, we can find that as an attractive MIMO technology, the research on SM have been widely carried out in different direction and topics for long time. Benefited form its single RF chain-multiple antenna MIMO structure, SM shows some attractive advantages such as the low system complexity and the high spectral energy efficiency when compared with

other conventional MIMO technologies. However, there are some drawbacks can not be neglected, which could be the future research direction to SM.

As a potential 5G technology, the research on SM regrading 5G systems development also have got fruitful achievements. Large number of technical papers on the development of SM for future 5G systems have been published. These papers cover important 5G issues such as the generalised SM, SM for green communications, SM in relay and distributed MIMO networks and Sm for VLC systems.

In 5G systems, some new communication scenarios will emerge. The channel modelling work for 5G communication systems is an important part of the research on 5G. Based on our survey, we can find some meaningful achievements in this topic, which will be helpful to the development of 5G technologies.

In this PhD thesis, these research works are clearly classified and surveyed. Based on the survey, a clear and deep understating to the research of SM and channel modelling for 5G scenarios is buried in my mind. Finally, the investigation of SM under different realistic 5G channel models is selected as the research focus of this PhD project.

Chapter 3

BER Performance of Spatial Modulation Systems Under 3D V2V MIMO Channel Models

3.1 Introduction

For 5G wireless systems, it is predicted that D2D communications will contribute most of the data traffic. As an important D2D issue, V2V communications have been treated as a hot research topic in recent years [112]. With multiple antennas equipped on the vehicle, MIMO technologies can be widely used by V2V communications for safety devices, ad hoc peer-to-peer networks and intelligent transportation systems [87], [112].

Compared with conventional F2M communications, the biggest challenge in V2V communications is the severe environment caused by the fast movement of both the Tx and Rx. And due to the special working environment for V2V communication systems, the physical layer transmit technologies should fulfil following requirements. 1) The system should be with high robustness, especially have good performance under the high VTD case. 2) Low system complexity and high spectral- energy efficiency.

In recent years, SM has attracted significant research interests due to its report enhancement in this system performance metrics, which indicates it a promising technology for V2V communications. In order to prove its advantages, it is necessary to investigate its performance under the potential working scenarios.

However, the BER performance of SM has so far mainly been investigated for some simple F2M channels such as Rayleigh, Rician, and Nakagami fading channels [22], [25], [26], [113]. In [114], the BER performance of SM systems was first studied under a simple 2D V2V MIMO channel model, which is a two-ring V2V RS-GBSM containing only DB components without considering the LoS component and SB components [85]. To the best of the author's knowledge, there is no relevant study on the BER performance of SM systems under more realistic 3D V2V MIMO channel models. To fulfil the research gap, this chapter investigates the BER performance of SM systems using the 3D V2V MIMO channel model in [87] with different VTD scenarios and system settings. The major contributions of this work are summarized as follows.

1. The BER performance of SM systems under the 3D V2V MIMO channel model was investigated with different channel configurations and system settings.
2. A tight closed-form upper bound of the theoretical average BER (ABER) for SM systems under a 3D V2V RS-GBSM was derived.
3. Different impacts of 3D and 2D V2V MIMO channel models on the BER performance of SM systems were studied.
4. BER performance of SM systems is compared with that of other MIMO technologies (spatial diversity and spatial multiplexing) under the realistic 3D V2V channel model.

The remainder of this chapter is organized as follows. In Section 3.2, the 3D V2V MIMO channel model and some important statistical properties are described. The theoretical expression of the ABER for SM under the 3D V2V MIMO channel model is derived in Section 3.3. In Section 3.4, numerical and simulation results are presented and analysed. Finally, conclusions are given in Section 3.5.

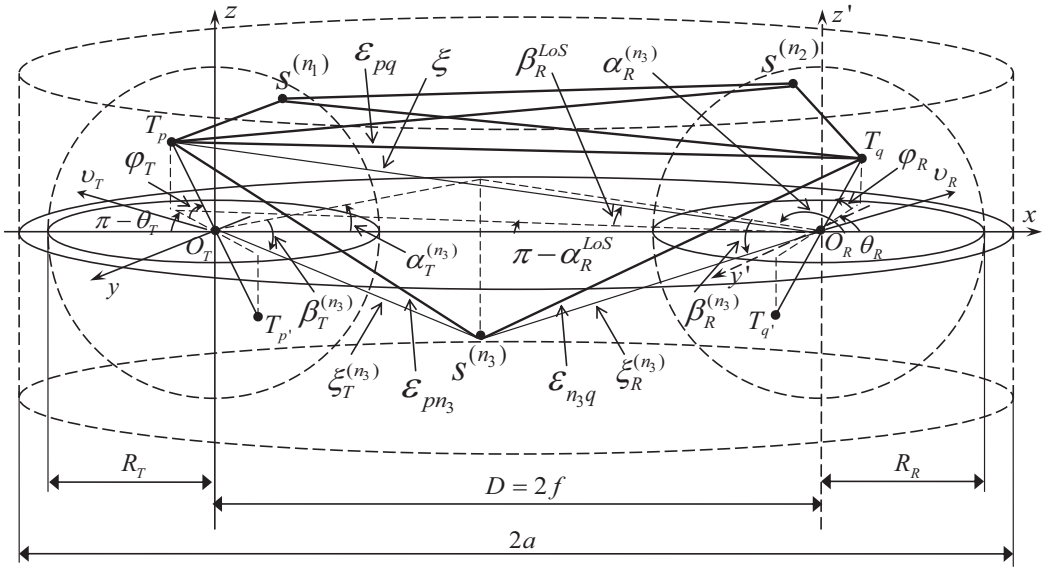

FIGURE 3.1: The 3D V2V RS-GBSM combining a two-sphere model and an elliptic-cylinder model (only the detailed geometry of LoS components and single-bounced rays in the elliptic-cylinder model). [81]

3.2 The 3D V2V MIMO Channel Model

In order to test the BER performance of SM systems, the narrowband 3D V2V MIMO channel model proposed in [87] by Yuan et al. is used in this work. In this model, the propagation environment is assumed to be a conventional urbane scenario. Along with the road, there are some fixed scatters such as buildings and trees. Two cars are assumed to move toward each other. Both cars are equipped with multiple omi-direction antennas at the top of cars.

The channel model consists of both LoS and Non-LoS components. For Non-Los components, they can be further classified as SB rays representing signals reflected only once during the propagation process and DB rays representing signals reflected more than once. This channel model is a RS-GBSM, where effective scatters are assumed to distribute on regular geometric shapes. In this channel model, two types of scatters are assumed. The first type is the stationary scatters such as buildings and trees which are abstracted as an elliptic-cylinder. The second type considers moving scatters, such as other vehicles which are abstracted and located on two spheres around the Tx and Rx.

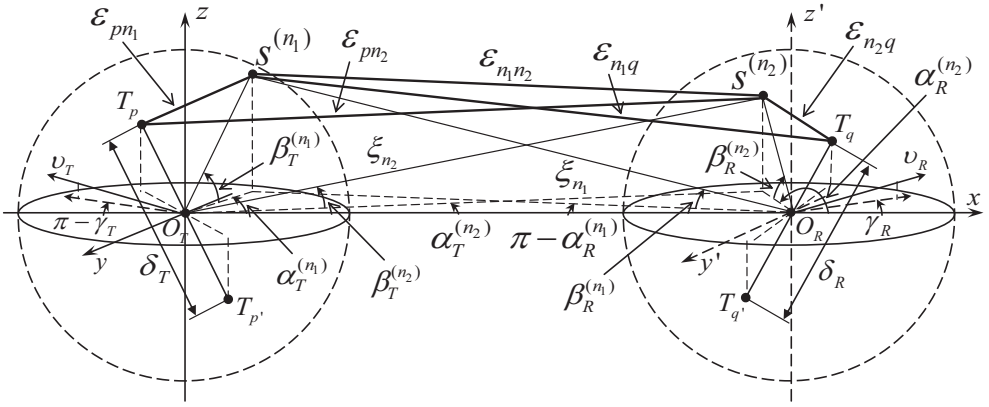

FIGURE 3.2: The detailed geometry of the single- and double-bounced rays in the two-sphere model of the proposed 3D V2V RS-GBSM.[81]

TABLE 3.1: Definition of parameters in Figs. 1 and 2. [81]

D	distance between the centres of the Tx and Rx spheres
R_T, R_R	radius of the Tx and Rx spheres, respectively
a, f	semi-major axis and half spacing between two foci of the elliptic-cylinder, respectively
δ_T, δ_R	antenna element spacing at the Tx and Rx, respectively
θ_T, θ_R	orientation of the Tx and Rx antenna array in the x-y plane, respectively
φ_T, φ_R	elevation of the Tx and Rx antenna array relative to the x-y plane, respectively
υ_T, υ_R	velocities of the Tx and Rx, respectively.
γ_T, γ_R	moving directions of the Tx and Rx in the x-y plane, respectively
$\alpha_T^{(n_i)}$ $(i=1,2,3)$	azimuth angle of departure (AAoD) of the waves that impinge on the effective scatterers $s^{(n_i)}$
$\alpha_R^{(n_i)}$ $(i=1,2,3)$	azimuth angle of arrival (AAoA) of the waves travelling from the effective scatterers $s^{(n_i)}$
$\beta_T^{(n_i)}$ $(i=1,2,3)$	elevation angle of departure (EAoD) of the waves that impinge on the effective scatterers $s^{(n_i)}$
$\beta_R^{(n_i)}$ $(i=1,2,3)$	elevation angle of arrival (EAoA) of the waves travelling from the effective scatterers $s^{(n_i)}$
α_R^{LoS}, β_R^{LoS}	AAoA and EAoA of the LoS paths, respectively
ε_q, ε_{pn_i}, $\varepsilon_{n_1n_2}$, ε_{n_iq}, ξ, $\xi_{T(R)}^{n_3}$, ξ_{n_1}, ξ_{n_2} $(i=1,2,3)$	distances $d(T_p,T_q)$, $d\left(T_p,s^{(n_i)}\right)$, $d\left(s^{(n_1)},s^{(n_2)}\right)$, $d\left(s^{(n_i)},T_q\right)$, $d(T_p,O_R)$, $d\left(O_T(O_R),s^{(n_3)}\right)$, $d\left(s^{(n_1)},O_R\right)$, $d\left(O_T,s^{(n_2)}\right)$, respectively

The geometry of the channel model is shown in Fig. 3.1 and Fig. 3.2. In Fig. 3.1, the geometry of LoS components and the single bounced elliptic-cylinder model are illustrated. While the detailed geometry of the single and double bounced two sphere model is shown in Fig. 3.2. The physical meaning of parameters in Fig. 3.1 and Fig. 3.2 are defined in Table I.

Let $h_{q,p}(t)$ represents the link between the *pth* antenna at the Tx and the *qth* antenna at the Rx. Corresponding to the channel model's assumption, each element $h_{q,p}(t)$ should contain three types of components: the LoS component, SB components, and DB components, which can be expressed as

$$h_{q,p}\left(t\right) = h_{qp}^{\mathrm{LoS}}\left(t\right) + \sum_{i=1}^{I} h_{qp}^{\mathrm{SB}_i}\left(t\right) + h_{q,p}^{\mathrm{DB}}\left(t\right) \tag{3.1}$$

where

$$h_{q,p}^{\mathrm{LoS}}(t) = \sqrt{\frac{K}{K+1}} e^{-j2\pi f_c \tau_{qp}} \times e^{j2\pi f_{T\max} t \cos\left(\alpha_T^{\mathrm{LoS}} - \gamma_T\right) \cos\beta_T^{\mathrm{LoS}}} \times e^{j2\pi f_{R\max} t \cos\left(\alpha_R^{\mathrm{LoS}} - \gamma_R\right) \cos\beta_R^{\mathrm{LoS}}} \tag{3.2a}$$

$$\begin{aligned} h_{q,p}^{\mathrm{SB}_i}\left(t\right) = \sqrt{\frac{\eta_{\mathrm{SB}_i}}{K+1}} \lim_{N_i\to\infty} \sum_{n_i=1}^{N_i} \frac{1}{\sqrt{N_i}} e^{j\left(\psi_{n_i} - 2\pi f_c \tau_{qp,n_i}\right)} \\ \times e^{j2\pi f_{T\max} t \cos\left(\alpha_T^{(n_i)} - \gamma_T\right) \cos\beta_T^{(n_i)}} \times e^{j2\pi f_{R\max} t \cos\left(\alpha_R^{(n_i)} - \gamma_R\right) \cos\beta_R^{(n_i)}} \end{aligned} \tag{3.2b}$$

$$\begin{aligned} h_{q,p}^{\mathrm{DB}}\left(t\right) = \sqrt{\frac{\eta_{\mathrm{DB}}}{K+1}} \lim_{N_1,N_2\to\infty} \sum_{n_1,n_2=1}^{N_1,N_2} \frac{1}{\sqrt{N_1 N_2}} \times e^{j\left(\psi_{n_1,n_2} - 2\pi f_c \tau_{qp,n_1,n_2}\right)} \\ \times e^{j2\pi f_{T\max} t \cos\left(\alpha_T^{(n_1)} - \gamma_T\right) \cos\beta_T^{(n_1)}} \times e^{j2\pi f_{R\max} t \cos\left(\alpha_R^{(n_2)} - \gamma_R\right) \cos\beta_R^{(n_2)}}, \end{aligned} \tag{3.2c}$$

with $\alpha_T^{\mathrm{LoS}} \approx \beta_T^{\mathrm{LoS}} \approx \beta_R^{\mathrm{LoS}} \approx 0$, $\alpha_R^{\mathrm{LoS}} \approx \pi$, $\tau_{qp} = \varepsilon_{qp}/c$, $\tau_{qp,n_i} = (\varepsilon_{pn_i} + \varepsilon_{n_i q})/c$, and $\tau_{qp,n_1,n_2} = (\varepsilon_{pn_1} + \varepsilon_{n_1 n_2} + \varepsilon_{n_2 q})/c$. Here, c is the speed of light and K designates the Rician factor, which indicates the power ratio of the LoS component to the Non-LoS components.

In this model, for SB components, the case number is setted as $I = 3$, which means there are three conditions for single-bounced rays. These conditions correspond to: SB_1 denotes the reflection from the Tx sphere, SB_2 is the reflection from the Rx sphere, and SB_3 denotes reflections from the elliptic-cylinder. Parameters η_{SB_i} and η_{DB} specify the amount of powers that the single- and double-bounced rays contribute to the total scattered power $1/(K+1)$. It is necessary to mention that these power-related

parameters satisfy $\sum_{i=1}^{I} \eta_{\mathrm{SB}_i} + \eta_{\mathrm{DB}} = 1$, which guarantees the power balance of the channel model. The phases ψ_{n_i} and ψ_{n_1,n_2} are assumed to be i.i.d. random variables with uniform distributions over $[-\pi, \pi)$. $f_{T_{\max}}$ and $f_{R_{\max}}$ are the maximum Doppler frequencies with respect to the Tx and Rx respectively, which can be calculated as

$$f_{T_{\max}/R_{\max}} = \frac{\upsilon_{T/R}}{c} f_c. \tag{3.3}$$

The next step is to obtain the delay of each path, which is determined by the distance of each component ε. In order to simplify the computation process, some appropriate triangles and small angle approximations in cosine are used (i.e., $\sin x \approx x$ and $\cos x \approx 1$ for small x), thus the distance ε of each component can be approximated as:

$$\varepsilon_{qp} \approx \xi - \frac{\delta_R}{2\xi}\left[\frac{\delta_T}{2}\sin\varphi_T \sin\varphi_R - Q\cos\varphi_R\cos\theta_R\right] \tag{3.4a}$$

$$\varepsilon_{pn_1} \approx R_T - \frac{\delta_T}{2}\Big[\sin\beta_T^{(n_1)}\sin\varphi_T + \cos\beta_T^{(n_1)}\cos\varphi_T\cos(\theta_T - \alpha_T^{(n_1)})\Big] \tag{3.4b}$$

$$\varepsilon_{n_1 q} \approx \xi_{n_1} - \frac{\delta_R}{2\xi_{n_1}}\Big[R_T\sin\beta_T^{(n_1)}\sin\varphi_R - Q_{n_1}\cos\varphi_R\cos(\alpha_R^{(n_1)} - \theta_R)\Big] \tag{3.4c}$$

$$\varepsilon_{pn_2} \approx \xi_{n_2} - \frac{\delta_T}{2\xi_{n_2}}\Big[R_R\sin\beta_R^{(n_2)}\sin\varphi_T + Q_{n_2}\cos\varphi_T\cos(\alpha_T^{(n_2)} - \theta_T)\Big] \tag{3.4d}$$

$$\varepsilon_{n_2 q} \approx R_R - \frac{\delta_R}{2}\Big[\sin\beta_R^{(n_2)}\sin\varphi_R + \cos\beta_R^{(n_2)}\cos\varphi_R\cos(\theta_R - \alpha_R^{(n_2)})\Big] \tag{3.4e}$$

$$\varepsilon_{n_1 n_2} \approx \left\{\Big[D - R_T\cos\alpha_T^{(n_1)} - R_R\cos(\alpha_R^{(n_1)} - \alpha_R^{(n_2)})\Big]^2 + \Big[R_T\cos\beta_T^{(n_1)} - R_R\cos\beta_R^{(n_2)}\Big]^2\right\}^{1/2} \tag{3.4f}$$

$$\varepsilon_{pn_3} \approx \xi_T^{(n_3)} - \frac{\delta_T}{2\xi_T^{(n_3)}}\Big[\xi_R^{(n_3)} \sin\beta_R^{(n_3)} \sin\varphi_T + Q_{n_3} \cos\varphi_T \cos(\alpha_T^{(n_3)} - \theta_T)\Big] \tag{3.4g}$$

$$\varepsilon_{n_3q} \approx \xi_R^{(n_3)} - \delta_R\Big[\sin\beta_R^{(n_3)} \sin\varphi_R + \cos\beta_R^{(n_3)} \cos\varphi_R \cos(\alpha_R^{(n_3)} - \theta_R)\Big], \tag{3.4h}$$

where

$$\xi \approx Q \approx D - \frac{\delta_T}{2} \cos\varphi_T \cos\theta_T \tag{3.5a}$$

$$\xi_{n_1} = \sqrt{Q_{n_1}^2 + R_T^2 \sin^2\beta_T^{(n_1)}} \tag{3.5b}$$

$$Q_{n_1} \approx D - R_T \cos\beta_T^{(n_1)} \times \cos\alpha_T^{(n_1)} \tag{3.5c}$$

$$\xi_{n_2} = \sqrt{Q_{n_2}^2 + R_R^2 \sin^2\beta_R^{(n_2)}} \tag{3.5d}$$

$$Q_{n_2} \approx D + R_R \cos\beta_R^{(n_2)} \cos\alpha_R^{(n_2)} \tag{3.5e}$$

$$\xi_R^{(n_3)} = \frac{2a - Q_{n_3}}{\cos\beta_R^{(n_3)}} \tag{3.5f}$$

$$\xi_T^{(n_3)} = \sqrt{Q_{n_3}^2 + (\xi_R^{(n_3)})^2 \sin^2\beta_R^{(n_3)}} \tag{3.5g}$$

$$Q_{n_3} = \frac{a^2 + f^2 + 2af\cos\alpha_R^{(n_3)}}{a + f\cos\alpha_R^{(n_3)}}. \tag{3.5h}$$

For double bounced reflections, we assume there is no correlation between azimuth/elevation angle of departure (A/EAoD, $\alpha_T^{(n_i)}$, $\beta_T^{(n_i)}$) and azimuth/elevation angle of arrival(A/EAoA, $\alpha_R^{(n_i)}$, $\beta_R^{(n_i)}$). However for single bounce reflections, they are related to each other based on their geometric relationship.

For the theoretical model of our channel, we assume there is infinite number of scatters. Thus AOAs and AODs are continuous random variables. In this channel model, the von Mises-Fisher (VMF) distribution is assumed to describe the distribution of these angles, which can represent the joint probability density function (PDF) of azimuth/elevation angles as [87] :

$$f(\alpha, \beta) = \frac{k \cos \beta}{4\pi \sinh k} \times e^{k[\cos \beta_0 \cos \beta \cos(\alpha - \alpha_0) + \sin \beta_0 \sin \beta]} \tag{3.6}$$

where $\alpha, \beta \in [-\pi, \pi)$, $\alpha_0 \in [-\pi, \pi)$ and $\beta_0 \in [-\pi, \pi)$ account for the mean values of the azimuth angle α and elevation angle β, respectively. k ($k \geq 0$) is a real-valued parameter that controls the concentration of the distribution relative to the mean direction identified by α_0 and β_0.

For the theoretical model, it is impossible to implement it either in software or hardware since it assumes infinite scatters. In order to use this 3D V2V channel model, the corresponding simulation model with finite number of scatters should be generated. To compensate for errors in such approximation, a novel parameter computation method called method of equal volume (MEV), is used to generate necessary parameters of the 3D channel model. Detail of this method can be found in [87].

If all EAoDs and EAoAs equal to zero as: $\beta_R^{LoS} = \beta_T^{LoS} = \beta_T^{(n_i)} = \beta_R^{(n_i)} = 0$ ($i = 1, 2, 3$), the 3D channel model becomes a 2D model with two rings and one ellipse. Relevant research has been carried out in [84], [87]. In this chapter, these works will not be repeated. However, in the following section, the different impact of 3D and 2D channel on the BER performance of SM system will be investigated.

3.2.1 Space-Time Correlation Function

There are various statistical properties of the considered channel model. However, in this work, only the space-time correlation function (STCF) property is considered as it indicates the spatial correlation among sub-channels. Such correlation has significant impact on the performance of SM systems. Mathematically and under the assumption of wide-sense stationary (WSS), the STCF between any two complex fading envelopes $h_{qp}(t)$ and $h_{q'p'}(t)$ is defined as

$$\rho_{h_{qp}h_{q'p'}}(\tau) = \mathrm{E}\left[h_{qp}(t)\, h^{*}_{q'p'}(t-\tau)\right] \tag{3.7}$$

where $(\cdot)^{*}$ denotes the complex conjugate operation, and $\mathrm{E}[\cdot]$ is the statistical expectation operator. For this V2V channel model, the STCF is calculated by adding correlation functions of the LoS component, SB components and DB components as

$$\rho_{h_{qp}h_{q'p'}}(\tau) = \rho_{h^{LoS}_{qp}h^{LoS}_{q'p'}}(\tau) + \sum_{i=1}^{I} \rho_{h^{SB_i}_{qp}h^{SB_i}_{q'p'}}(\tau) + \rho_{h^{DB}_{qp}h^{DB}_{q'p'}}(\tau)\,. \tag{3.8}$$

The STCF of LoS component is expressed as

$$\rho_{h^{LoS}_{pq}h^{LoS}_{p'q'}}(\tau) = K e^{\frac{j2\pi}{\lambda}A^{LoS} + j2\pi\tau(f_{T_{max}}\cos\gamma_T - f_{R_{max}}\cos\gamma_R)} \tag{3.9}$$

where $A^{LoS} = 2D\cos\varphi_R\cos\theta_R$.

For SB components SB_i $(i = 1, 2, 3,)$, the STCF is

$$\rho_{h^{SB_i}_{qp}h^{SB_i}_{q'p'}}(\tau) = \eta_{SB_i}\int_{-\pi}^{\pi}\int_{-\pi}^{\pi}\Big[e^{\frac{j2\pi}{\lambda}A^{(i)}} \times e^{j2\pi\tau\left(f_{T_{max}}B^{(i)} + f_{R_{max}}C^{(i)}\right)} f(\alpha^{(i)}_{T/R}, \beta^{(i)}_{T/R})\Big] d(\alpha^{(i)}_{T/R}, \beta^{(i)}_{T/R}) \tag{3.10}$$

where $A^{(i)}, i = 1, 2, 3$ is expressed as

$$\begin{aligned} A^{(1)} = {} & \delta_T\left[\sin\beta^{(1)}_T\sin\varphi_T + \cos\beta^{(1)}_T\cos\varphi_T\cos\left(\theta_T - \alpha^{(1)}_T\right)\right] \\ & + \frac{\delta_R}{\xi_{n_1}}\left[R_T\sin\beta^{(1)}_T\sin\varphi_R - Q_{n_1}\cos\varphi_R\cos\left(\theta_R - \alpha^{(1)}_R\right)\right] \end{aligned} \tag{3.11a}$$

$$A^{(2)} = \delta_R\big[\sin\beta_R^{(2)}\sin\varphi_R + \cos\beta_R^{(2)}\cos\varphi_R\cos\Big(\theta_R - \alpha_R^{(2)}\Big)\big] + \frac{\delta_T}{\xi_{n_2}}\big[R_R\sin\beta_R^{(2)}\sin\varphi_T + Q_{n_2}\cos\varphi_T\cos\Big(\theta_T - \alpha_T^{(2)}\Big)\big] \tag{3.11b}$$

$$A^{(3)} = \frac{\delta_T}{\xi_T^{(n_3)}}\big[\xi_R^{(n_3)}\sin\beta_R^{(3)}\sin\varphi_T + Q_{n_3}\cos\varphi_T\cos\Big(\theta_T - \alpha_T^{(3)}\Big)\big] + \delta_R\big[\sin\beta_R^{(3)}\sin\varphi_R + \cos\beta_R^{(3)}\cos\varphi_R\cos\Big(\theta_R - \alpha_R^{(3)}\Big)\big] \tag{3.11c}$$

with

$$B^{(i)} = \cos\Big(\alpha_T^{(i)} - \gamma_T\Big) \times \cos\Big(\beta_T^{(i)}\Big) \tag{3.11d}$$

$$C^{(i)} = \cos\Big(\alpha_R^{(i)} - \gamma_R\Big) \times \cos\Big(\beta_R^{(i)}\Big). \tag{3.11e}$$

The expressions of $\alpha_R^{(i)}$, $\beta_R^{(i)}$, Q_{n_i}, ξ_{n_1}, ξ_{n_2}, and $\xi_{T(R)}^{n_3}$ are given in Table II. Note that the subscripts T and R are applied to $i = 1$ and $i = 2, 3$, respectively.

For the double-bounced component resulting from the Tx and Rx spheres, the STCF is expressed as

$$\rho_{h_{qp}^{DB}h_{q'p'}^{DB}}(\tau) = \rho_{qq'}^{R}(\tau)\rho_{pp'}^{T}(\tau) = \eta_{DB}\int_{-\pi}^{\pi}\int_{-\pi}^{\pi}\int_{-\pi}^{\pi}\int_{-\pi}^{\pi} \Big[e^{\frac{j2\pi}{\lambda}A^{DB}} \times e^{j2\pi\tau\left(f_{T_{max}}B^{DB} + f_{R_{max}}C^{DB}\right)} \times f(\alpha_T^{(1)}, \beta_T^{(1)}) \cdot f(\alpha_R^{(2)}, \beta_R^{(2)})\Big] d(\alpha_T^{(1)}, \beta_T^{(1)}) d(\alpha_R^{(2)}, \beta_R^{(2)}) \tag{3.12}$$

with

$$A^{DB} = \delta_T\big[\sin\beta_T^{(1)}\sin\varphi_T + \cos\beta_T^{(1)}\cos\varphi_T\cos\Big(\theta_T - \alpha_T^{(1)}\Big)\big] + \delta_R\big[\sin\beta_R^{(2)}\sin\varphi_R + \cos\beta_R^{(2)} \times \cos\varphi_R\cos\Big(\theta_R - \alpha_R^{(2)}\Big)\big] \tag{3.13a}$$

$$B^{DB} = \cos\Big(\alpha_T^{(1)} - \gamma_T\Big)\cos\beta_T^{(1)} \tag{3.13b}$$

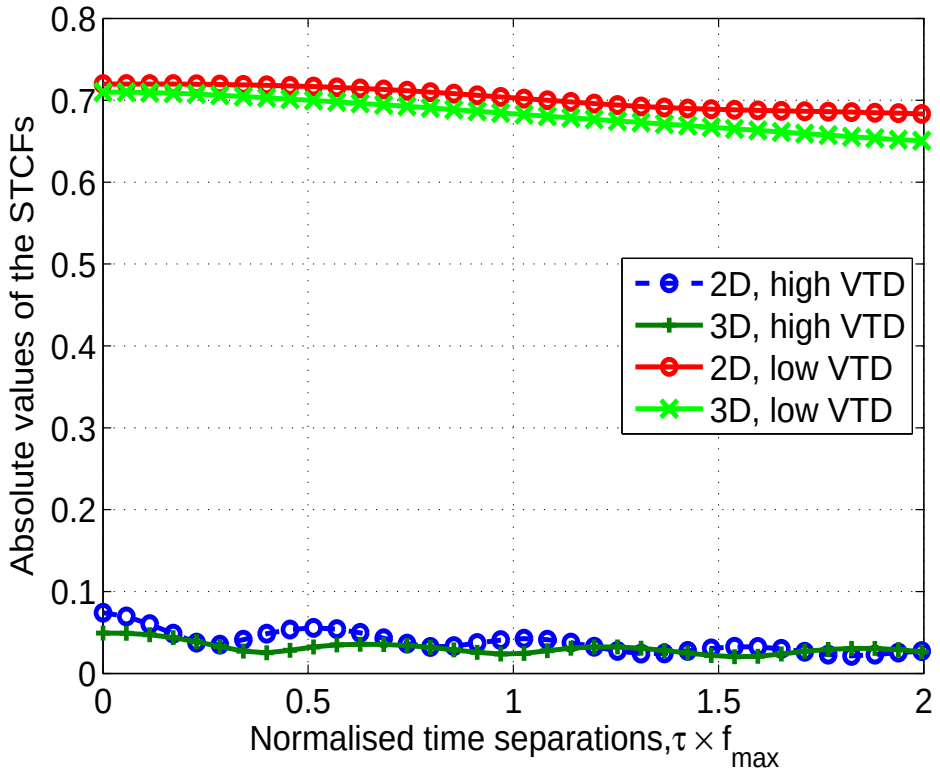

FIGURE 3.3: Absolute values of STCFs for V2V MIMO channel models with different dimensions and VTD settings.

$$C^{DB} = \cos\left(\alpha_R^{(2)} - \gamma_R\right) \cos\beta_R^{(2)}. \tag{3.13c}$$

In Fig. 3.3 and Fig. 3.4, the STCF of the V2V channel model with different configurations are shown. The difference in STCF cased by 3D and 2D channel model, different VTD scenario, are stated in Fig. 3.3. While in Fig. 3.4, the difference caused by VTD scenario and Doppler shift are investigated. In following sections, we will further explain these difference and try to use them analysis simulation results on BER performance.

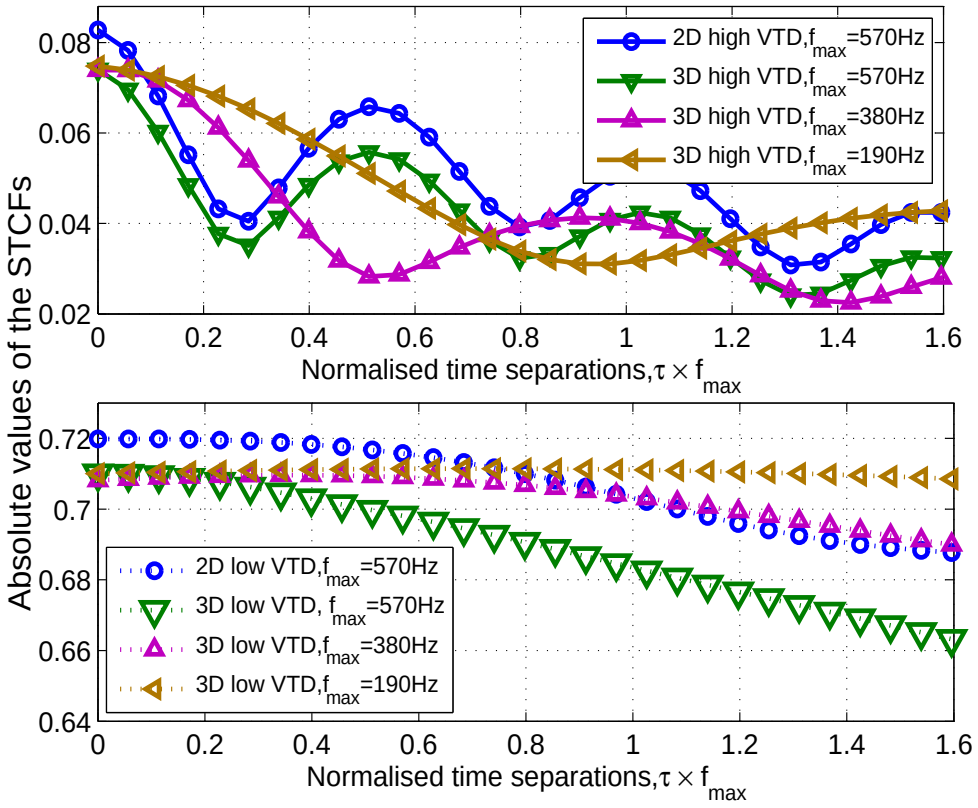

FIGURE 3.4: Absolute values of STCFs for V2V MIMO channel models with different Doppler frequency and VTD scenarios.

3.3 Theoretical ABER Analysis of SM Systems Under the 3D V2V GBSM

The theoretical ABER of SM systems can be obtained via the union bound method [26]–[28], [115]–[117]. In [26], an improved upper-bound method is presented which classifies errors into 3 categories : 1) error only occurs in the digital modulation part with the probability $\underset{\text{Signal}}{\text{ABER}}$; 2) error only occurs in spatial modulation part with the probability $\underset{\text{Spatial}}{\text{ABER}}$ and 3) error occurs in both parts with the probability $\underset{\text{Joint}}{\text{ABER}}$. The overall upper-bound expression of the BER is the combination of these three parts, which can be expressed as:

$$\underset{\text{SM}}{\text{ABER}} \leqslant \underset{\text{Signal}}{\text{ABER}} + \underset{\text{Spatial}}{\text{ABER}} + \underset{\text{Joint}}{\text{ABER}} \tag{3.14}$$

Compared to other approaches [27], [28], [115]–[117], this method is shown to offer better accuracy [26].

$\underset{\text{Signal}}{\text{ABER}}$ means error only occurs in the digital modulation part and the transmit antenna index is correctly detected. It is similar to the single-input-multiple-output (SIMO) case. The BER expression is given by

$$\underset{\text{Signal}}{\text{ABER}} = \frac{1}{N_t}\frac{\log_2(M)}{m}\sum_{n_t=1}^{N_t}\underset{\text{MOD}}{\text{APEB}}(n_t), \tag{3.15}$$

and

$$\underset{\text{MOD}}{\text{APEB}}(n_t) = \frac{1}{M}\frac{1}{\log_2(M)}N_H\left(\chi \to \tilde{\chi}\right)P(\chi \to \tilde{\chi}, n_t). \tag{3.16}$$

In (3.16), $N_H\left(\chi \to \tilde{\chi}\right)$ is the Hamming distance between modulated symbols χ and $\tilde{\chi}$, $P(\chi \to \tilde{\chi}, n_t)$ denotes the pairwise error probability (PEP) that the transmitted symbol χ is detected as $\tilde{\chi}$ when antenna n_t is used to transmit. In (3.15) and (3.16), $\underset{\text{Signal}}{\text{ABER}}$ is determined by the digital modulation scheme. For example, if M-PSK modulation scheme is used, (3.16) is given as [26], [115]

$$\underset{\text{MOD}}{\text{APEB}}(n_t) = \frac{1}{\log_2(M)}\sum_{l=1}^{M-1}\left[\left(2\left|\frac{l}{M} - \left\lfloor\frac{l}{M}\right\rfloor\right| + 2\sum_{k=2}^{\log_2(M)}\left|\frac{l}{2^k} - \left\lfloor\frac{l}{2^k}\right\rfloor\right|\right)\right]P_l(n_t), \tag{3.17}$$

where:

$$P_l(n_t) = \frac{1}{2\pi}\int_0^{\pi[1-(2l-1)/M]}T_l^-(\theta, n_t)d\theta - \frac{1}{2\pi}\int_0^{\pi[1-(2l+1)/M]}T_l^+(\theta, n_t)d\theta, \tag{3.18}$$

and:

$$\begin{aligned} T_l^-(\theta, n_t) &= M_r(2\gamma\frac{\sin^2\left[\pi(2l-1)/M\right]}{\sin^2\theta}) \\ T_l^+(\theta, n_t) &= M_r(2\gamma\frac{\sin^2\left[\pi(2l+1)/M\right]}{\sin^2\theta}) \end{aligned}. \tag{3.19}$$

In (3.19), γ is the signal-to-noise ratio (SNR), which can be defined as $\gamma = \frac{E_m}{N}$, where E_m is the transmit power and N is the noise power. $M_r(.)$ is the moment generation function (MGF) of $\sum_{n_r=1}^{N_R}\|h_{n_t,n_r}e\|^2$, where $e = \chi - \tilde{\chi}$. The close form expression of

$M_r(.)$ is

$$M_r(s) = \prod_{i=1}^{N_R} (1 - s\lambda_i e)^{-1}. \tag{3.20}$$

In (3.20), λ_i is the eigenvalue of Rx correlation indicator matrix R_{Rx}. Similarly, we can define R_{Tx} as the correlation indicator matrix of Tx. Considering the this GBSM channel model and referring [118], these two matrices are expressed as

$$\begin{aligned} R_{Tx}(p, \tilde{p}) &= \rho_{h_{q,p} h_{q,\tilde{p}}}(0) \\ R_{Rx}(q, \tilde{q}) &= \rho_{h_{q,p} h_{\tilde{q},p}}(0) \end{aligned}, \tag{3.21}$$

where $\rho_{h_{q,p} h_{q,\tilde{p}}}(.)$ is the STCF of the V2V channel model, which indicates the correlation between $h_{q,p}$ and $h_{q,\tilde{p}}$. As an ideal channel estimation is assumed at Rx side, $\tau = 0$.

For the case that error only occurs in the spatial modulation part, which is expressed as $\underset{\text{Spatial}}{\text{ABER}}$ previously, we can refer to related investigations on space shift keying (SSK) systems, [27], [28]. This part can be expressed as

$$\underset{\text{Spatial}}{\text{ABER}} = \frac{1}{M} \frac{\log_2(N_t)}{m} \sum_{l=1}^{M} \underset{\text{SSK}}{\text{APEB}}(l). \tag{3.22}$$

$\underset{\text{SSK}}{\text{APEB}}$ can be further expressed as

$$\underset{\text{SSK}}{\text{APEB}}(l) = \frac{1}{N_t} \frac{1}{\log_2(N_t)} \times \sum_{n_t=1}^{N_t} \sum_{\tilde{n}_t=1}^{N_t} \left[N_H \left(n_t \to \tilde{n}_t \right) P(\kappa_l, n_t \to \tilde{n}_t) \right], \tag{3.23}$$

where $N_H \left(n_t \to \tilde{n}_t \right)$ is the Hamming distance between the antenna indices n_t and $\tilde{n}_t$, $P(\kappa_l, n_t \to \tilde{n}_t)$ is the PEP that the active antenna $\tilde{n}_t$ is detected given that n_t was transmitted with the modulation modulus κ_l. Referring to the ML detector algorithm in [24], this error can only occurs when $\|y - h_{n_t,n_r}\kappa_l\|^2 > \|y - h_{\tilde{n}_t,n_r}\kappa_l\|^2$. Thus, $P(\kappa_l, n_t \to \tilde{n}_t)$ can be written as

$$\begin{aligned} P(\kappa_l, n_t \to \tilde{n}_t) &= P(\|y - h_{n_t,n_r}\kappa_l\|^2 > \|y - h_{\tilde{n}_t,n_r}\kappa_l\|^2) \\ &= Q(\gamma \|h_{n_t,n_r}\kappa_l - h_{n_t,n_r}\kappa_l\|^2), \end{aligned} \tag{3.24}$$

where $Q(.)$ is the Q-function. Based on the alternative integral expression of Q-function and MGF-based approach [115], [116], (3.24) can be written as

$$P(\kappa_l, n_t \to \tilde{n}_t) = \frac{1}{\pi}\int_0^{\pi/2} M_{n_t,\tilde{n}_t}(\gamma\frac{\kappa_l^2}{2\sin^2\theta})d\theta. \tag{3.25}$$

In (3.25), $M_{n_t,\tilde{n}_t}(.)$ is the MGF of $\sum_{n_r=1}^{N_R}\|h_{n_t,n_r} - h_{\tilde{n}_t,n_r}\|^2$, which can be expressed as:

$$M_{n_t,\tilde{n}_t}(s) = \prod_{j=1}^{N_T}\prod_{i=1}^{N_R}(1 - s\lambda_i u_j)^{-1}, \tag{3.26}$$

where u_j is the eigenvalue of receivers correlation indicator matrix R_{Tx}. If constant modulus modulation schemes such as M-PSK are used, κ_l is a constant value as κ and (3.22) can be simplified as

$$\underset{\text{Spatial}}{\text{ABER}} = \frac{1}{N_t m}\sum_{n_t=1}^{N_t}\sum_{\tilde{n}_t=1}^{N_t}\left[N_H\left(n_t \to \tilde{n}_t\right) \times \frac{1}{\pi}\int_0^{\pi/2} M_{n_t,\tilde{n}}(\gamma\frac{k^2}{2\sin^2\theta})d\theta\right]. \tag{3.27}$$

For the third case, $\underset{\text{Joint}}{\text{ABER}}$, both digital modulation and spatial modulation parts are incorrect. It can be expressed as:

$$\underset{\text{Joint}}{\text{ABER}} = \frac{1}{N_t m}\sum_{n_t=1}^{N_t}\sum_{\tilde{n}_t\neq n_t=1}^{N_t}\left[N_H\left(n_t,\chi \to \tilde{n}_t,\tilde{\chi}\right) \times P\left(n_t,\chi \to \tilde{n}_t,\tilde{\chi}\right)\right], \tag{3.28}$$

where $N_H\left((n_t,\chi) \to (\tilde{n}_t,\tilde{\chi})\right)$ is the Hamming distance for the error case that symbol χ transmitted by antenna n_t is detected as $\tilde{\chi}$ sent by antenna $\tilde{n}_t$ and $P\left((n_t,\chi) \to (\tilde{n}_t,\tilde{\chi})\right)$ is the corresponding PEP. Similar to the case of $\underset{\text{Spatial}}{\text{ABER}}$, it can be expressed as:

$$\begin{aligned} P\left((n_t,\chi)\to(\tilde{n}_t,\tilde{\chi})\right) &= P(\|y - h_{n_t,n_r}\chi\|^2 > \|y - h_{\tilde{n}_t,n_r}\tilde{\chi}\|^2) \\ &= Q(\gamma\|h_{n_t,n_r}\chi - h_{\tilde{n}_t,n_r}\tilde{\chi}\|^2). \end{aligned} \tag{3.29}$$

Using the MGF-based approach, (3.29) can be represented as

$$P\left((n_t,\chi) \to (\tilde{n}_t,\tilde{\chi})\right) = \frac{1}{\pi}\int_0^{\frac{\pi}{2}} M_{n_t\chi,\tilde{n}_t\tilde{\chi}}(\frac{\gamma}{2\sin^2\theta})d\theta. \tag{3.30}$$

In (3.30), $M_{n_t\chi,\tilde{n}_t\tilde{\chi}}(.)$ is the MGF of $\sum_{n_r=1}^{N_r} |h_{n_t,n_r}\chi - h_{\tilde{n}_t,n_r}\tilde{\chi}|^2$, with the expression of

$$M_{n_t\chi,\tilde{n}_t\tilde{\chi}}(s) = \prod_{j=1}^{N_T}\prod_{i=1}^{N_R}(1 - s\lambda_i e u_j)^{-1}. \tag{3.31}$$

3.4 Simulation Results and Discussions

In this section, different simulation results are presented to evaluate the performance of SM systems under the 3D V2V channel model. Based on the reported measurement results in [119], following key parameters are used to obtain these simulation results: the carrier frequency is setted as $f_c = 5.9$ GHz, the speed of two cars are assumed to be $v = 110$ km/h, and the corresponding maximum Doppler shifts are defined as $f_{Tmax} = f_{Rmax} = 570$ Hz, the distance between Tx and Rx is setted as $D = 300$ m. In the simulation, two cars are assumed to move toward each other, thus the moving direction angles $\gamma_T = \gamma_R = 0°$, and the space between two antenna elements is configured as 0.5λ.

TABLE 3.2: Key parameters of different VTD scenarios.

	K	η_{SB_1}	η_{SB_2}	η_{SB_3}	η_{DB}	$k^{(1)}$	$k^{(2)}$	$k^{(3)}$
Low VTD	3.786	0.335	0.203	0.411	0.051	9.6	3.6	11.5
High VTD	0.156	0.126	0.126	0.063	0.685	0.6	1.3	11.5

For different VTD scenarios, corresponding parameters are used, especially the K factor, which is configured as 3.786 and 0.756 for low and high VTD scenario respectively. Rest parameters can be found in Table 3.2. All simulation results are obtained through Monte Carlo simulation, for each point in following figures, results of 10 runs (each run transmits 100000 symbols) are averaged to get the final value.

3.4.1 Theoretical BER Results Vs. Simulation Results

The theoretical result in this work is the upper bound of the ABER, which Indicates the maximum value of the ABER, in principle theoretical results should be higher

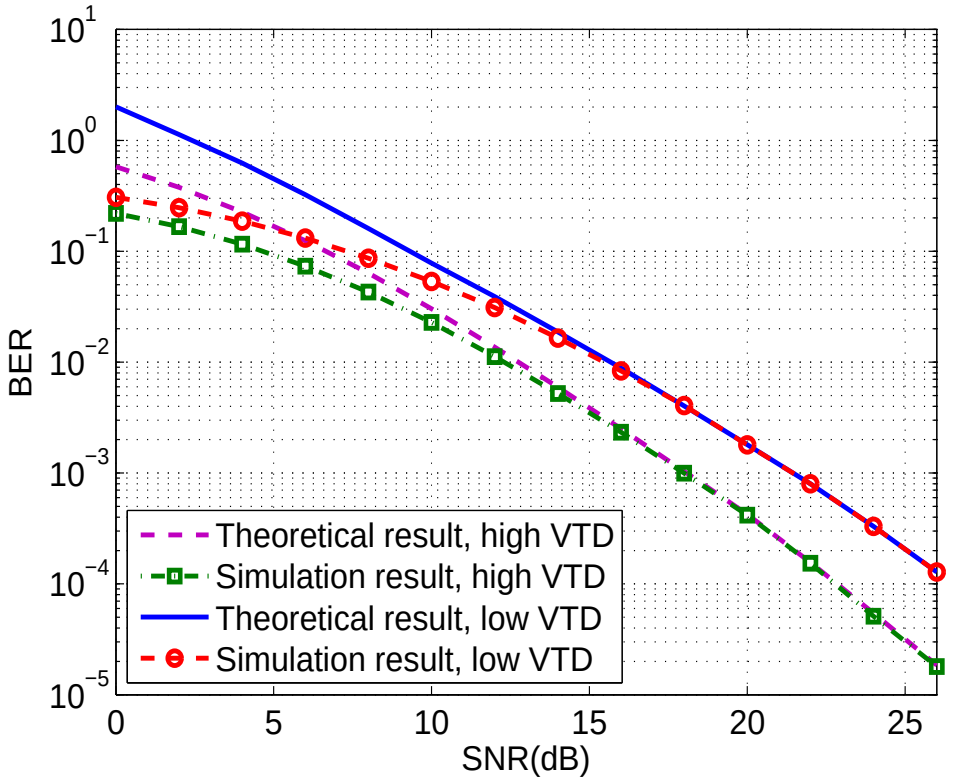

FIGURE 3.5: Theoretical and simulated BER results of SM systems under the 3D V2V MIMO channel model.

than the simulation results at the low SNR range as theoretical results considered all error cases. While at the high SNR range, these two results should match with each other.

In Fig. 3.5, theoretical results of ABER for SM systems under the 3D V2V channel model of different VTD scenarios are compared with simulation results. This figure exactly follows our observation. An excellent approximation of the theoretical derivation with simulation results can be found, especially in the high SNR range where SNR $\geq$ 15 dB. The theoretical ABER upper-bound offers a reasonable accuracy, which indicates the correctness of the theoretical derivation.

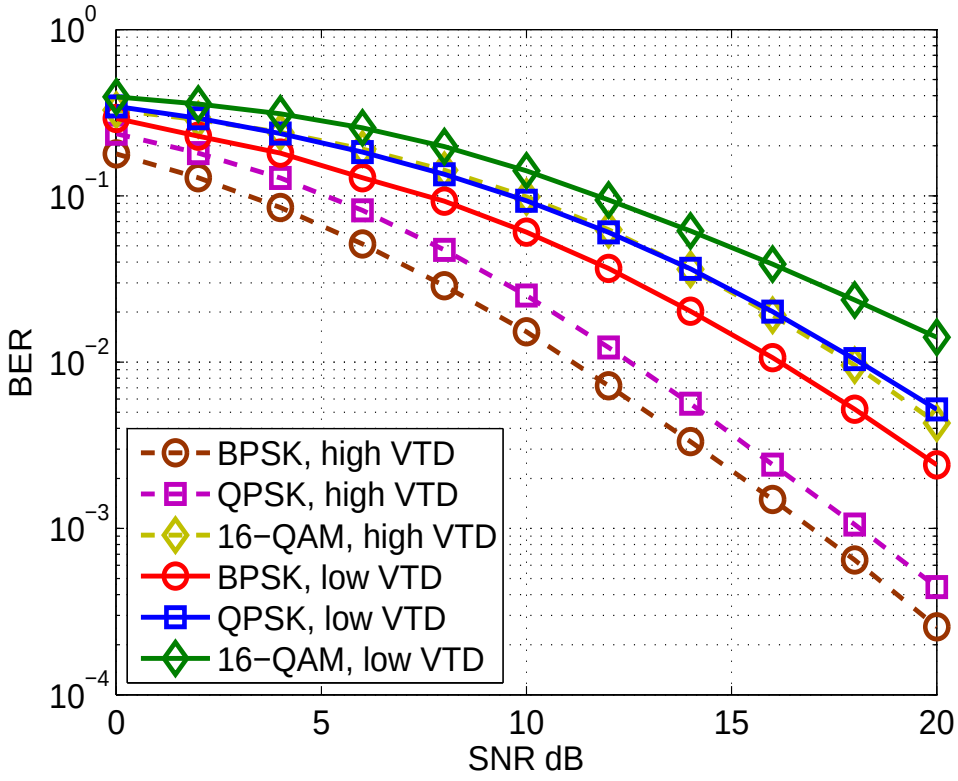

FIGURE 3.6: BER performance of SM systems under the 3D V2V channel model with different modulation schemes and VTD settings.

3.4.2 BER Performance of SM Systems Under Different VTD Scenarios and Modulation Schemes

In Fig. 3.6, we investigate the performance of SM systems under the 3D channel model with different modulation schemes under both high and low VTD scenarios. From simulation results, we can find that under both VTD scenarios, the higher order modulation scheme will result in the poorer BER performance due to the lower energy allocated to each bit.

In addition, it is noted that when using the same modulation scheme, the SM system has better performance under the high VTD scenario. This phenomenon can be explained through Fig. 3.3, where the STCF of the 3D V2V channel model with different VTD assumptions can be found. It can be observed that under the high VTD scenario, the correlation between sub-channels is much lower than the low VTD scenario. That is because the 3D V2V channel model is a Rician style channel model

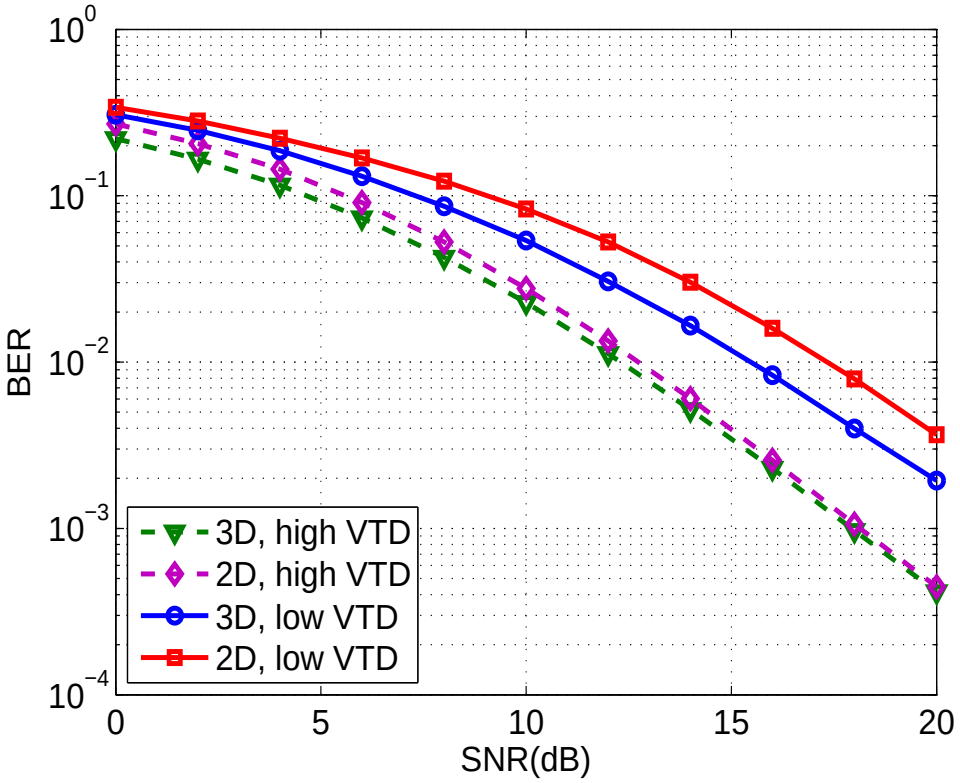

FIGURE 3.7: BER performance of SM systems under the 3D and 2D V2V MIMO channel models with different VTD settings.

and its K factor is determined by the VTD scenario. Higher K factor values correspond to the case of stronger LoS component. Considering the detailed expression of the channel model and the expression of STCF, it can be observed that higher K factor leads to higher correlation among sub-channels. With strong LoS components, it is hard for the receiver to detect which antenna was used to transmit data. Thus, it will result in poor BER performance. This viewpoint was also noted in [27], where the performance of the SSK system under the Rician fading channel is investigated. It is shown that the higher K factor will result in the worse performance of the SSK system.

3.4.3 BER Performance of SM Under 2D and 3D Channel Models

In Fig. 3.7, the performance of SM systems over the 3D and 2D V2V channel models with the same system setting are compared. It is shown that when using the same system configuration and under the same VTD scenario, the SM system has better performance under the 3D channel model.

That is because the 3D channel has lower similarity of sub-channels as compared to 2D channel, and as such lower correlation. This observation is supported also by Fig. 3.3, which shows that the correlation between sub-channels of 3D channel models is always lower than the 2D model for both high VTD and low VTD scenarios.

3.4.4 BER Performance of SM Under the 3D V2V Channel Model with Different Doppler Frequencies

In Fig. 3.8, we investigated the performance of SM systems with different Doppler frequencies under both high and low VTD scenarios. Firstly, it is noticed that the higher Doppler frequency will result in the poorer BER performance.

This phenomenon can be explained through Fig. 3.4, where the STCF of the channel model is shown. It can be observed that higher Doppler frequency will result in faster fading speed, which will reduce the probability that the strength of signals maintains a reasonable level. This problem is known as the signal outages probability problem. Again, from Fig. 3.8, it is found that the SM system has better performance under the high VTD scenario.

3.4.5 Comparison Between SM and Other MIMO Technologies Under the 3D V2V Channel Model

The spatial multiplexing and spatial diversity have widely been used in 4G wireless communication systems [6]. As these two MIMO schemes have achieved great success

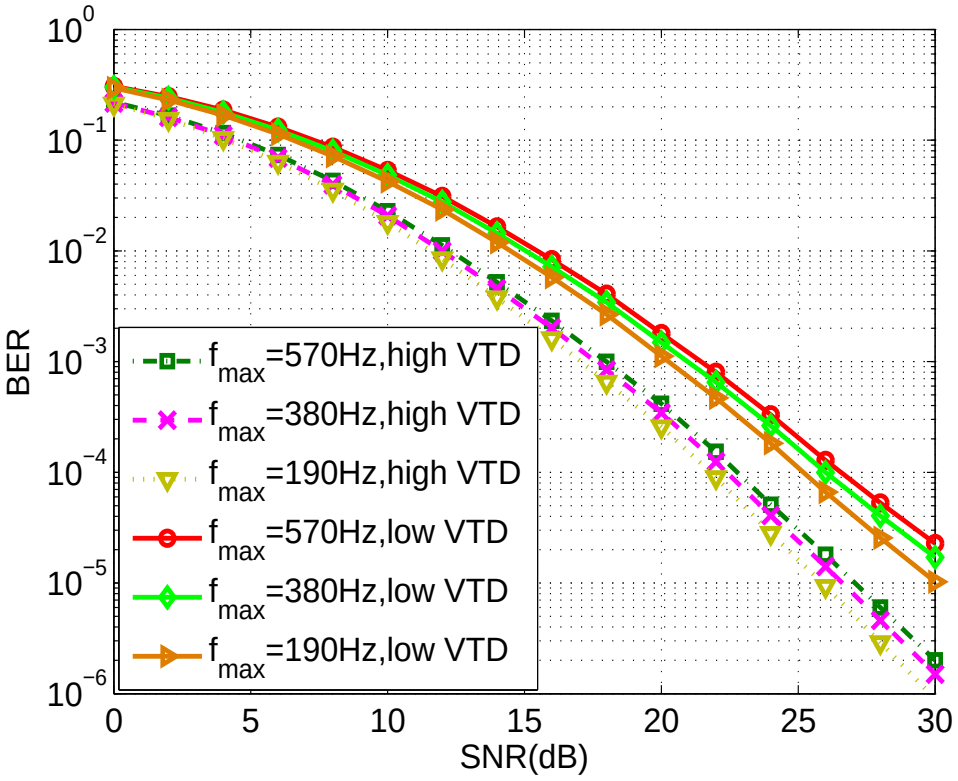

FIGURE 3.8: BER performance of SM systems under the 3D V2V MIMO channel models with different Doppler frequency and VTD scenarios, a 2×2 system using QPSK modulation scheme..

in real use and therefore they are suitable benchmarks to be compared with other MIMO technologies in terms of system performance. In this work, two typical spatial multiplexing and spatial diversity technologies, the V-BLAST and the Alamouti scheme, are employed to evaluate the performance SM system under the 3D V2V channel model . In Figs. 3.9–3.12, simulation results are proposed.

In this work, besides different VTD scenarios, different spectral efficiency values and systems settings are also considered. It is necessary to note that for the V-BLAST and the Alamouti systems, the ML are also employed as the receiver algorithm for fair comparison.

From Figs. 3.9 and 3.10, it is observed that for 4 bits/symbol spectral efficiency and under high VTD scenario, the SM system using the 4×4 antenna setting obtains the best performances among all systems, especially within the range of SNR $\geq$ 15 dB.

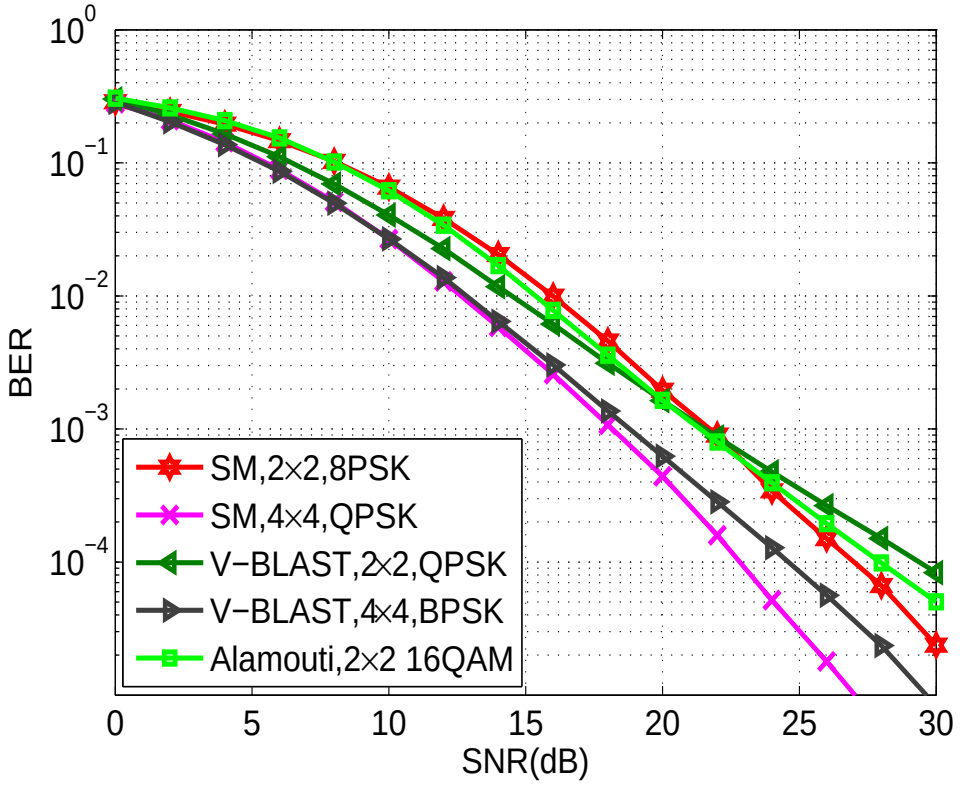

FIGURE 3.9: BER performance of three different MIMO technologies under the 3D V2V MIMO channel model for the high VTD scenario, with the spectral efficiency of 4 bits/symbol.

Further investigate, the V-BLAST system can obtain the similar performance within the range of SNR $\leq$ 15 dB. Even using the higher order modulation scheme, the Alamouti scheme can still indicate good performance within the high SNR range (SNR$\geq$ 14 dB) as a result of diversity gain. When under the low VTD scenario, the Alamouti scheme shows significant performance enhancement due to the strong LoS component while both SM and V-BLAST suffer form the high correlation among sub-channels. However, compared with the V-BLAST system, the SM system demonstrates a 3 dB enhancement at the BER around 10^{-3}.

In Figs. 3.11 and 3.12, similar comparisons are carried out with the spectral efficiency of 8 bits/symbol. Under both scenario, the Alamouti scheme shows the worst performance due to using higher order modulation scheme. The V-BLAST system can obtain similar or even better performance as the SM system within the range of SNR$<$ 14 dB, but the SM system is superior at high SNR range. However when we

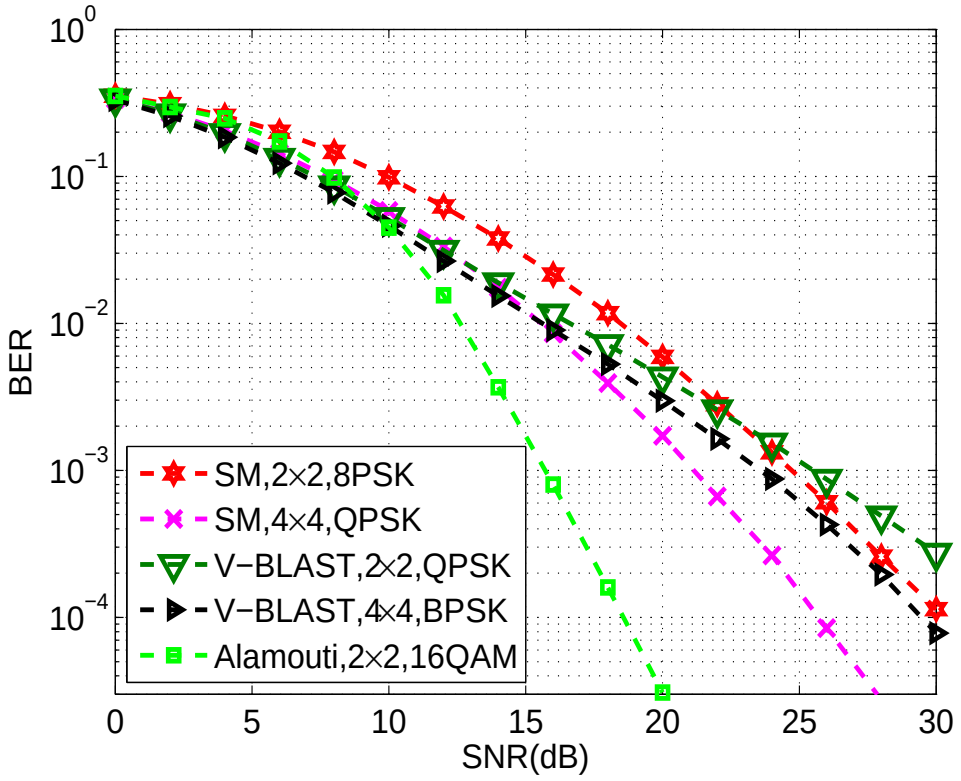

FIGURE 3.10: BER performance of three different MIMO technologies under the 3D V2V MIMO channel model for the low VTD scenario, with the spectral efficiency of 4 bits/symbol.

use the ML receiver algorithm, the system complexity of V-BLAST is much higher than SM.

3.5 Summary

In this chapter, we have investigated the performance of SM systems under a 3D V2V channel model with different system settings and VTD scenarios. Numerical and simulation results have shown that lower order modulation schemes can lead to better BER performance due to the higher energy per bit. When using the same modulation scheme, the SM system has better performance under the high VTD scenario than the low VTD scenario due to the lower correlation between sub-channels caused by weaker LoS components. Besides, higher Doppler effect can result in worse BER performance due to higher outage probability. Additionally, compared with 2D models,

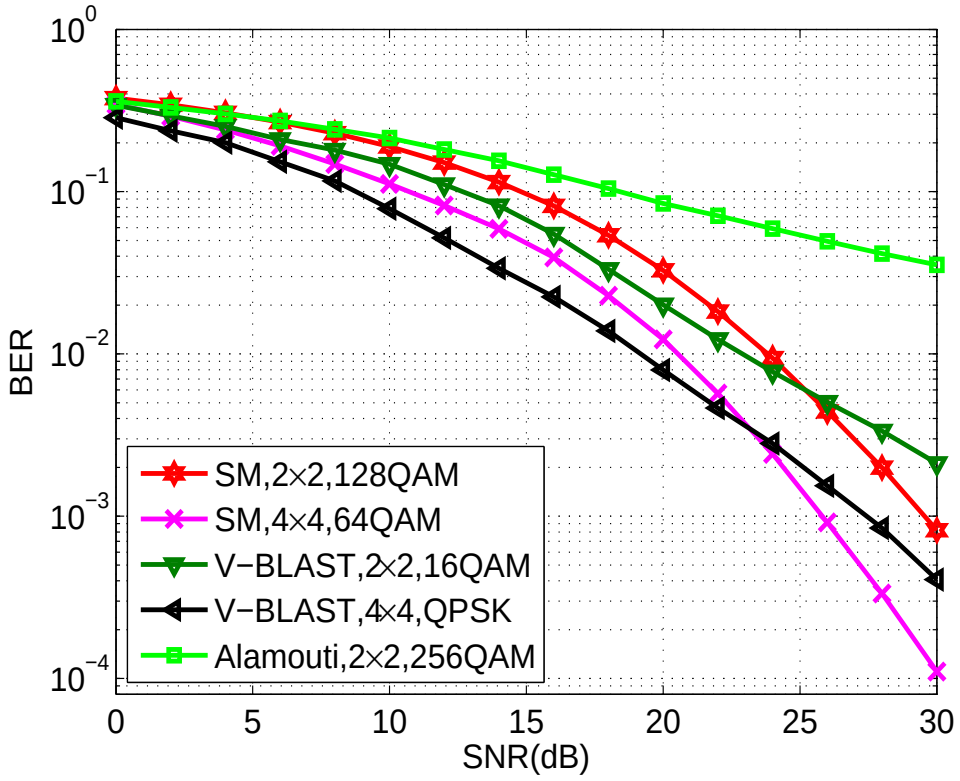

FIGURE 3.11: BER performance of three different MIMO technologies under the 3D V2V MIMO channel model for the high VTD scenario, with the spectral efficiency of 8 bits/symbol.

SM systems can obtain better BER performance under 3D models due to the extended vertical dimension which results in lower correlation of sub-channels. When compared with other MIMO technologies such as the V-BLAST and the Alamouti scheme, SM systems can yield relative good performance under the 3D V2V channel model considering its spectral efficiency and system complexity. From above mentioned simulation results, the advantage of SM can be declared. SM can offer higher reliability under the harsh high VTD scenario. Also, it is a better option for communication systems requiring high spectral efficiency.

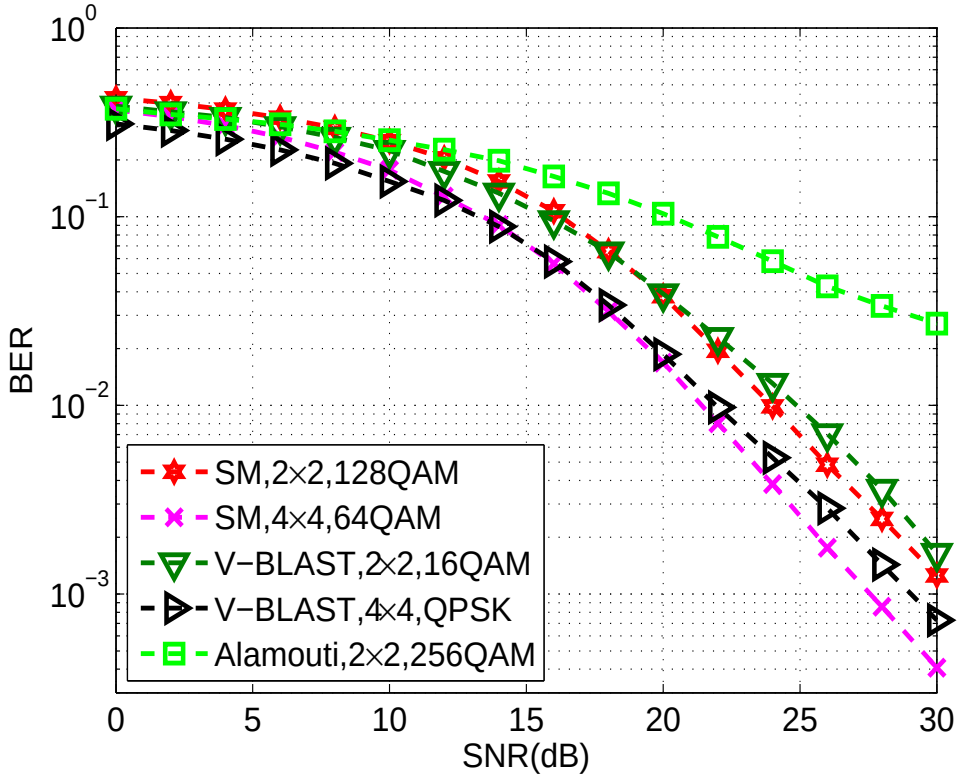

FIGURE 3.12: BER performance of three different MIMO technologies under the 3D V2V MIMO channel model for the low VTD scenario, with the spectral efficiency of 8 bits/symbol.

Chapter 4

Performance Investigation of Spatial Modulation Systems Under Non-Stationary Wideband High-Speed Train Channel Models

4.1 Introduction

In recent years, HST systems with the operating speed of more than 250 km/h have obtained significant developments. It is reported that the maximum speed of HSTs can easily reach 500 km/h within the next decade, and the passenger number will be explosively increased [120].

With the large volume of passengers, there is a great demand for high data rate and reliable wireless communication services [121]. However, the existed wireless communication systems (include 4G system) can only support the movement speed up to 350 km/h. Thus, reliable wireless communication services for future HST systems have been considered as an important issue for 5G wireless communication systems [9].

Compared with conventional communication systems, the HST wireless communication system suffers more challenges. For example, as the speed of HST systems can easily reach over 250 km/h, more serious Doppler shift will occur. Besides, the handover will happen more frequently, which will result in the higher probability of handover failure and connection lost. Also, as cabins of HST are usually built with metal like aluminium, there will be huge penetration losses when signal gets into carriages [122].

In order to solve these problems, many new cellular architectures such as distributed antenna system (DAS) [123], [124] and mobile relay station (MRS) [125], [126] (or mobile Femtocell [9], [127]) were investigated. In our work, the MRS solution is assumed, and its multiple receive antennas are distributed on the surface of HST carriages. Signals will be passed to transmit antennas of MRS within carriages through cables in order to avoid huge penetration losses. MSs will communicate with the MRS rather than with BSs directly, which can significantly improve the link quality.

Besides new cellular architectures, novel physical layer transmit technologies will also be used to improve the service quality of HST wireless communication systems. Among various technologies, spatial modulation [22] has attracted lots of research interests in recent years due to its outstanding performance in enhancing the system performance such as system robustness and spectral-energy efficiency. Besides, the system complexity on SM systems can be controlled under a reasonable level benefit form it uses single RF chain [22], [24].

The BER performance of SM, so far, has only been investigated for some simple F2M channels such as Rayleigh, Rician, and Nakagami channels [22], [24]–[26], and in V2V channel models in [87], [114]. However these channel models [22], [24]–[26], [114] were all narrowband channels and under the WSS assumption. Therefore, the influence of inter-symbol-interference (ISI) and time-varying channels on the BER performance of SM systems cannot be investigated. To the best of the author's knowledge, there is no relevant study on the performance of SM systems under realistic non-stationary wideband HST MIMO channel models. In order to fill this research gap, this work will investigate the BER performance of SM using the novel non-stationary wideband HST

MIMO channel model proposed in [97], with the assumption of channel estimation error. To be closer to the real environment, this channel model will be configured using time-varying parameters form measurement results reported in [90]. The impact of estimation delay and Doppler frequency on the BER performance will be studied both theoretically and by simulation.

In the following, we highlight main contributions and novelties of this work.

1. We investigate the BER performance of SM systems under a HST non-stationary wideband channel model. The non-ideal channel estimation case is considered. An accurate theoretical BER expression is derived to compared with all simulation results. BER simulation results are comprehensively analysed together with the investigation of STCF. The link between the BER performance and the STCF has been established.

2. We propose a new statistical property: stationary interval in terms of STCF, and investigate the BER performance of SM systems in terms of this property. The aim to propose this statistical property is to accurately and straightforward describe the non-stationary behaviour of the HST channel model, especially to find the time interval within which the channel can be treated as relatively stationary. Since the STCF directly affect the BER performance of SM systems, in this work, the STCF will be used as the object to obtain the stationary interval.

The remainder of the chapter will be organised as follows. In Section 4.2, the wideband HST channel model and related important statistical properties including the novel non-stationary statistic property are described. The theoretical expression of the ABER for SM under the non-stationary HST wideband channel is derived in Section 4.3. In Section 4.4, simulation results are presented and analysed. Finally, conclusions are drawn in Section 4.5.

4.2 The Non-stationary Wideband HST Channel Model

For HST wireless communication systems, in general, their channel environments can be classified in to following scenarios: open space, cutting, tunnels and viaduct. Among all scenarios, the open space is the most common one. In this scenario, the train is usually moving at a very high speed. Antennas of the BS are located at a much higher position than the surroundings, thus there is LoS component in the channel.

In this work, the HST system is assumed working at an open space environment and use MRS to improve the wireless service quality, thus the wireless communication link between MSs and the BS will be divided into two parts: BS to MRS and MRS to mobile devices. Correspondingly, there are two types of wireless channels existing, the outdoor channel between BS and MRS and indoor channel between MRS and mobile devices which are illustrated in Fig. 4.1. The indoor channel is similar to the conventional indoor scenario, which has already been widely investigated. In this work, only the outdoor channel will be considered.

In this channel model, it is assumed a MIMO HST system equipped with S transmit and U receive omni-directional antenna elements. The BS is located on the track-side where a minimum distance between the BS and the track denoted as $D_{\min} = 50$ m [92] is considered. The time-varying distance between the BS and MRS is defined as $D_s(t) = \sqrt{(D_{min}^2 + D^2(t))}$, where $D(t)$ stands for the projection of $D_s(t)$ on the railway track plane. Fig. 4.2 illustrates the abstracted multiple-confocal-ellipses GBSM. These ellipses represent multiple taps of the channel model. For different taps, corresponding propagation cases are considered, includes direct links represented by LoS components, and single reflected signals represented as single-bounced rays. In this work, a 2×2 MIMO channel model are used in Fig. 4.2 as an example. The parameters in Fig. 3 are defined in Table I.

Let us assume there are N_i effective scatterers on the ith ellipse (means the ith tap,), where $i = 1, 2, ..., I$ and I is the total number or taps. Let $a_i(t)$ and $s^{(n_i)}$ denote the semi-major axis of the ith ellipse and the n_ith $(n_i = 1, ..., N_i)$ effective scatterer

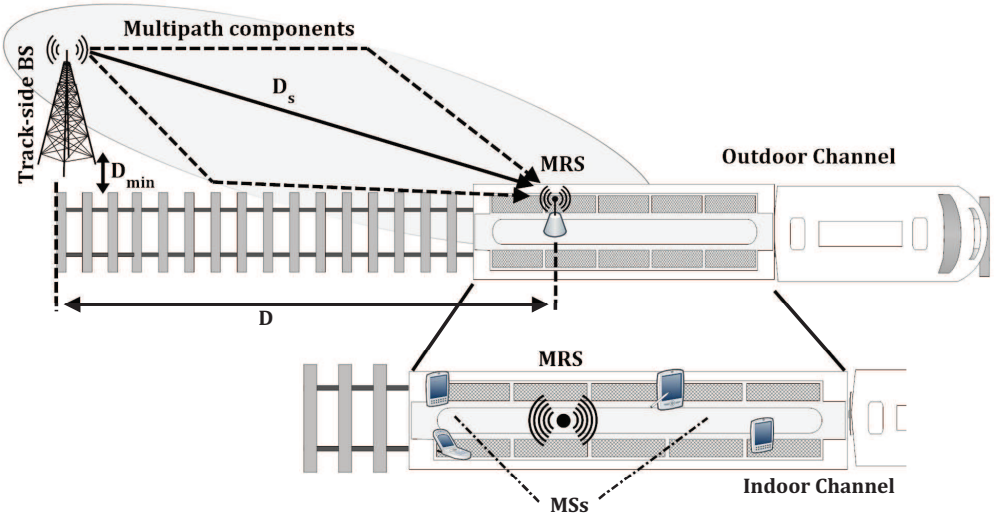

FIGURE 4.1: A HST communication system deploying MRSs [112].

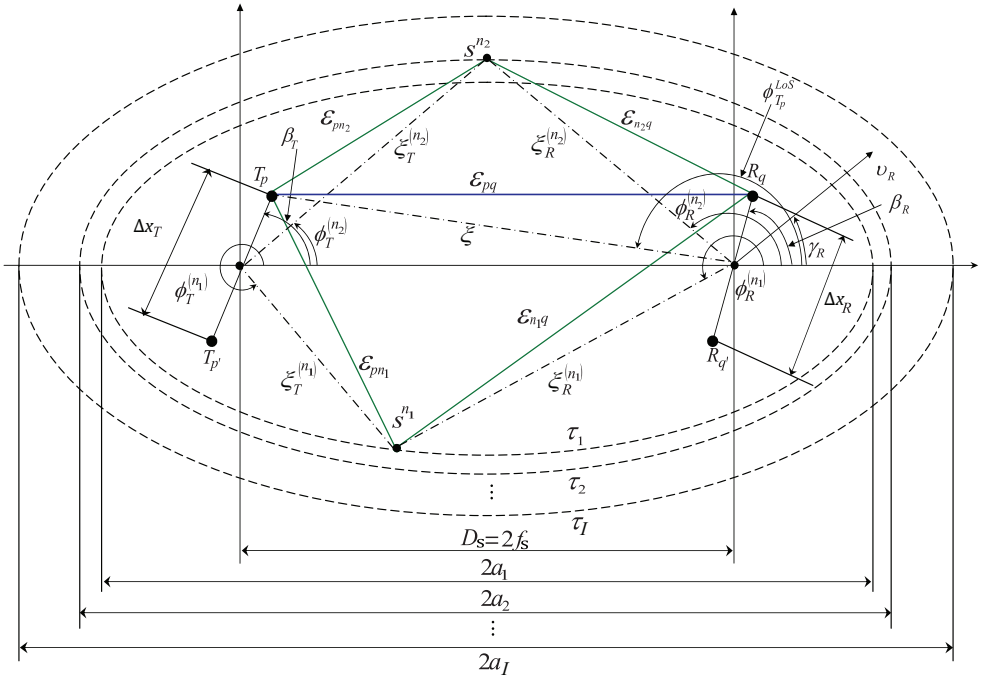

FIGURE 4.2: The GBSM for a wideband MIMO HST channel [112].

TABLE 4.1: Definition of parameters in Fig. 3 [112].

Parameters	**Definition**
$D_s(t)$	distance between the BS and MRS
$f_s(t)$	half length of the distance between the two foci of ellipses
$a_i(t)$, $b_i(t)$	semi-major axis and semi-minor axis of the ith ellipse, respectively
υ_R, γ_R	MRS speed and angle of motion, respectively
Δx_T, Δx_R	antenna element spacings of the BS and MRS
β_T, β_R	tilt angles of the BS and MRS antenna arrays in the x-y plane (relative to the x-axis)
$\phi_{T_p}^{\mathrm{LoS}}(t)$, $\phi_R^{(n_i)}(t)$	AoA of the LoS path and AoA of the wave travelling from an effective scatterer $s^{(n_i)}$
$\phi_T^{(n_i)}(t)$	AoD of the wave that impinges on the effective scatterer $s^{(n_i)}$
ξ, $\xi_T^{(n_i)}(t)$, and $\xi_R^{(n_i)}(t)$	distances $d(T_p, \mathrm{MRS})$, $d\left(\mathrm{BS}, s^{(n_i)}\right)$, and $d\left(s^{(n_i)}, \mathrm{MRS}\right)$
ε_{pq}, ε_{pn_i}, ε_{n_iq}	distances $d(T_p, R_q)$, $d\left(T_p, s^{(n_i)}\right)$, and $d\left(s^{(n_i)}, R_q\right)$, respectively

respectively. Based on the geometric relationship, the time-varying semi-minor axis of the ith ellipse can be expressed as $b_i(t) = \sqrt{a_i^2(t) - f_s^2(t)}$, where $f_s(t) = D_s(t)/2$ means the half distance between the two foci of ellipses. The tilt angles of the BS and MRS antenna arrays are represented by β_T and β_R, respectively. The MRS is assumed to move with the speed of υ_R in the direction determined by the angle of motion γ_R. The AoA of the wave travelling from an effective scatterer $s^{(n_i)}$ to the MRS is denoted by $\phi_R^{(n_i)}(t)$. The AoD of the wave that reflected through the effective scatterer $s^{(n_i)}$ is denoted by $\phi_T^{(n_i)}(t)$, while $\phi_{T_p}^{\mathrm{LoS}}(t)$ is the AoA of a LoS path.

The complex space-time-variant channel impulse response represents the link between the pth $(p = 1, ..., S)$ element of the Tx, T_p, and the qth $(q = 1, ..., U)$ element of the Rx, R_q, can be expressed as $h_{pq}(t, \tau) = \sum_{i=1}^{I} h_{i,pq}(t)\,\delta(\tau - \tau_i)$, where $h_{i,pq}(t)$ and τ_i are the complex space-time-variant coefficients and the propagation delay of the ith tap, respectively. From the assumption of the above GBSM, only the complex coefficients for the first tap (i=1) of the $T_p - R_q$ link contains the LoS component and SB components, which can be expressed as the superposition of $h_{pq}(t, \tau)$ and $h_{1,pq}(t)$

$$h_{1,pq}(t) = h_{1,pq}^{\mathrm{LoS}}(t) + h_{1,pq}^{\mathrm{SB}}(t) \tag{4.1}$$

where

$$h_{1,pq}^{\mathrm{LoS}}(t) = \sqrt{\frac{K_{pq}\Omega_{1,pq}}{K_{pq}+1}} e^{-j2\pi f_c \tau_{pq}(t)} e^{j2\pi f_{\max} t \cos\left(\phi_{T_p}^{\mathrm{LoS}}(t) - \gamma_R\right)} \tag{4.2a}$$

$$h_{1,pq}^{\mathrm{SB}}(t) = \sqrt{\frac{\Omega_{1,pq}}{K_{pq}+1}} \lim_{N_1\to\infty} \sum_{n_1=1}^{N_1} \frac{1}{\sqrt{N_1}} e^{j\left(\psi_{n_1} - 2\pi f_c \tau_{pq,n_1}(t)\right)} \times e^{j2\pi f_{\max} t \cos\left(\phi_R^{(n_1)}(t) - \gamma_R\right)}. \tag{4.2b}$$

For other taps ($1 < i \leq I$), their complex tap coefficients of the link of $T_p - R_q$, contains only SB component, which can be expressed as

$$h_{i,pq}(t) = h_{i,pq}^{\mathrm{SB}}(t) = \sqrt{\Omega_{i,pq}} \lim_{N_i\to\infty} \sum_{n_i=1}^{N_i} \frac{1}{\sqrt{N_i}} \times e^{j\left(\psi_{n_i} - 2\pi f_c \tau_{pq,n_i}(t)\right)} e^{j2\pi f_{\max} t \cos\left(\phi_R^{(n_i)}(t) - \gamma_R\right)}, 1 < i \leq I. \tag{4.3}$$

This channel model is designed to represent the non-stationary behaviour of HST scenarios. Thus in (4.2a), (4.2b), and (4.3), time-varying parameters $\tau_{pq}(t)$, $\phi_{T_p}^{\mathrm{LoS}}(t)$, $\tau_{pq,n_i}(t)$ $(i = 1, ..., I)$, and $\phi_R^{(n_i)}(t)$ are involved, which makes the underlying GBSM shows non-stationary characteristic. In the following part, we will define and calculate these time-varying parameters.

In (4.2a), (4.2b), and (4.3), $\Omega_{i,pq}$ denotes the mean power for the ith tap, $\tau_{pq}(t) = \varepsilon_{pq}(t)/c$, and $\tau_{pq,n_i}(t) = (\varepsilon_{pn_i}(t) + \varepsilon_{n_i q}(t))/c$ are propagation times of the waves travel through the links $T_p - R_q$ and $T_p - s^{(n_i)} - R_q$, respectively, as shown in Fig. 3. Here, c is the speed of light and K_{pq} is the Ricean factor which indicates the ratio of the power of the LoS component over non-LoS components. The phases ψ_{n_1} and ψ_{n_i} are assumed as i.i.d. random variables with uniform distributions over $[-\pi, \pi)$, $f_{\max}$ is the maximum Doppler shift which is related to carrier frequency and the speed of HST. From Fig. 3 and based on the geometric relationship, we can calculate the following distances for different propagation paths as

$$\varepsilon_{pq}(t) \approx D_s(t) - k_p \Delta x_T \cos\beta_T - k_q \Delta x_R \cos(\phi_{T_p}^{\mathrm{LoS}}(t) - \beta_R) \tag{4.4a}$$

$$\varepsilon_{pn_i}(t) \approx \xi_T^{(n_i)}(t) - k_p \Delta x_T \cos\left(\phi_T^{(n_i)}(t) - \beta_T\right) \tag{4.4b}$$

$$\varepsilon_{n_i q}(t) \approx \xi_R^{(n_i)}(t) - k_q \Delta x_R \cos\left(\phi_R^{(n_i)}(t) - \beta_R\right) \tag{4.4c}$$

where $k_p = (S - 2p + 1)/2$, $k_q = (U - 2q + 1)/2$, and $\xi_R^{(n_i)}(t) = b_i^2(t) / \left(a_i(t) + f_s(t)\cos\phi_R^{(n_i)}(t)\right)$

with $\xi_T^{(n_i)}(t) = \Big(a_i^2(t)+f_s^2(t)+2a_i(t)f_s(t)\cos\phi_R^{(n_i)}(t)\Big)/\Big(a_i(t)+f_s(t)\cos\phi_R^{(n_i)}(t)\Big)$. For the LoS component, we can calculate the time-variant AoA $\phi_{T_p}^{\mathrm{LoS}}(t)$ as [91]

$$\phi_{T_p}^{\mathrm{LoS}}(t)=\begin{cases}\phi_{T_p}^{\mathrm{LoS}}(t_0)+\arccos\Big(\frac{D_s(t_0)+v_R t\cos\gamma_R}{D_s(t)}\Big), -\pi\le\gamma_R\le 0\\ \phi_{T_p}^{\mathrm{LoS}}(t_0)-\arccos\Big(\frac{D_s(t_0)+v_R t\cos\gamma_R}{D_s(t)}\Big),\ 0\le\gamma_R\le\pi\end{cases} \tag{4.5}$$

where $\phi_{T_p}^{\mathrm{LoS}}(t_0)=\arcsin\Big(\frac{k_p\Delta x_T}{D_s(t_0)}\sin\beta_T\Big)$ denotes the initial LoS AoA at time $t=t_0$.

For this channel model, the von Mises PDF is employed to describe the distribution of time-varying AoAs for SB components. This PDF is widely used in channel models assumed non-isotropic propagation case,which are expressed as $f(\phi)\triangleq \exp\left[k\cos(\phi-\mu)\right]/[2\pi I_0\left(k\right)]$, where μ is the mean value of angle $\phi\in[-\pi,\pi)$, $I_0(\cdot)$ is the zeroth-order modified Bessel function of the first kind, and k ($k\ge 0$) is a positive real-valued parameter that controls the spread of ϕ.

Based on von Mises distribution, the PDF of the time-varying AoAs can be defined as $f\Big(\phi_R^{(i)}\Big)(t)\triangleq \exp\Big[k_R^{(i)}\cos\Big(\phi_R^{(i)}-\mu_R^{(i)}(t)\Big)\Big]/\Big[2\pi I_0\Big(k_R^{(i)}\Big)\Big]$, where $\mu_R^{(i)}(t)$ is the time-varying mean angular value of the AoAs $\phi_R^{(i)}$, which will determine the time-varying behaviour of AoAs and AoDs. $k_R^{(i)}$ is the parameter that controls the spread of $\phi_R^{(i)}$.

For SB rays, their AoDs $\phi_T^{(n_i)}(t)$ and AoAs $\phi_R^{(n_i)}(t)$ are assumed interdependent in geometry. The relationship between the AoD and AoA for each tap can be expressed as:

$$\sin\phi_T^{(n_i)}(t)=\frac{b_i^2(t)\sin\phi_R^{(n_i)}(t)}{a_i^2(t)+f_s^2(t)+2a_i(t)f_s(t)\cos\phi_R^{(n_i)}(t)} \tag{4.6a}$$

$$\cos\phi_T^{(n_i)}(t)=\frac{2a_i(t)f_s(t)+(a_i^2(t)+f_s^2(t))\cos\phi_R^{(n_i)}(t)}{a_i^2(t)+f_s^2(t)+2a_i(t)f_s(t)\cos\phi_R^{(n_i)}(t)}. \tag{4.6b}$$

Thus, if we have AoA, the corresponding AoD can be calculated from this relationship.

For the theoretical model, the number of scatters are assumed infinite. In a real system, this assumption can not be implemented neither by software nor hardware, thus

corresponding simulation should be generated, which means using suitable parameters computation methods to generate necessary discrete channel parameters. For this channel model, time-varying angles $\phi_T^{(n_i)}(t)$ and $\phi_R^{(n_i)}(t)$ for simulation model will be computed by the modified method of equal areas (MMEA). Detailed information can be obtained from [96]. In Fig. 4.3, the time-varying behaviour of the GBSM is presented, where the MRS is assumed to move with the speed of v_R in the direction defined by the angle of motion γ_R. The distance between the BS and the MRS can be calculated as $D_s(t) = 2f_s(t) = \left(\sqrt{D_s^2(t_0) + (v_R t)^2 + 2D_s(t_0) v_R t \cos\gamma_R}\right)$. The AoAs and the axes of the ellipses is also time-varying which can be calculated based on the geometric relationship. The time-varying function of mean AoA $\mu_R^{(i)}(t)$ can be derived as (4.7).

TABLE 4.2: Power-delay profile of the measurement results in [105].

Scenario	**Tap Number**	**Relative time delay** $[\mu S]$	**Average path gain** $[dB]$
CA	1	0	0
	2	0.5	-12.9
	3	1.2	-15.7
	4	1.6	-18.9
	5	2.0	-20.8
	6	3.1	-19.8
	7	3.5	-21.3
	8	5.6	-20.0
CEA	1	0	0
	2	0.4	-15.2
	3	1.2	-19.7

In order to make our channel model more accurate and realistic, measurement results (power-delay profile) presented in [90] are employed. In [90], based on measurement results, authors further classified the HST channel into 5 sub-scenarios in terms of the relative position of the MRS and the BS. In this work, two typical scenario will be used. The Close Area (CA) scenario, which contains the maximum number of taps, and the Closer Area (CEA) scenario, which involved the time-varying K-factor. For the CA scenario, $D(t) \in (250, 1550]$ m, and $D(t_0) = 800$m is selected as the initial value, $K_{pq} = 5.9$. For the CEA scenario, $D(t) \in (20, 250]$ m (we select $D(t_0) = 135$m as the initial value), K_{pq} is time-varying which depend on D(t), which can be expressed as $K_{pq}(t) = -0.0337D(t) + 23.05$, within the range of $[16.31, 22.376)$. For these two

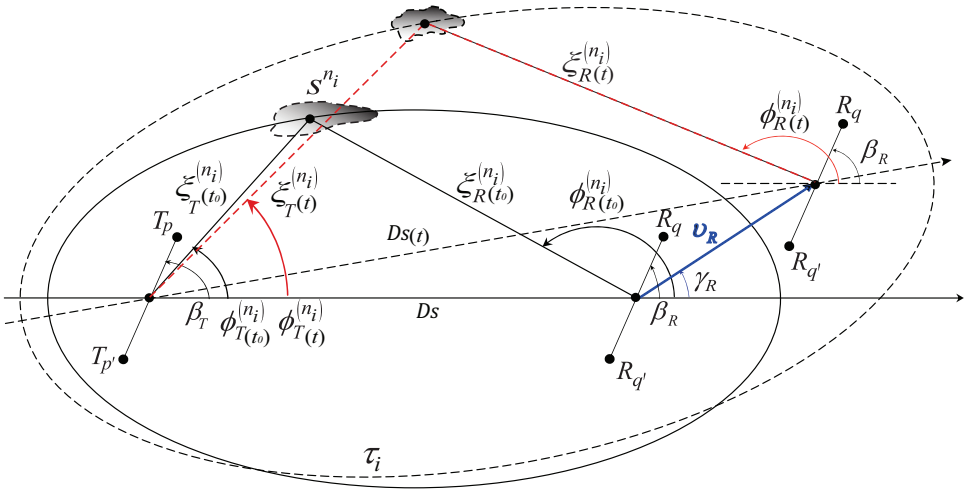

FIGURE 4.3: The time-varying angular parameters in the HST channel model [112].

scenarios, distances between different confocal-ellipses $a_i(t)$ are calculated based on the power-delay profile repetitively.

$$\mu_R^{(i)}(t)=\begin{cases}\gamma_R-\arccos\left(\dfrac{v_R t-\xi_R^{(n_i)}(t_0)\cos\left(\gamma_R-\mu_R^{(i)}(t_0)\right)}{\sqrt{\xi_R^{2\,(n_i)}(t_0)+(v_R t)^2-2\xi_R^{(n_i)}(t_0)v_R t\cos\left(\gamma_R-\mu_R^{i}(t_0)\right)}}\right), & -\pi\leq\gamma_R\leq 0\\ \gamma_R+\arccos\left(\dfrac{v_R t-\xi_R^{(n_i)}(t_0)\cos\left(\gamma_R-\mu_R^{(i)}(t_0)\right)}{\sqrt{\xi_R^{2\,(n_i)}(t_0)+(v_R t)^2-2\xi_R^{(n_i)}(t_0)v_R t\cos\left(\gamma_R-\mu_R^{i}(t_0)\right)}}\right), & 0\leq\gamma_R\leq\pi.\end{cases} \tag{4.7}$$

4.2.1 The Space-Time Correlation Function of the HST Channel Model

There are various statistical properties of the considered channel model. However, in this work, the STCF property is considered as it indicates the spatial correlation among sub-channels, and this correlation has significant impact on the performance of SM systems. The STCF between two arbitrary channel impulse responses $h_{pq}(t,\tau)$ and $h_{p'q'}(t,\tau)$ can be defined as:

$$R_h(t,\Delta x_T,\Delta x_R,\Delta t)=\mathrm{E}\left\{h_{pq}(t)\,h_{p'q'}^{*}(t-\Delta t)\right\} \tag{4.8}$$

For this wideband MIMO HST channel, since it assumes uncorrelated scattering, there is no correlation between the underlying processes in different taps. Thus, the over-all STCF is determined by the correlation properties of $h_{i,pq}(t)$ and $h_{i,p'q'}(t)$ in each tap, and expressed as the superposition of STCF of each taps:

$$R_h(t, \Delta x_T, \Delta x_R, \Delta t) = \sum_{i=1}^{I} \Omega_{i,pq} R_{h_i}(t, \Delta x_T, \Delta x_R, \Delta t) \tag{4.9}$$

For the first tap, as it includes both LoS and SB propagation case, its STCF R_{h_1} should contains both components, which can be expressed as:

$$\begin{aligned} R_{h_1}(t, \Delta x_T, \Delta x_R, \Delta t) = & \\ & \sqrt{\frac{K_{pq} K_{p'q'}}{(K_{pq}+1)(K_{p'q'}+1)}} \; R_h^{\mathrm{LoS}}(t, \Delta x_T, \Delta x_R, \Delta t) \\ & + \sqrt{\frac{1}{(K_{pq}+1)(K_{p'q'}+1)}} \; R_h^{\mathrm{SB}_1}(t, \Delta x_T, \Delta x_R, \Delta t) \end{aligned} \tag{4.10}$$

For rest taps, as it only contains SB components, its STCF $R_{h_i}(i = 2...I)$ is only determined by the STCF of SB component which can be expressed as:

$$R_{h_i}(t, \Delta x_T, \Delta x_R, \Delta t) = R_h^{\mathrm{SB}_i}(t, \Delta x_T, \Delta x_R, \Delta t), (i = 2...I). \tag{4.11}$$

– In the case of the LoS component,

$$R_h^{\mathrm{LoS}}(t, \Delta x_T, \Delta x_R, \Delta t) = e^{j2\pi\left[P\cos\beta_T - Q\cos\left(\phi_{T_p}^{\mathrm{LoS}}(t) - \beta_R\right)\right]} \times e^{j2\pi f_{\max}\cos\left(\phi_{T_p}^{\mathrm{LoS}}(t-\Delta t) - \gamma_R\right)\Delta t} \tag{4.12}$$

where $P = (p' - p)\,\Delta x_T/\lambda$, $Q = (q' - q)\,\Delta x_R/\lambda$,

– In the case of the SB component, $i = 1...I$

$$R_h^{\mathrm{SB}_i}(t, \Delta x_T, \Delta x_R, \Delta t) = \frac{1}{2\pi I_0\left(k_R^{(i)}\right) U}$$

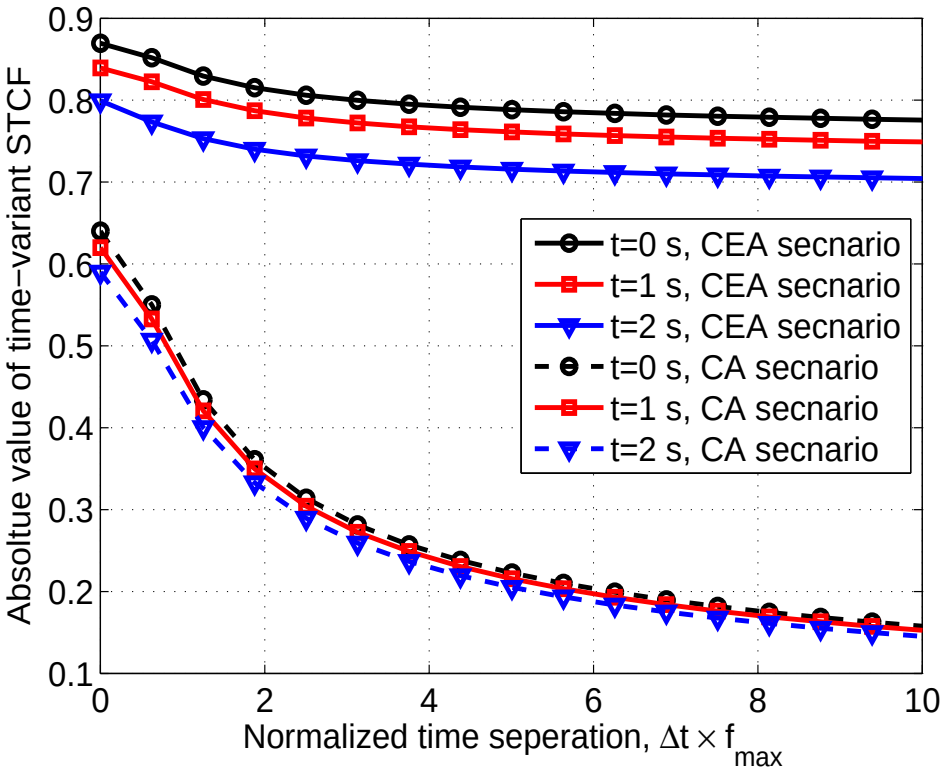

FIGURE 4.4: Absolute values of STCFs for HST channel models with different scenarios.

$$\times \int_{-\pi}^{\pi} e^{k_R^{(i)} \cos\left(\phi_R^{(i)} - \mu_R^{(i)}(t)\right)} e^{j2\pi\left[P\cos\left(\phi_T^{(i)} - \beta_T\right) + Q\cos\left(\phi_R^{(i)} - \beta_R\right)\right]} \times e^{j2\pi\xi_{TR}^{(n_i)}(t,\Delta t)} e^{j2\pi f_{\max}\cos\left(\phi_R^{(i)} - \gamma_R\right)\Delta t} \mathrm{d}\phi_R^{(i)} \tag{4.13}$$

where $\xi_{TR}^{n_i}(t, \Delta t) = \xi_T^{n_i}(t - \Delta t) - \xi_T^{n_i}(t) + \xi_R^{n_i}(t - \Delta t) - \xi_R^{n_i}(t)$.

In Fig. 4.4, STCFs of the HST channel model under the CA and CEA scenarios are plotted out. It can offer support to our later analysis on the system BER performance. From this figure, firstly, we can find the STCF for both scenario appears time-varying behaviour. However, it can be observed that the CEA scenario shows the stronger time-varying behaviour than the CA scenario due to the influence of time-varying K factor. Secondly, if we compare the STCF of the CA and the CEA scenario, we can find that for the CA scenario, its correlation of sub-channels is much lower than the CEA scenario due to the higher K factor. In this case we can find that in the HST

channel model, the K factor which indicates the ratio of LoS powers has significant influence on the channel's statistical properties.

4.2.2 Stationary Interval in Terms of STCF

For this HST channel model, its most unique characteristic is the non-stationary behaviour. As conventional statistical properties will not be able to represent the non-stationary behaviour, it is necessary to involve some new metrics to accurately describe the time-varying characteristic of the channel model. In [93], researcher used a new statistic property called the stationary interval in terms of local region of stationariness (LRS) to describe the non-stationary characteristic.

In our system, as the STCF will directly affect the BER performance, the stationary interval in term of STCF is important to our research. Thus, in our work, referring the idea of [93], we will investigate a similar statistic property in term of STCF. This statistic property is defined as the maximum time instant that within with the behaviour of STCF can maintain the required similarity. In mathematics, we can explain this definition as the time instant that make the autocorrelation function (ACF) of the STCF maintains a given threshold, which can be expressed as:

$$t_{\text{int}} = \max\{t_{\text{int}} | \text{ACF}(R_h(t, \Delta x_T, \Delta x_R), R_h(t + t_{\text{int}}, \Delta x_T, \Delta x_R)) \leqslant C_{threshold}\} \quad (4.14)$$

In Fig. 4.5, the stationary interval in terms of STCF for the non-stationary HST channel model under the CA and the CEA scenario are presented. The similarity threshold $C_{threshold} = 0.9$ is used. From this figure, it can be observed that the CA scenario has longer stationary interval than the CEA scenario, which can match our previous observations that the CA scenario is more stable than the CEA scenario.

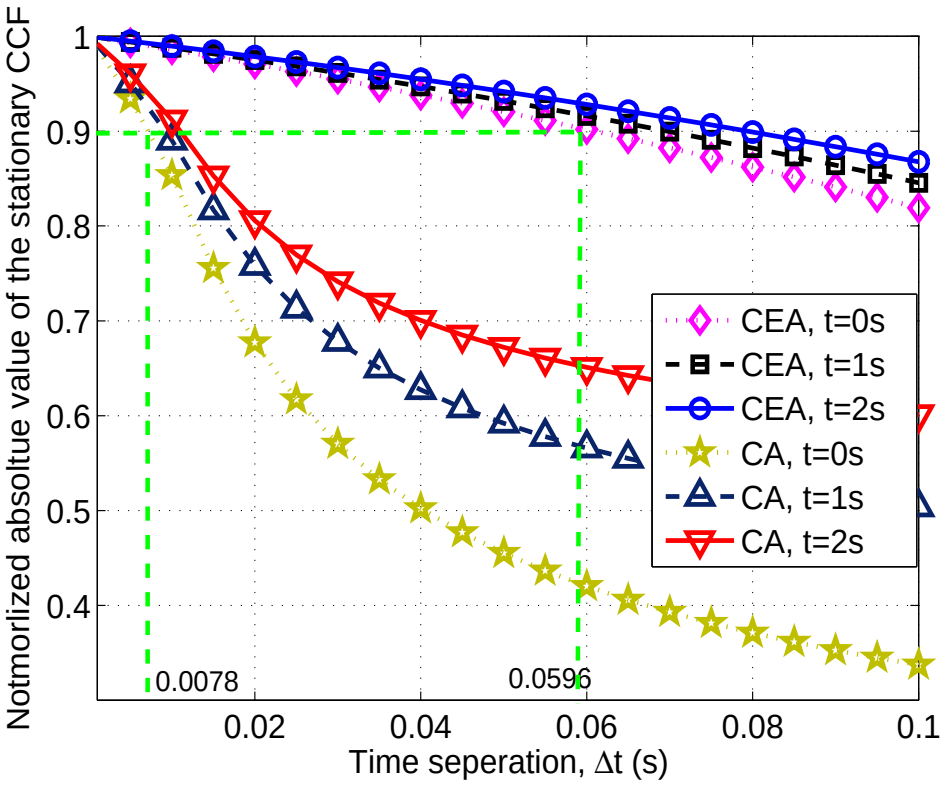

FIGURE 4.5: Stationary interval of the HST channel model under CA and CEA scenarios.

4.2.3 Tap-Delay Line Based Channel Simulator

Mathematically, the process of simulating the signal pass channel models can be represented by the convolution operation between the signal vector and the impulse response of the channel model as 2.1. We can further express the receiver vector as

$$y(t) = \int_0^{\infty} H(t,\tau)S(t-\tau)d\tau \tag{4.15}$$

However, in practical, the channel impulse response and signal vector are discrete, 4.15 should be written to

$$y(t) = \sum_{m=0}^{n} H(t, m\Delta\tau)S(t-m\Delta\tau). \tag{4.16}$$

From this expression, it can be observed that when under wideband channel, the receiver signal suffers from the interference from previous symbols which is known as

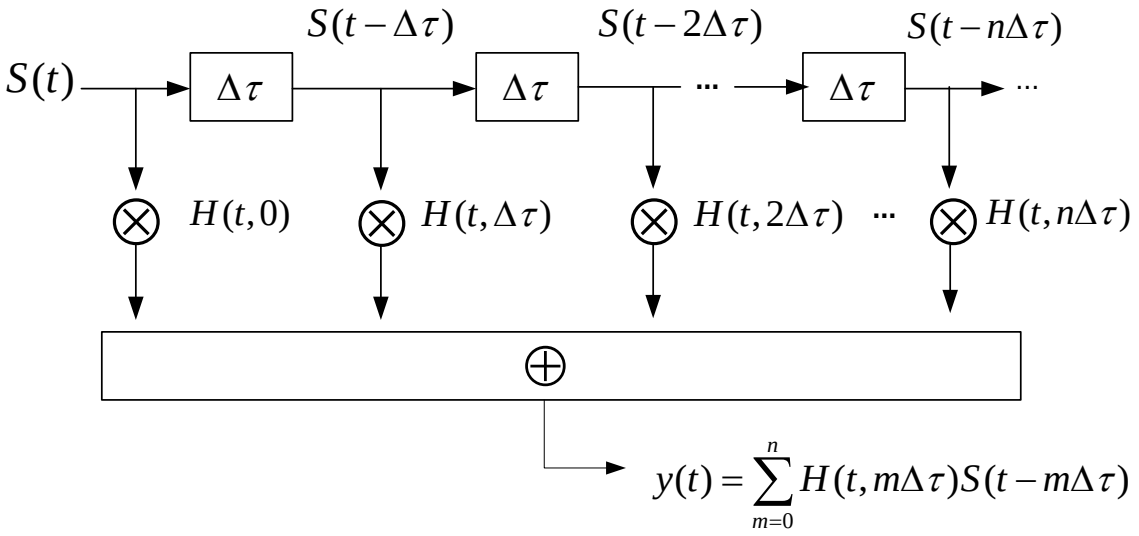

FIGURE 4.6: The tap-delay line based channel simulator.

the ISI. In order to simulate communication systems under wideband channel models, the tap-delay line based channel simulator should be used [80]. In Fig. 4.6, the principle diagram is shown.

4.2.4 Channel Estimation Error Model

In a real communication system, at the Rx side, the estimated channel coefficient is used to recover the transmitted signal. The estimated channel coefficient always comes with estimation errors. Research work regarding estimated error model has been reported in [128] and [129]. However, these error models can not be directly used in our system as they all only assumed narrowband propagation case. In this work, we present a novel estimation error scheme for the wideband HST channel model in the expression of

$$H_{est}(t,\tau_{est}) = \sum_{i=1}^{I} \rho_i(t+\tau_{est}) H_{i,}(t) + \sum_{i=1}^{I} \Omega_i \left(1-\rho_i(t+\tau_{est})\right) \cdot \varepsilon_{est}. \tag{4.17}$$

In (4.17), $\rho_i(t+\tau_{est})$ is the ACF for the ith tap of the channel at time t with the estimation delay τ_{est}. And ε_{est} is the random error vector which is assumed to obey the unit-variance zero-mean complex Gaussian distribution.

4.3 Time-varying Theoretical BER Analysis

By using the union bound method mentioned in [26]–[28], [115], [116], the theoretical ABER of SM systems can be calculated. In this work, the improved upper-bound method presented in [26] is used, which further classifies errors into 3 categories: 1) error only occurs in the digital modulation part with the probability $\underset{\text{Signal}}{\text{ABER}}$; 2) error only occurs in spatial modulation part with the probability $\underset{\text{Spatial}}{\text{ABER}}$ and 3) error occurs in both parts with the probability $\underset{\text{Joint}}{\text{ABER}}$. The overall upper-bound expression of the BER is the combination of these three parts, and in this work, as the channel is time-varying, the theoretical derivation should also consider to be time-varying, which is expressed as:

$$\underset{\text{SM}}{\text{ABER}}\,(t) \leqslant \underset{\text{Signal}}{\text{ABER}}\,(t) + \underset{\text{Spatial}}{\text{ABER}}\,(t) + \underset{\text{Joint}}{\text{ABER}}\,(t) \tag{4.18}$$

$\underset{\text{Signal}}{\text{ABER}}(t)$ represents the case that at time t the error only occurs in the digital modulation part while the transmit antenna index is correctly detected. It is similar to the SIMO case. The BER expression is given by

$$\underset{\text{Signal}}{\text{ABER}}(t) = \frac{1}{N_t}\frac{\log_2(M)}{m}\sum_{n_t=1}^{N_t}\underset{\text{MOD}}{\text{APEB}}(t, n_t), \tag{4.19}$$

and

$$\underset{\text{MOD}}{\text{APEB}}(t, n_t) = \frac{1}{M}\frac{1}{\log_2(M)}N_H\left(\chi \to \tilde{\chi}\right)P(t, \chi \to \tilde{\chi}). \tag{4.20}$$

In (4.20), $N_H\left(\chi \to \tilde{\chi}\right)$ is the Hamming distance between modulated symbols χ and $\tilde{\chi}$, $P(t, \chi \to \tilde{\chi})$ denotes the pairwise error probability (PEP) that the transmitted symbol χ is detected as $\tilde{\chi}$ at time t. In (4.19) and (4.20), $\underset{\text{Signal}}{\text{ABER}}$ is determined by the digital modulation scheme. For example, if M-PSK modulation scheme is used, (4.20) can be derived out referring [26], [115] as

$$\underset{\text{MOD}}{\text{APEB}}(t, n_t) = \frac{1}{\log_2(M)}\sum_{l=1}^{M-1}\left[\left(2\left|\frac{l}{M} - \left\lfloor\frac{l}{M}\right\rfloor\right| + 2\sum_{k=2}^{\log_2(M)}\left|\frac{l}{2^k} - \left\lfloor\frac{l}{2^k}\right\rfloor\right|\right)\right]P_l(t, n_t), \tag{4.21}$$

where:

$$P_l(t,n_t)=\frac{1}{2\pi}\int_0^{\pi[1-(2l-1)/M]}T_l^-(\theta,n_t,t)d\theta-\frac{1}{2\pi}\int_0^{\pi[1-(2l+1)/M]}T_l^+(\theta,n_t,t)d\theta, \quad (4.22)$$

and:

$$T_l^-(\theta,n_t,t)=M_r(2\gamma\frac{\sin^2\left[\pi(2l-1)/M\right]}{\sin^2\theta},t), T_l^+(\theta,n_t,t)=M_r(2\gamma\frac{\sin^2\left[\pi(2l+1)/M\right]}{\sin^2\theta},t). \quad (4.23)$$

In (4.23), γ is the signal-to-interference-plus-noise ratio (SINR). Under the condition with channel estimation error, the SINR can be defined as:

$$\gamma=\frac{E_m\cdot\sum_{i=1}^{I}\rho_i(t+\tau_{est})\,\Omega_i}{N+I+\sum_{i=1}^{I}\Omega_i\left(1-\rho_i(t+\tau_{est})\right)} \quad (4.24)$$

where E_m is the transmit power, N is the noise power. $M_r(.,t)$ is the time-varying moment generation function (MGF) of $\sum_{n_r=1}^{N_R}\|h_{n_t,n_r,est}(t)e\|^2$, where $e=\chi-\tilde{\chi}$. The close form expression of $M_r(.,t)$ is

$$M_r(s,t)=\prod_{i=1}^{N_R}(1-s\lambda_i(t+\tau_{est})e)^{-1}. \quad (4.25)$$

In (4.25), $\lambda_i(t)$ is the eigenvalue of time-varying Rx correlation indicator matrix $R_{Rx}(t)$. Similarly, we can define $R_{Tx}(t)$ as the time-varying correlation indicator matrix of Tx. Considering this GBSM channel model and referring [118], these two matrices are expressed as

$$R_{Tx}(p,\tilde{p})=\rho_{h_{q,p}h_{q,\tilde{p}}}(t), R_{Rx}(q,\tilde{q})=\rho_{h_{q,p}h_{\tilde{q},p}}(t), \quad (4.26)$$

where $\rho_{h_{q,p}h_{q,\tilde{p}}}(t)$ is the STCF of the HST channel model at time t, which indicates the correlation between $h_{q,p}$ and $h_{q,\tilde{p}}$.

For the case that the error only occurs in the spatial modulation part, which is expressed as $\underset{\text{Spatial}}{\text{ABER}}$ previously, we can refer to related investigations on space shift

keying (SSK) systems, [27], [28]. This part can be expressed as

$$\underset{\text{Spatial}}{\text{ABER}}(t) = \frac{1}{M}\frac{\log_2(N_t)}{m}\sum_{l=1}^{M}\underset{\text{SSK}}{\text{APEB}}(t,l). \tag{4.27}$$

$\underset{\text{SSK}}{\text{APEB}}$ can be further expressed as

$$\underset{\text{SSK}}{\text{APEB}}(t,l) = \frac{1}{N_t}\frac{1}{\log_2(N_t)} \times \sum_{n_t=1}^{N_t}\sum_{\tilde{n}_t=1}^{N_t}\left[N_H\left(n_t \to \tilde{n}_t\right) P(t,\kappa_l, n_t \to \tilde{n}_t)\right], \tag{4.28}$$

where $N_H\left(n_t \to \tilde{n}_t\right)$ is the Hamming distance between the antenna indices n_t and $\tilde{n}_t$, the PEP that at time t is represented as $P(t,\kappa_l, n_t \to \tilde{n}_t)$, the active antenna $\tilde{n}_t$ is detected given that n_t was transmitted with the modulation modulus κ_l. Referring to the ML detector algorithm in [24], this error can only occurs when $\|y - h_{n_t,n_r,est}(t)\kappa_l\|^2 > \|y - h_{\tilde{n}_t,n_r,est}(t)\kappa_l\|^2$. Thus, $P(t,\kappa_l, n_t \to \tilde{n}_t)$ can be written as

$$\begin{aligned} P(t,\kappa_l, n_t \to \tilde{n}_t) &= P(\|y - h_{n_t,n_r,est}(t)\kappa_l\|^2 > \|y - h_{\tilde{n}_t,n_r,est}(t)\kappa_l\|^2) \\ &= Q(\gamma\|h_{n_t,n_r,est}(t)\kappa_l - h_{n_t,n_r,est}(t)\kappa_l\|^2), \end{aligned} \tag{4.29}$$

where $Q(.)$ is the Q-function. Based on the alternative integral expression of Q-function and MGF-based approach [115], [116], (4.29) can be written as

$$P(t,\kappa_l, n_t \to \tilde{n}_t) = \frac{1}{\pi}\int_0^{\pi/2} M_{n_t,\tilde{n}_t}(\gamma\frac{\kappa_l^2}{2\sin^2\theta}, (t))d\theta. \tag{4.30}$$

In (4.30), $M_{n_t,\tilde{n}_t}(.,t)$ is the MGF of $\sum_{n_r=1}^{N_R}\|h_{n_t,n_r,est}(t) - h_{\tilde{n}_t,n_r,est}(t)\|^2$, which can be expressed as:

$$M_{n_t,\tilde{n}_t}(s,t) = \prod_{j=1}^{N_T}\prod_{i=1}^{N_R}(1 - s\lambda_i(t+\tau_{est})u_j(t+\tau_{est})^{-1}), \tag{4.31}$$

where $u_j(t)$ is the eigenvalue of receivers correlation indicator matrix R_{Tx}. If constant modulus modulation schemes such as M-PSK are used, κ_l is a constant value as κ and

(4.27) can be simplified as

$$\underset{\text{Spatial}}{\text{ABER}}(t) = \frac{1}{N_t m} \sum_{n_t=1}^{N_t} \sum_{\tilde{n}_t=1}^{N_t} \left[N_H\left(n_t \to \tilde{n}_t\right) \times \frac{1}{\pi} \int_0^{\pi/2} M_{n_t,\tilde{n}}(\gamma \frac{k^2}{2\sin^2\theta}, t) d\theta \right]. \quad (4.32)$$

For the third case, $\underset{\text{Joint}}{\text{ABER}}$, both digital modulation and spatial modulation parts are incorrect. It can be expressed as:

$$\underset{\text{Joint}}{\text{ABER}}(t) = \frac{1}{N_t m} \sum_{n_t=1}^{N_t} \sum_{\tilde{n}_t \neq n_t=1}^{N_t} \left[N_H\left(n_t, \chi \to \tilde{n}_t, \tilde{\chi}\right) \times P\left(t, n_t, \chi \to \tilde{n}_t, \tilde{\chi}\right) \right], \quad (4.33)$$

where $N_H\left((n_t, \chi) \to (\tilde{n}_t, \tilde{\chi})\right)$ is the Hamming distance for the error case that symbol χ transmitted by antenna n_t is detected as $\tilde{\chi}$ sent by antenna $\tilde{n}_t$ and $P\left(t, (n_t, \chi) \to (\tilde{n}_t, \tilde{\chi})\right)$ is the corresponding PEP. Similar to the case of $\underset{\text{Spatial}}{\text{ABER}}$, it can be expressed as:

$$\begin{aligned} &P(t,(n_t,\chi) \to (\tilde{n}_t,\tilde{\chi})) \\ &\quad = P(\|y - h_{n_t,n_r,est}(t)\chi\|^2 > \|y - h_{\tilde{n}_t,n_r,est}(t)\tilde{\chi}\|^2) = Q(\gamma \|h_{n_t,n_r,est}(t)\chi - h_{\tilde{n}_t,n_r,est}(t)\tilde{\chi}\|^2). \end{aligned} \quad (4.34)$$

Using the MGF-based approach, (4.34) can be represented as

$$P(t, (n_t, \chi) \to (\tilde{n}_t, \tilde{\chi})) = \frac{1}{\pi} \int_0^{\frac{\pi}{2}} M_{n_t\chi, \tilde{n}_t\tilde{\chi}}(\frac{\gamma}{2\sin^2\theta}, (t)) d\theta. \quad (4.35)$$

In (4.35), $M_{n_t\chi,\tilde{n}_t\tilde{\chi}}(., t)$ is the MGF of $\sum_{n_r=1}^{N_r} |h_{n_t,n_r,est}(t)\chi - h_{\tilde{n}_t,n_r,est}(t)\tilde{\chi}|^2$, with the expression of

$$M_{n_t\chi,\tilde{n}_t\tilde{\chi}}(s,t) = \prod_{j=1}^{N_T} \prod_{i=1}^{N_R} (1 - s\lambda_i(t + \tau_{est}) e u_j(t + \tau_{est}))^{-1}. \quad (4.36)$$

4.4 Simulation Results and Discussions

In this section, different simulation results are presented to evaluate the performance of SM systems under the non-stationary wideband HST channel model. The system

is assumed to be a LTE system working with 1.4 MHz bandwidth, using a 2x2 MIMO system and BPSK modulation scheme.

Referring [90] and [130], following key parameters are used to configure all simulations: the carrier frequency is $f_c = 2.6$ GHz, the speed of the HST is $\upsilon_R = 300$ km/h with the movement angle $\gamma_R = 30°$, the corresponding maximum Doppler shift is $f_{max} = 722$ Hz. The initial AoAs $\mu_R^{(i)}(t_0)$ are selected referring the WINNER II channel model [92], from the D2A moving networks scenario. The concentration parameter of von Mise distribution is chosen as $k_R^{(i)} = 6$. The space between two antenna elements of Tx and Rx sides is configured as 0.5λ with tilt angles as $\beta_R = \beta_T = 60°$. The distance between the BS and the track is defined as $D_{\min} = 50$ m. It necessary to note that in this work, in order purely investigate the effect of the channel, no equalizer is involved. As the channel model is with time-varying behaviour, in order to make simulation results be stable, we tried to make the simulation time short (1000 symbols each time), but repeat large numbers of time (1000 times each point) to get the final smooth curves.

The research focus of this work is to investigate the impact of the non-stationary behaviour of the channel model on the BER performance of SM systems. As the channel model is novel and complex, in this work, some further investigations on the non-stationary behaviour of the channel model are also important research issues and some interesting results on the channel behaviour are obtained. We are interested in how these unique characteristics affect the BER performance of SM. Thus, the comparison between SM and other MIMO technologies are not carried out in this work.

4.4.1 Comparison Between Theoretical Results and Simulation Results

In Fig. 4.7, theoretical results of ABER for SM systems under the non-stationary wideband HST channel model of the CA scenarios are compared with simulation results. This figure indicates an excellent approximation of the theoretical derivation

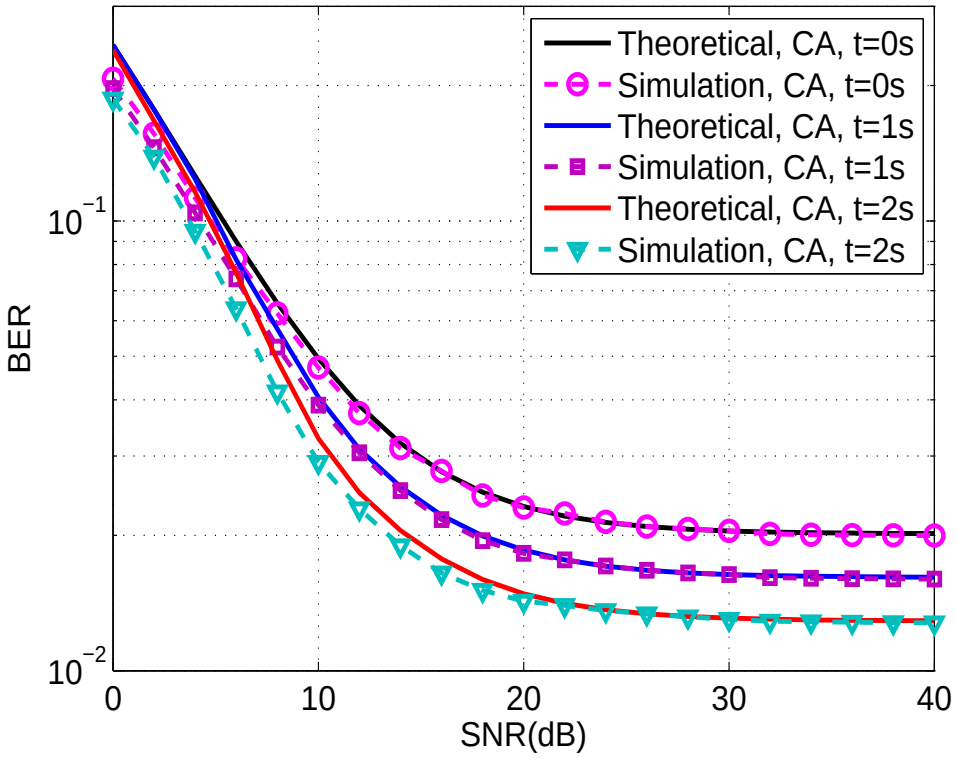

FIGURE 4.7: BER performance of SM system under the CA scenario at different time instants, compared between theoretical results and simulation results.

with simulation results at each time point. Based on this figure, we can conclude that our theoretical ABER upper-bound can offer a great accuracy. It can be used to estimate BER for SM system under the wideband channels and the non-stationary case.

In Fig. 4.8, similar observations can be obtained. Under the CEA scenario, theoretical results can also match simulation results very well even involved time-varying K factor.

4.4.2 Performance of SM Under CA and CEA Scenarios

From Fig. 4.7, we can also observe that the BER performance of the SM system shows the time-varying characteristic. And at the high SNR range (SNR$\geq$ 20dB), even the signal power is increased, the BER performance still keeps the same level. That is because for wideband channels, beside the noise, the received signal also suffers from

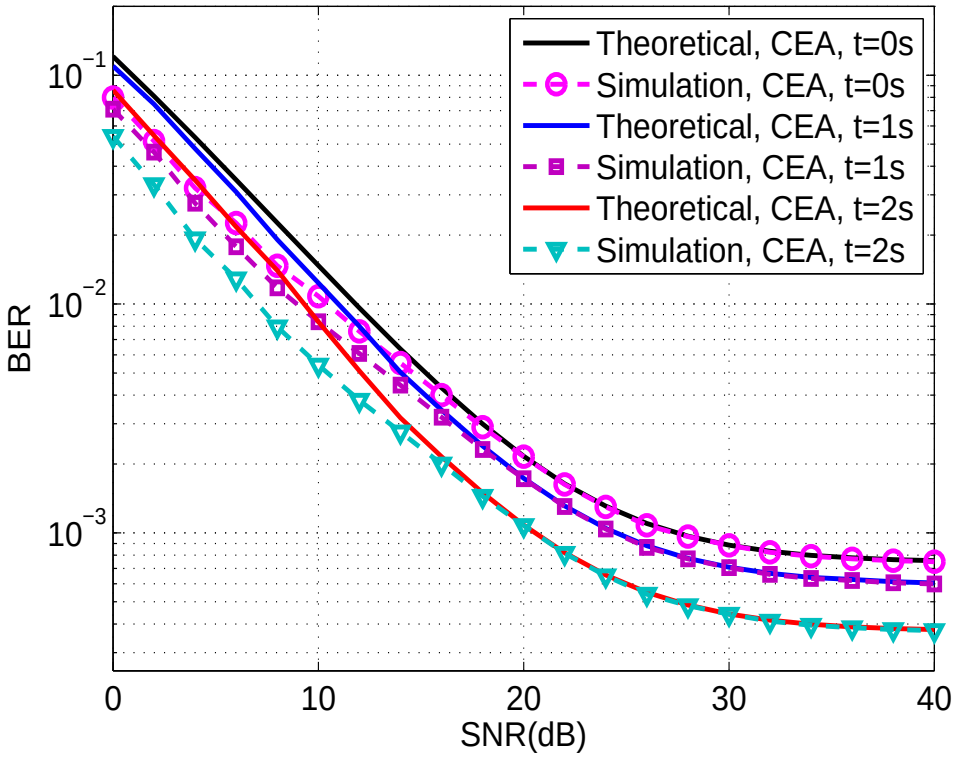

FIGURE 4.8: BER performance of SM system under the CEA scenario at different time instant, compared between theoretical results and simulation results.

the ISI. When the transmit power increases, the ISI increases at the same time. This is the reason why communication systems in reality use equalisers to improve the system performance.

Similar to the CA scenario, at the high SNR range, the system's performance also suffers from the ISI. However, for the CEA scenario, due to the ISI level is lower than the CA scenario, the SM system can offer the better performance than it under the CA scenario. The BER performance also appears the time-varying characteristic. If it compared with results of CA scenario, we can find that under the CEA scenario, the time-varying characteristic is much stronger. With the same time change, the BER result in the CEA scenario appears the higher change ratio. The reason behind this phenomena is that for the CA scenario, only the distance between the BS and the MRS and AoA are time-varying, but for the CEA scenario, besides these pro-mentioned parameters, the K factor which has significantly influence on the correlation properties of the channel is also time-varying.

If we look back to Fig.4.4, we can find that the correlation of sub-channels for CA scenario is much lower than that of the CEA scenario. In principle, the BER performance of the CA scenario should be better than the CEA scenario. However, from Fig. 4.7 and Fig. 4.8, it is clear the SM system has superior performance under the CEA scenario. That is because under the CA scenario, the SM system suffers much stronger ISI than the CEA scenario. From this comparison, we can conclude that the ISI is the key effector to the performance of SM system under the wideband channel. Again, it indicates the importance of using equaliser in real systems.

4.4.3 Influence of Stationary Interval on BER Performance

In Fig. 4.9 and 4.10, the BER performance are investigated in terms of the stationary interval. In our simulation, the stationary interval are selected for threshold $C_{threshold} = 0.9$. From simulation results, it is clear that within the stationary interval, due to the correlation between sub-channels maintains relatively stationary, the BER performance can also keep a stable behaviour. However, as the time difference increased, due to the correlation property becomes below the necessary threshold, the behaviour on BER performance changes.

4.4.4 Impact of Non-ideal Channel Estimation Errors and Doppler Shift on BER Performance

In Fig. 4.11 and Fig. 4.12, the BER performance of SM system are investigated under the CA scenario with the non-ideal channel estimation, impacts of channel estimation delay and Doppler frequency are considered. It can be observed that theoretical upper bounds and simulation results can match very well for all cases. The accuracy and the flexibility of our theoretical BER framework can be noticed, it can capture the BER behaviour of SM system under the complex HST propagation scenarios.

In Fig. 4.11, the BER performance is investigated with different estimation delay while under the case of fixed Doppler frequency (f_{max}=722 Hz). It can be observed

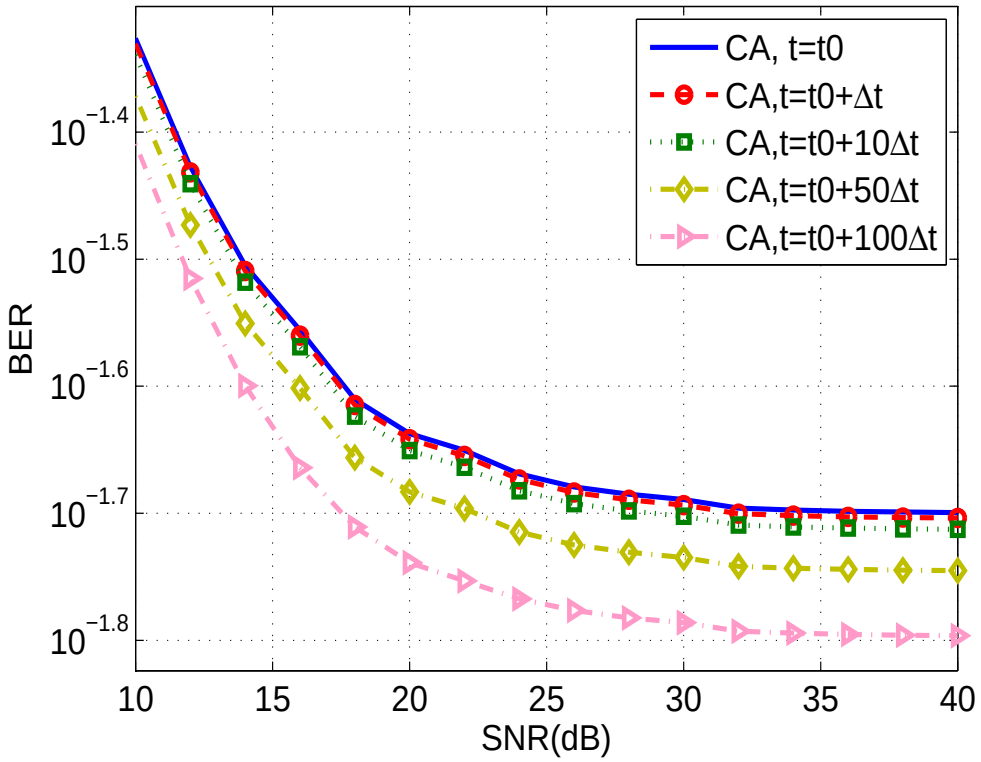

FIGURE 4.9: BER performance for SM system under the CA scenario in terms of stationary interval,$\Delta t = t_{\text{int}}$=0.0596 s.

that better BER performance can be achieved with the smaller channel estimation. This predominance can be explained by Fig. 4.13. It can be observed that with the fixed Doppler frequency, the shorter time difference (also refers to channel estimation delay) will result in the better coherence between the estimated channel and the real channel.

In Fig. 4.12, the BER performance of SM with fixed estimation delay (τ=0.2ms) but different Doppler frequency are illustrated. It can be found that with the fixed estimation delay, the higher Doppler frequency which corresponding to the higher speed will cause the poor BER performance. That is because the higher Doppler frequency will shorten the coherence time of the channel. In our system, it will make the bigger difference between the estimated channel and the real channel. From this figure, it can be concluded that when under the high movement speed, communication systems should spend more resource on channel estimation in order to provide the reliable service.

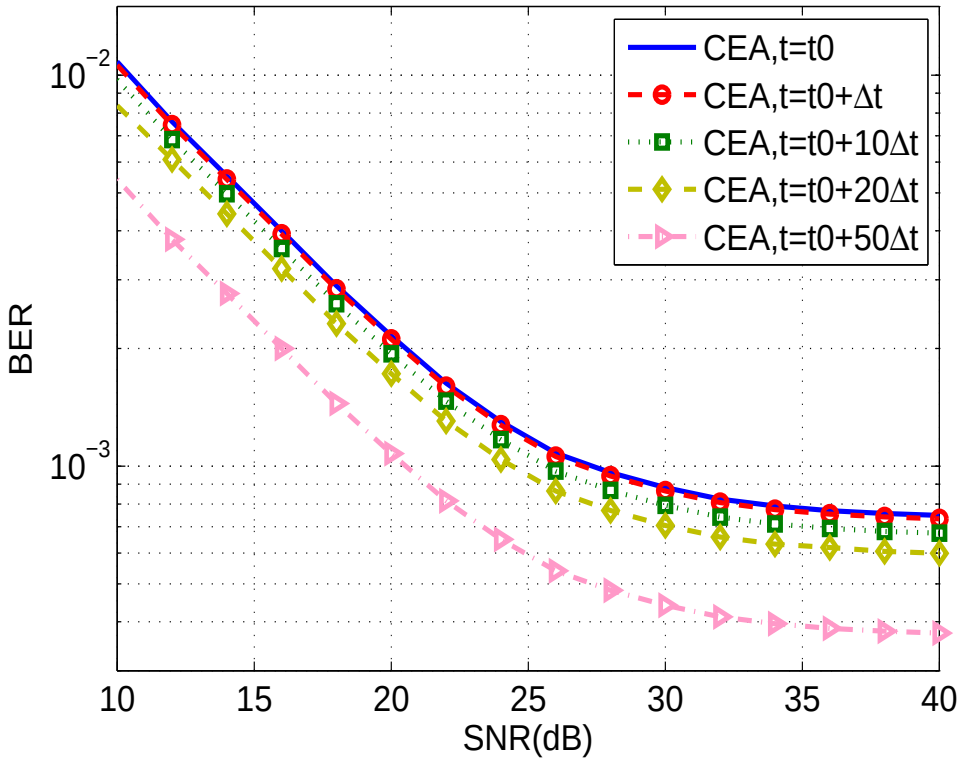

FIGURE 4.10: BER performance for SM system under the CEA scenario in terms of stationary interval,$\Delta t = t_{\text{int}}$=0.0078 s.

4.5 Summary

In this chapter, we have investigated the performance of SM systems under a non-stationary wideband HST channel model with different propagation scenarios. Measurement results are involved which make the channel more accurate to capture the reality of HST communication scenarios. Accurate theoretical BER expression of SM under non-stationary wideband channel assumed non-ideal channel estimation has been derived. The influence of different time-varying parameters on the BER performance of SM system have comprehensively been studied. Additionally, a novel statistic property to accurate describe the non-stationary behaviour named stationary interval in terms of the STCF has been presented, and its influence on the BER performance of SM system has been investigated. Form theoretical and simulation results, we have observed that the BER performance of SM system shows a timing-varying behaviour due to the non-stationary HST channel model. Also, the BER

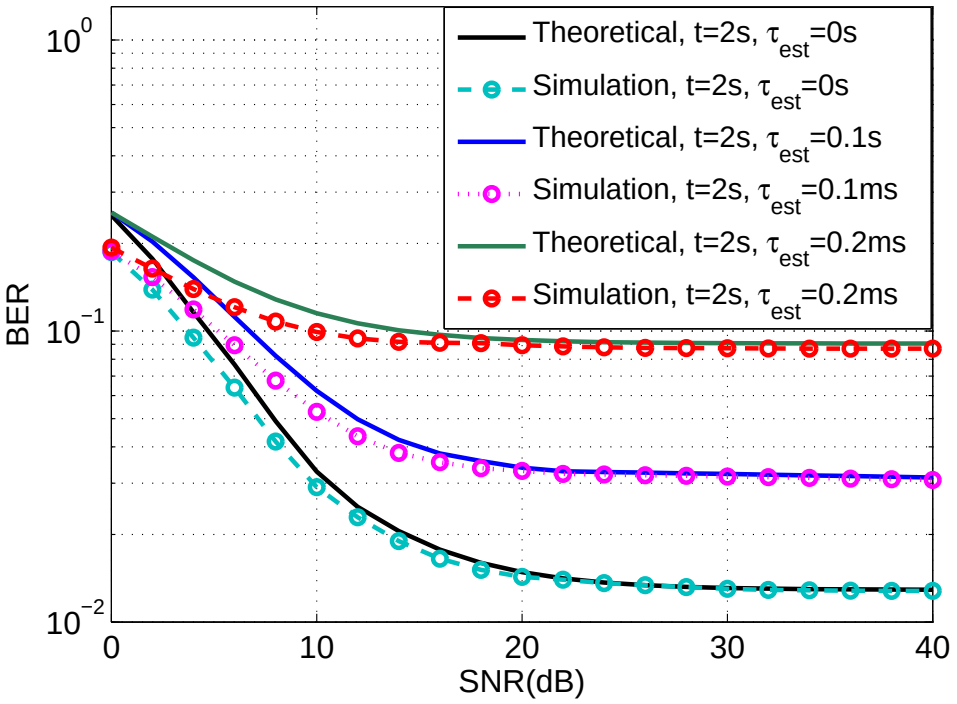

FIGURE 4.11: BER performance for SM system under the CA scenario in terms of different estimation delays, f_{max}=722 Hz.

performance of SM system under the HST channel model are mainly affected by the correlation between sub-channels, ISI, Doppler shift, and channel estimation delay.

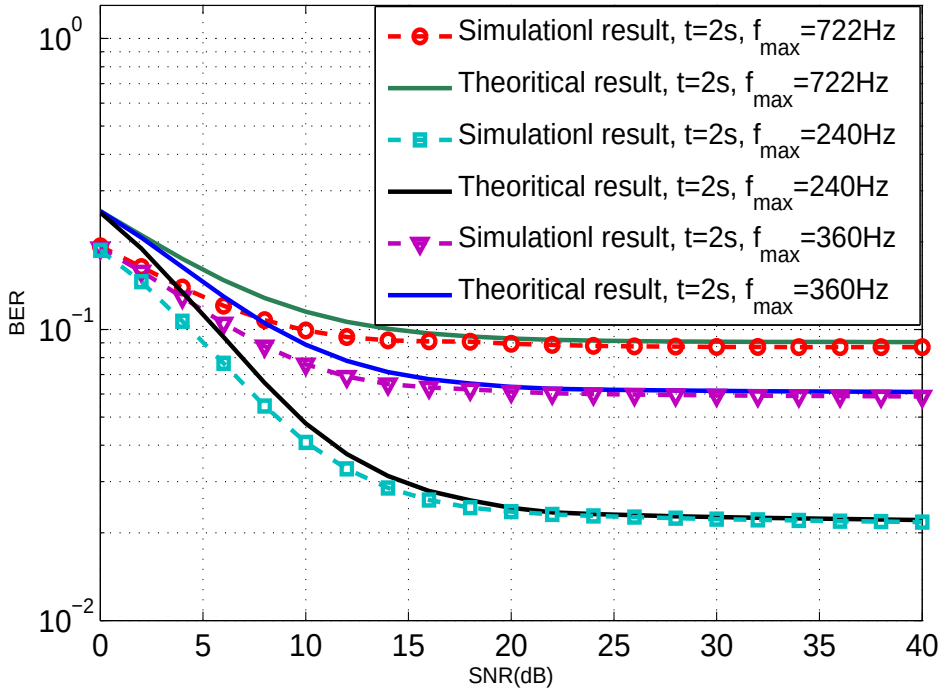

FIGURE 4.12: BER performance for SM system under the CA scenario in terms of different Doppler frequencies,τ_{est}=0.2 ms.

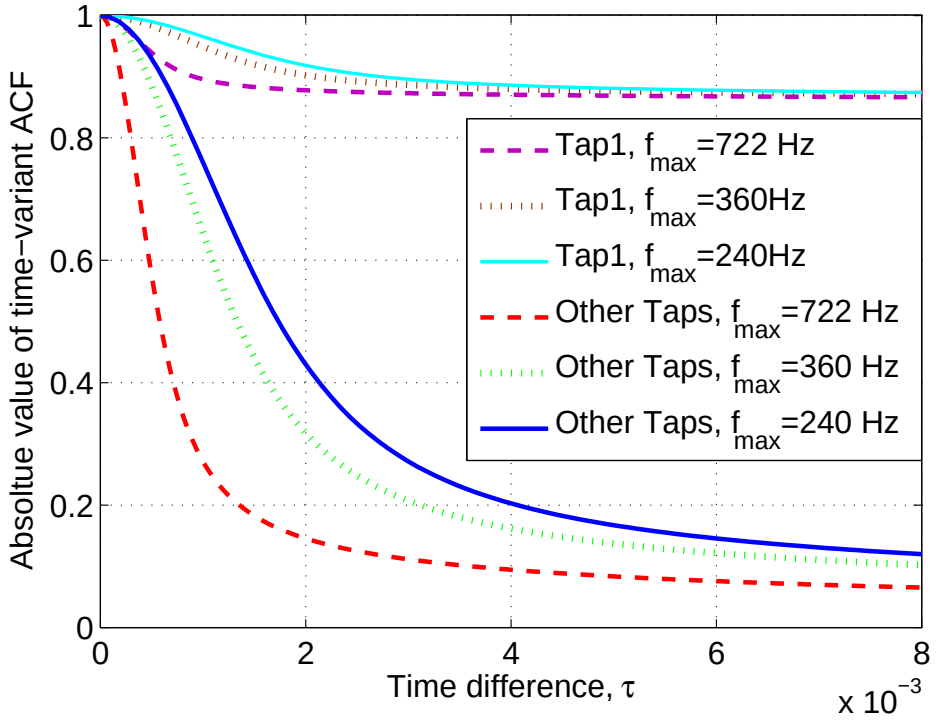

FIGURE 4.13: The absolute values of the time-variant ACF of different Taps of the HST channel model with different Doppler frequency at the time instant of t=2 s.

Chapter 5

Performance Investigation of Spatial Modulation Systems Under A Kronecker-Based Massive-MIMO Channel Model of Multiple User Scenarios

5.1 Introduction

In order to fulfil the dramatically increasing demand on reliability, capacity and energy-spectral efficiency for wireless communications systems, novel physical layer transmit technologies have been widely investigated [9]. In recent years, massive MIMO systems which are equipped with tens even hundreds of antennas, have attracted significant research interests due to their potential capability to fulfil aforementioned requirements [98]–[101].

How to implement a massive MIMO system is still a challenge in practical. Existing MIMO technologies including the spatial multiplexing and the spatial diversity [131], [132], have achieved great success in current wireless communication systems [99]. However, these technologies suffer from various of drawbacks such as the ICI and high system complexity, and hence they are not suitable for massive MIMO systems. In

recent years, SM has attracted lots of research interests due to it outstanding performance in achieving good trade-off between the system performance and the complexity [21]–[23]. These advantages make SM be considered as a promising candidate technology for Massive MIMO systems.

In realistic conditions, a massive MIMO system usually works in the multi-user (MU) case, and how to eliminate the inter-user-interference (IUI) is an important technical issue. In general, there are two ways to solve this problem. The first method is to use the TDMA scheme [133], [134], which means at a certain time slot, all antennas will serve only one user. Under the TDMA scheme, the IUI problem can be totally avoided, and as it does not require channel knowledge at the Tx side, the system complexity is significantly reduced. However, when combining the TDMA scheme with SM systems, as it uses only one active antenna to transmit data to one user, the utilization of antenna elements and the system achievable sum rate are lower than other technologies. For the second framework, precoding methods were employed to enable the TX to send signals to all users at the same time using all transmit antennas. In [135]–[137], research works for precoding schemes for MU-MIMO systems have been reported, in which some well-known precoding schemes such as minimum mean-squared error (MMSE), zero-forcing (ZF), matched filter (MF) have been investigated. However, these methods are not suitable for SM systems as they all eliminate the channel's effects, which will lose the data carried by antenna indexes [138]. Besides, all of these methods can only support using a single receive antenna for each user, which will deprive the benefit of receive diversity. It is necessary to involve some specific precoding methods for SM. In [139], [140], a method named block diagonalization (BD) was introduced, its basic idea is to compose the precoding matrix that represents the null-space of IUI using the singular value decomposition (SVD). The most attractive characteristics of this method are it can support multiple receive antennas and with the ability to keep the channel's effects, which make it possible to establish precoding SM systems with the receive diversity gain.

Most existing researches on the performance of SM technologies so far only focus on single-user point to point scenarios [26], [43], [114], [141] for small scale MIMO

systems. In recent years, some researchers attempted to investigate SM under MU massive MIMO scenarios, related works have been reported in [142]–[146]. However, there are following research gaps for the researches on MU-SM systems. Firstly, to the best of author's knowledge, most researches on MU-SM only focus on the uplink scenario, there is rarely research on the downlink case. Secondly, most researchers tried to use precoding schemes to eliminate the IUI. However, due to the limitation of selected precoding methods, each user can use only single receive antenna, and hence the study of receive diversity is missing. Thirdly, there is not sufficient research on practical massive MIMO systems. In some so-called massive MIMO systems, the number of transmit antennas was even less than 32, and for most of these research works, only conventional MIMO channel models and even i.i.d channel models were used to investigate the performance of massive MIMO systems. These channel models are not able to accurately represent the fading characteristics of massive MIMO channels.

In order to fulfil these research gaps, in this work, the performance of SM in the massive MIMO systems under MU scenarios is investigated under a KBSM that specifically developed for massive MIMO scenarios. In this work, massive MIMO SM systems are established using both the TDMA scheme and the BD based precoding scheme, different channel configurations (cluster evolution factors) and different system settings are considered to comprehensively analyse and compare the BER performance of both solutions.

Over all, we can highlight the main contributions and novelties of this work as follows.

1. SM is investigated under MU scenarios using a channel model that specifically proposed for massive MIMO systems. A comprehensive study on the BER performance of SM systems under this massive MIMO channel model is carried out. How different channel factors affect the system BER performance such as evolution factors of cluster, number of users are thoroughly studied.

2. An accurate theoretical BER expression for MU-SM system using BD-precoding scheme is presented. To the best of author's knowledge, there is no relevant

study to derive out the theoretical BER expression of MU-SM systems under the precoding scheme supporting multiple receive antennas for each user.

3. The BER performance of different MIMO technologies include TD-SM, BD-SM, BD-V-BLAST and the conventional channel inversion [147] are compared. The influence of different system settings on the system performance such as the number of users and data rate are considered. This is the first time that SM using the BD percoding scheme is compared with other MIMO technologies under multiple-user scenarios.

The remainder of this chapter will be organized as follows. In Section 5.2, systems architectures of MU-massive MIMO systems using the TDMA-SM and BD-SM schemes are introduced. In Section 5.3, the KBSM for the massive MIMO scenario are described. The theoretical BER expression of TD-SM and BD-SM massive MIMO systems under the KBSM for the massive MIMO scenario is derived in Section 5.4. In Section 5.5, simulation results are presented and analysed. Finally, conclusions are drawn in Section 5.6.

5.2 Systems Architectures of MU-SM Massive MIMO systems

5.2.1 The Time-Division Multiple-users SM System

For a MU system using the TDMA scheme, at each time instant, BS only transmits data to one user. Thus, compared with other multiple access schemes, the system complexity of the TDMA system can be significantly decreased as it is not necessary to employ complex precoding process to mitigate IUI. Let us assume there is a system with K users, the BS is equipped with N_t antenna elements. At each instant, only one antenna is used to transmit data to a single user. The bit stream for each user is divided into two parts, the first $\log_2(N_t)$ bits are carried by the antenna index, which is also used for the antenna selection. The other $\log_2(M)$ bits are transmitted

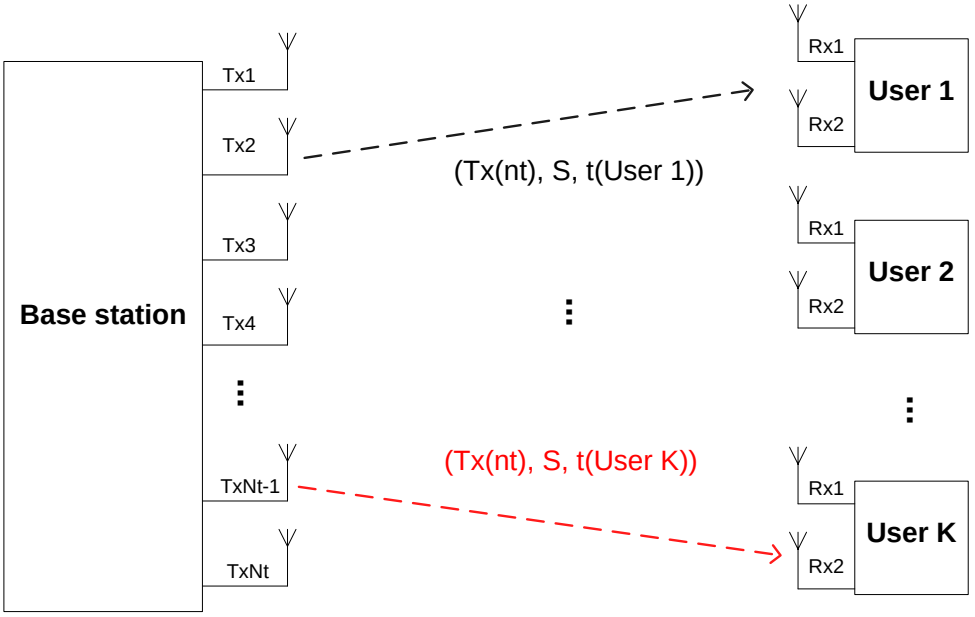

FIGURE 5.1: Block diagram of TD multiple users Spatial Modulation system

through the digital modulated symbol, where M is the modulation order. Thus, at each time instant, $m = \log_2(N_t) + \log_2(M)$ bits are transmitted, where m is the spectral efficiency of the SM system in the unit of bits/symbol. An example of a TD-MU-SM system is given in Fig. 5.1, at the time instant for a selected user, modulated symbol S is transmitted through the selected active antenna to the user.

Mathematically, the detailed expression of the K users TDMA system at the time slot of the kth user can be written as

$$\boldsymbol{Y}(t_k) = \boldsymbol{H}\boldsymbol{S}(t_k) + \boldsymbol{N}, k = 1.2...K. \tag{5.1}$$

$\boldsymbol{H}$ is the channel matrix vector, its dimension is $K \times 1$, which can be expressed as

$$\boldsymbol{H} = \begin{bmatrix} \boldsymbol{H_1^T} & \boldsymbol{H_2^T} & ... & \boldsymbol{H_k^T} & ... & \boldsymbol{H_K^T} \end{bmatrix}^T \tag{5.2}$$

each element $\boldsymbol{H_k}(1 \leqslant k \leqslant K)$ is the channel matrix for the corresponding kth user. $\boldsymbol{N}$ is the complex AWGN vector for the system, $[.]^T$ denotes transpose operation. $\boldsymbol{S}(t_k)$ is the transmit vector for K users at the time slot for the kth user t_k, while each element is the signal vector for the corresponding user. As the system works under the TDMA scheme, thus at the time instant of the kth user, only the element of the

kth user in $\boldsymbol{S}(t_k)$ is not zero, which is with the expression of

$$\boldsymbol{S}(t_k) = [\ 0 \quad ... \quad \boldsymbol{S_k}(t_k) \quad ... \quad 0\ ]^T_{K\times 1} \tag{5.3}$$

Let $\boldsymbol{S_k}(t_k)$ denote the transmit signal vector of the kth user at the Tx side at time t_k, which is a $N_t \times 1$-size vector. For SM, as only one transmit antenna is active at each time instant, $\boldsymbol{S_k}(t_k)$ can be further expressed as $\boldsymbol{S_k}(t_k) = [0, ..., s, ..., 0]_{N_t}{}^T$. As each user is equipped with N_r antennas, at the Rx side of the kth user, the received $N_r \times 1$-dimensional signal vector $y_k(t_k)$ can be written as:

$$\boldsymbol{y_k}(t_k) = \boldsymbol{H_k}(t_k)\boldsymbol{S_k}(t_k) + \boldsymbol{n_k}. \tag{5.4}$$

In addition, $\boldsymbol{H_k}(t_k)$ is the $N_r \times N_t$ channel matrix of the kth user at time t_k, each element $h_{q,p}(t_k)$ is the channel impulse response between the pth Tx and the qth Rx. Detailed procedure of generating channel impulse responses for the massive channel model will be introduced in next section. $\boldsymbol{n}$ is the AWGN vector of each user.

In this system, the Tx and the Rx are assumed to be with the perfect synchronization in both time and frequency domains. Besides, it is assumed that the full channel state information (CSI) is available at the Rx in this work. The optimum ML detector proposed in [56] is employed to estimate the transmit antenna index $\hat{p}$ and the transmitted data symbol s for each user as

$$\begin{gathered}[\hat{p}, s]_k = \arg\min_{p,m} \left(\|\boldsymbol{y_k} - \boldsymbol{H_k} S_{l,m}\|_F^2\right) \\ p \in \{1 : N_T\}\ ,\ m \in \{1 : M\} \text{and } k \in \{1 : K\}\end{gathered}\ , \tag{5.5}$$

where $\|\cdot\|_F$ denotes the Frobenius norm.

5.2.2 The BD Precoding Based MU SM System

The principle of the BD precoding has been introduced in [139], [140], its basic idea is to generate the precoding matrix represents the null space of IUI. In Fig. 5.2,

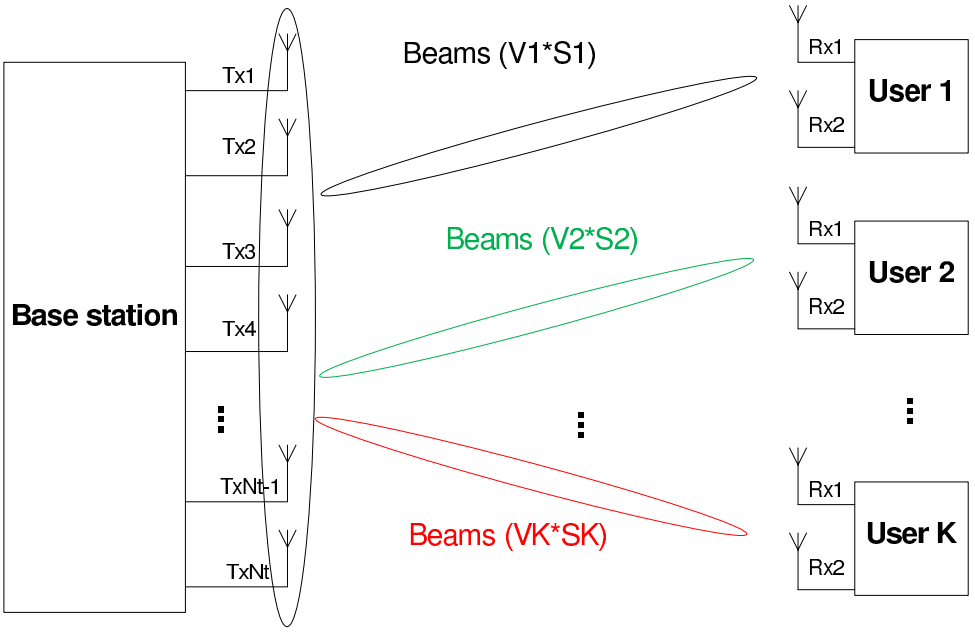

FIGURE 5.2: Block diagram of BD multiple users Spatial Modulation system

the system architecture of a precoding based MU-SM system is shown. Let us still assume a system has K users, and in this system, each user is equipped with N_r receive antennas, while the BS uses N_t antennas. Thus, the channel matrix can still be expressed by (5.2). For the kth user ($1 \leqslant k \leqslant K$), its interference channel matrix $\tilde{H}$ can be defined as:

$$\tilde{\boldsymbol{H}}_{\boldsymbol{k}} = \left[\begin{array}{cccccc} \boldsymbol{H}_{\boldsymbol{1}}^{\boldsymbol{T}} & \ldots & \boldsymbol{H}_{\boldsymbol{k-1}}^{\boldsymbol{T}} & \boldsymbol{H}_{\boldsymbol{k+1}}^{\boldsymbol{T}} & \ldots & \boldsymbol{H}_{\boldsymbol{k-1}}^{\boldsymbol{T}} \end{array} \right]^{T} \tag{5.6}$$

The precoding matrix for this user can be obtained through the SVD product of $\tilde{H}_k$ as:

$$\tilde{\boldsymbol{H}}_{\boldsymbol{k}} = \tilde{U}_k \tilde{\Sigma}_k \left[\begin{array}{cc} \tilde{V}_k^{(1)} & \tilde{V}_k^{(0)} \end{array} \right]^{H}. \tag{5.7}$$

In (5.7), $[.]^H$ is the Hermitian transpose. In order to clearly describe the principle, let us define $J_k = N_t - (K-1) \times N_r$, which is the maximum number beamforming patterns of the system and it should be a positive number. Thus for an BD based MU system, it should firstly fulfil the condition that $N_t > \sum_{k=1}^{K-1} Nr$. The precoding matrix $\tilde{V}_k^{(0)}$ is with the dimension of $N_t \times J_k$. In a conventional SM system, antenna indexes are used to carry information. However, for a MU-BD-SM system, it uses the BD precoding scheme to generate beams to eliminate IUI, and all antenna are

active. Thus, in a BD-SM system, what is used to carry out spatial modulation is the beamforming pattern index rather than the antenna index. So, for a BD-SM system, following conditions should be fulfilled. Firstly, in order to use the beam pattern index to carry information, the minimum pattern numbers should be not less than 2 as $J_k \geqslant 2$. Secondly, the maximum bits that can be carried by the pattern index is $\lfloor \log_2(\mathrm{J_k}) \rfloor$, where $\lfloor \rfloor$ is the floor function. We can observe that in a BD-MU-SM system, the pattern number of each user is $2 \leqslant N \leqslant J_k$, the precoding matrix $\tilde{V}_k$ is with the dimension of $N_t \times N$. The spectral efficiency m can be expressed as $m = \log_2(N) + \log_2(M)$.

Let us define the coded transmit signal vector $\boldsymbol{S}$ as

$$\boldsymbol{S} = \left[\begin{array}{cccccc} \tilde{V}_1 \boldsymbol{S_1} & ... & \tilde{V}_k \boldsymbol{S_k} & ... & \tilde{V}_K \boldsymbol{S_K} \end{array} \right]. \tag{5.8}$$

$\boldsymbol{S_k} (1 \leqslant k \leqslant K)$ is the transmitted signal vector for the kth user with the dimension of $N \times 1$, and there is only one non-zero element in the vector $\boldsymbol{S_k}$. For the system, mathematically, this procedure can be expressed as

$$\begin{aligned} \boldsymbol{Y} &= \begin{bmatrix} \boldsymbol{y_1} \\ \vdots \\ \boldsymbol{y_k} \\ \vdots \\ \boldsymbol{y_K} \end{bmatrix} = \begin{bmatrix} \boldsymbol{H_1} \\ \vdots \\ \boldsymbol{H_k} \\ \vdots \\ \boldsymbol{H_K} \end{bmatrix} \left[\begin{array}{cccccc} \tilde{V}_1 \boldsymbol{S_1} & \cdots & \tilde{V}_k \boldsymbol{S_k} & \cdots & \tilde{V}_K \boldsymbol{S_K} \end{array} \right] + \boldsymbol{n} \\ &= \begin{bmatrix} \boldsymbol{H_1} \tilde{V}_1 \boldsymbol{S_1} & \cdots & 0 & \cdots & 0 \\ \vdots & \ddots & \cdots & \cdots & \vdots \\ 0 & \cdots & \boldsymbol{H_k} \tilde{V}_k \boldsymbol{S_k} & \cdots & 0 \\ \vdots & \cdots & \cdots & \ddots & \vdots \\ 0 & \cdots & 0 & \cdots & \boldsymbol{H_K} \tilde{V}_K \boldsymbol{S_K} \end{bmatrix} + \boldsymbol{N}. \end{aligned} \tag{5.9}$$

It can be observed from (5.9) that IUI can be totally avoided. For each user, its $N_r \times 1$ received signal vector can be expressed as

$$\boldsymbol{y_k} = \boldsymbol{H_k}\rho_k\tilde{V}_k\boldsymbol{S_k} + \boldsymbol{n_k}. \tag{5.10}$$

where ρ_k is the scaling factor to normalize the power, which is with the expression of :

$$\rho_k = \sqrt{\frac{E_{Tr}}{tr((\tilde{V}_k)\cdot(\tilde{V}_k)^H)}} \tag{5.11}$$

where E_{T_r} is the transmit power, and $tr(.)$ is the trace of a matrix.

In BD based precoding schemes, the effective channel can be expressed as: $H_E = H\tilde{V}$. Under this channel, there are N beamforming patterns generated which also equals to the dimension of the precoding matrix. If we investigate the cross correlation function (CCF) of different beam patterns p_i and p_k, we can write

$$CCF_{p_ip_k} = (H\tilde{V}(i))(H\tilde{V}(k))^* = H\tilde{V}(i)\tilde{V}(k)^*H^* \tag{5.12}$$

From the feature of SVD process, it is easy to prove that $\tilde{V}(i)$ and $\tilde{V}(k)$ are orthogonal. Thus, the CCF of two beam patterns can be derived to be zero, which means these is no correlation between two beamforming patterns. In this work,beamforming patterns can be treated as sub channels in conventional SM systems, and it is well-known that low correlation between sub channels can greatly improve the performance of SM systems. Thus, the advantage of using the BD based precoding scheme can be announced as it can generate 'i.i.d propagation channels' for spatial modulation systems even under highly correlated channel conditions (for example, TX and Rx are close to each other, which is the very common environment for millimetre wave communications systems).

The ML detector can still work under the BD frame-work. However, the task of the detector is to estimate the beamforming pattern number p rather than the antenna index, and the transmitted symbol s is jointly detected at the same time, which can

be expressed as:

$$[\hat{p}, s]_k = \arg\min_{p,l} \left(\left\| \boldsymbol{y_k} - \boldsymbol{H_k} \tilde{V}_k \boldsymbol{S_{p,m}} \right\|_F^2 \right) , \quad p \in \{1:N\} \ , \ m \in \{1:M\} \text{and } k \in \{1:K\} \tag{5.13}$$

5.3 The Massive MIMO Channel Model

In principle, in massive MIMO system, both the base station and the Rx can equip large numbers of antennas. However, in reality, limited by the device size and power assumption, only the base station can use large numbers of antenna. Thus, the massive MIMO system usually be assumed as a 'unbalanced' system [98]. In this work, under this assumption, a MU-Massive MIMO system is considered as each user is equipped with two antennas, while the base station employed 64 transmit antennas. Correspondingly, the channel model used in this work is under this assumption.

For a conventional KBSM MIMO channel model, its general expression can be composed as

$$H = R_R^{\frac{1}{2}} H_W R_T^{\frac{1}{2}}, \tag{5.14}$$

where H_W is the i.i.d. Gaussian entries with the dimension of $N_r \times N_t$, R_R ($N_r \times N_r$ dimension) and R_T ($N_t \times N_t$ dimension) are the correlation matrices of Tx and Rx receptively, and can be assumed as Toeplitz matrices when using uniform linear antennas. The Tx and Rx correlation matrices are composed by spatial correlation coefficients $T_{R/T,mn}$, which indicate the correlations between the mth and the nth antenna. As mentioned earlier, due to the widely spread of antennas in Massive MIMO systems, different cluster sets may be observed by different antennas. In [111], Wu et al. optimized the channel model by considering the evolution of clusters on the array axis. In this model, the scatter survival probability with the expression of [109], [110]

$$E_{R/T,mn} = e^{-\beta|m-n|} \tag{5.15}$$

which describes the probability that the mth antenna shares the same clusters with the nth antenna. β is the evolution factor which indicates how fast the scatters disappear.

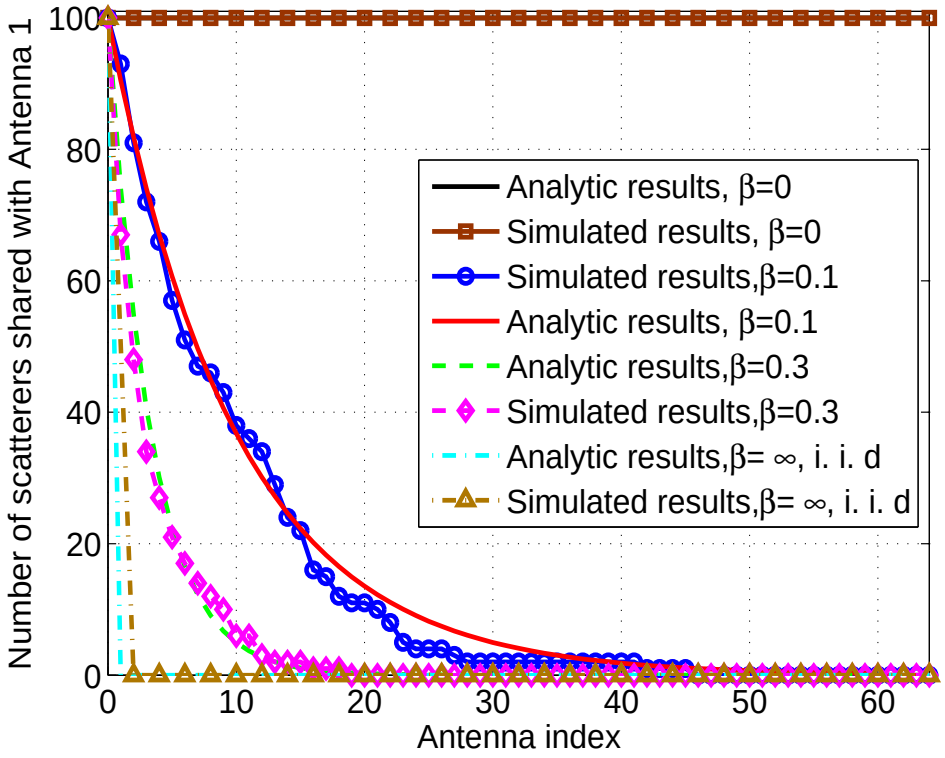

FIGURE 5.3: Number of scatterers shared with Antenna 1 in terms of antenna indices (100 initial scatterers in Antenna 1)

At the Rx, a similar analysis can also be carried out. Thus, the correlation coefficient can be expressed as:

$$R^{E}_{R/T,mn} = E_{R/T,mn} R_{R/T,mn} \tag{5.16}$$

Finally, the channel impulse response can be generated based on (5.14) and (5.16) as

$$H = (R^{E}_{R})^{\frac{1}{2}} H_W (R^{E}_{T})^{\frac{1}{2}} = (E_R \odot R_R)^{\frac{1}{2}} H_W (E_T \odot R_T)^{\frac{1}{2}} \tag{5.17}$$

where $\odot$ is the Hadamard product of two matrices. In the following chapters, this model is used to test the performance of different massive MIMO systems.

5.3.1 Evolution of Clusters in the Massive MIMO Channel Model

In Fig. 5.3, the number of scatters that other antennas shared with antenna 1 is shown considering different cluster evolution factors. It is necessary to note that when $\beta = 0$, all antennas share the same set of clusters, thus the channel model becomes a conventional MIMO channel model. When $\beta = \infty$, the channel becomes a i.i.d channel model as there in no same cluster that shared by different antennas.

5.3.2 Spatial Correlation Function

In order to describe the correlation of sub-channels, the statistic property named spatial correlation function is involved with the expression of

$$R_h(\Delta x_T,\ \Delta x_R) = E\{h_{p,q}(t)h^*_{p'q'}(t)\} \tag{5.18}$$

where Δx_R and Δx_T are antenna spacing at receiver and transmitter side.

In Fig. 5.4, the spatial correlation function of the Tx side is shown. From these two figures, it can be observed that under the massive MIMO channel model, with higher cluster evolution factors, the number of clusters shared by different antennas will be smaller. This phenomenon will further result in lower correlation between sub-channels. Compared with conventional MIMO and i.i.d MIMO channel models, the fading characteristic of this massive MIMO channel model used in this work is significantly different, which indicates the necessity to use specific massive MIMO channel models to design and test the performance of massive MIMO systems.

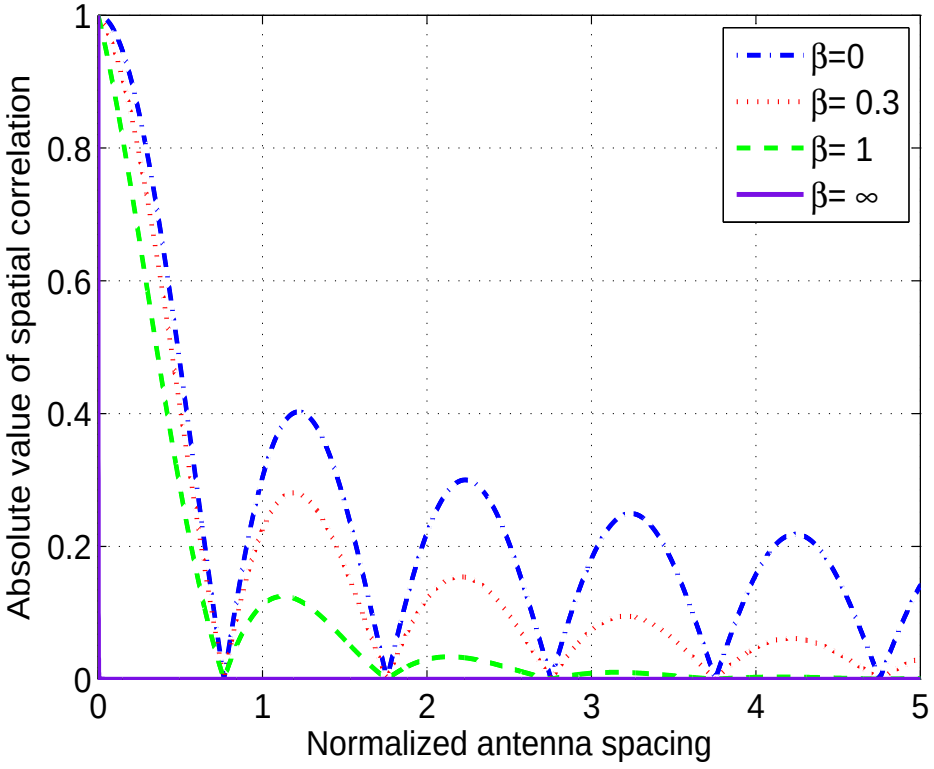

FIGURE 5.4: The spatial correlation of the KBSM for Massive MIMO system.

5.4 Theoretical BER Analysis

5.4.1 The Theoretical BER Expression of TD-MU-SM Systems

For a TD-MU-SM system, at each time instant, all Tx antennas only transmit data to one user. Thus, this case is similar to the conventional point-to-point scenario, and its theoretical BER can be approached via the union bound method mentioned in [26], [115], [116]. Here, we can define $x_{n_t,l}$ as the transmitted symbol l from antenna n_t, $l = 1, 2...M, n_t = 1, 2...N_t$. The theoretical upper-bound expression of the BER for the kth user can be expressed as

$$\mathrm{ABER_k} \leqslant \frac{1}{N_t M} \frac{1}{m} \sum_{n_t \neq \tilde{n}_t} \sum_{l \neq \tilde{l}} \left[N_H(x_{n_t,l} \to x_{\tilde{n}_t,\tilde{l}}) P(x_{n_t,l} \to x_{\tilde{n}_t,\tilde{l}} | H_k) \right] \tag{5.19}$$

where $N_H(x_{n_t,l} \to x_{\tilde{n}_t,\tilde{l}})$ is the Hamming distance between $x_{n_t,l}$ and $x_{\tilde{n}_t,\tilde{l}}$, and the pairwise error probability (PEP) that $x_{n_t,l}$ is detected to $x_{\tilde{n}_t,\tilde{l}}$ under the channel H_k is expressed as $P(x_{n_t,l} \to x_{\tilde{n}_t,\tilde{l}}|H_k)$. For a ML detector, the error only happens when $\|y_k - H_k x_{n_t,l}\|^2 > \left\|y_k - H_k x_{\tilde{n}_t,\tilde{l}}\right\|^2$. If we define $e = x_{n_t,l} - x_{\tilde{n}_t,\tilde{l}}$, the PEP can be expressed as [116]

$$P(x_{n_t,l} \to x_{\tilde{n}_t,\tilde{l}}|H_k) = P(\|y - H_k x_{n_t,l}\|^2 > \left\|y - H_k x_{\tilde{n}_t,\tilde{l}}\right\|^2) = Q(\gamma\|H_k e\|^2), \quad (5.20)$$

where γ is the signal-to-noise ratio (SNR), $Q(.)$ is the Q-function. Based on the alternative integral expression of Q-function using MGF-based approach [116], [115], (5.20) can be rewritten as

$$P(x_{n_t,l} \to x_{\tilde{n}_t,\tilde{l}}|H_k) = \frac{1}{\pi}\int_0^{\pi/2} M(\gamma\frac{1}{\sin^2\theta})d\theta. \quad (5.21)$$

In (5.21), $M(.)$ is the MGF of $\|H_k e\|^2$, which can be expressed as

$$M(s) = \prod_{j=1}^{N_r}(1 - s\lambda_i\mu)^{-1}, \quad (5.22)$$

where λ_i is the eigenvalue of R_R and μ is the eigenvalue of $ee^H R_T$. Substituting (5.21), (5.22) into (5.19), the final expression of the theoretical BER expression for the kth user of a TD-MU-SM is

$$ABER_k \leqslant \frac{1}{\pi}\frac{1}{N_t M}\frac{1}{m}\sum_{n_t \neq \tilde{n}_t}\sum_{l \neq \tilde{l}}\left[N_H(x_{n_t,l} \to x_{\tilde{n}_t,\tilde{l}})\int_0^{\frac{\pi}{2}}\prod_{j=1}^{N_r}(1 - \frac{\gamma}{\sin^2\theta}\lambda_i\mu)^{-1}d\theta\right] \quad (5.23)$$

5.4.2 The Theoretical BER Expression of BD-MU-SM Systems

For the BD-MU-SM system, we can still follow the similar principle as stated above to derive the theoretical BER expression. However, due to some data are mapped to the beamforming pattern index, the error case should be expressed as $x_{n_b,l} \to x_{n_{\tilde{b}},\tilde{l}}$,

which means the transmitted symbol l using the beamforming pattern n_b is detected to symbol $\tilde{l}$ carried by the $n_{\tilde{b}}$ beamforming pattern, $(l, \tilde{l}) = 1, 2...M; (n_b, n_{\tilde{b}}) = 1, 2...N$.

The theoretical upper-bound expression of the BER for the kth user can be expressed as

$$\mathrm{ABEP_k} \leqslant \frac{1}{\mathrm{NM}} \frac{1}{\mathrm{m}} \sum_{\mathrm{n_b} \neq \tilde{\mathrm{n}}_\mathrm{t}} \sum_{\mathrm{l} \neq \tilde{\mathrm{l}}} \left[\mathrm{N_H}(\mathrm{x_{n_b,l}} \rightarrow \mathrm{x_{n_{\tilde{b}},\tilde{l}}}) \mathrm{P}(\mathrm{x_{n_b,l}} \rightarrow \mathrm{x_{n_{\tilde{b}},\tilde{l}}} \left| \mathrm{H_E{}^k} \right.) \right]. \tag{5.24}$$

where $N_H(x_{n_b,l} \rightarrow x_{n_{\tilde{b}},\tilde{l}})$ is the Hamming distance between $x_{n_b,l}$ and $x_{n_{\tilde{b}},\tilde{l}}$, and $P(x_{n_b,l} \rightarrow x_{n_{\tilde{b}},\tilde{l}} \left| {H_E}^k \right.)$ is the PEP of the error that occurs under the effective channel H_E. From (5.9), we can write the expression of ${H_E}^k$ as

$${H_E}^k = H_k \tilde{V}_k = R_{R,k}^{\frac{1}{2}} H_W R_{T,k}^{\frac{1}{2}} \tilde{V}_k = R_{R,k}^{\frac{1}{2}} H_W (R_{T,k} \tilde{V}^2)^{\frac{1}{2}}. \tag{5.25}$$

Thus, for the effective channel, its Rx correlation matrix is not changed, but the Tx correlation matrix is changed by the precoding matrix, and the Tx effective correlation matrix is $R_{E,T,k} = R_{T,k} \tilde{V}^2$. For the ML detector of the BD-MU-SM system, the error will occur under the case that $\left\| y_k - {H_E}^k \rho_k x_{n_b,l} \right\|^2 > \left\| y_k - {H_E}^k \rho_k x_{n_{\tilde{b}},\tilde{l}} \right\|^2$. We can also defined the error vector $e = x_{n_b,l} - x_{n_{\tilde{b}},\tilde{l}}$.

The expression of PEP in (5.24) can be expressed as

$$\begin{aligned} P(x_{n_b,l} \rightarrow x_{n_{\tilde{b}},\tilde{l}} \left| {H_E}^k \right.) &= P(\left\| y_k - {H_E}^k \rho_k x_{n_b,l} \right\|^2 > \left\| y_k - {H_E}^k \rho_k x_{n_{\tilde{b}},\tilde{l}} \right\|^2) \\ &= Q(\gamma_E \left\| {H_E}^k e \right\|^2), \end{aligned} \tag{5.26}$$

γ_E is the effective SNR, which can be expressed as $\gamma_E = \rho_k^2 \gamma$. Similar to the TD-MU-SM case, the PEP can be expressed by the MGF-based approach in (5.21) using the MGF of $\left\| {H_E}^k e \right\|^2$. However, for the BD case, the value of μ in (5.22) is the eigenvalue of $ee^H R_{E,T,k}$. Finally, we can express the final theoretical BER expression for the kth user of a BD-MU-SM as

Finally, we can express the final theoretical BER expression for the kth user of a BD-MU-SM as

$$ABER_k \leqslant \frac{1}{\pi}\frac{1}{NM}\frac{1}{m}\sum_{n_b \neq \tilde{n}_b}\sum_{l \neq \tilde{l}}\left[N_H(x_{n_b,l} \to x_{\tilde{n}_b,\tilde{l}})\int_0^{\frac{\pi}{2}}\prod_{j=1}^{N_r}(1-\frac{\gamma_E}{\sin^2\theta}\lambda_i\mu)^{-1}d\theta\right] \quad (5.27)$$

5.5 Simulation Results and Discussions

In this section, different simulation results are used to evaluate the performance of SM systems under the massive MIMO channel model for multiple user cases. For all simulations, the base station is assumed to be equipped with 64 transmit antennas, and for each user, 2 receive antennas are equipped. For a fair comparison, we assume that the transmit power and the data rate of each user are the same. All simulation results are obtained through Monte Carlo simulation. For each point in following figures, results of 10 runs (each run transmits 100000 symbols) are averaged to get the final value.

5.5.1 Comparison between Theoretical Results and Simulation Results

In Fig. 5.5, theoretical results of BER performance for the TD-MU-SM and BD-MU-SM systems under the massive channel model, are compared with simulation results considering different cluster evolution factors β. For both systems, the data rate is m=7 bits/symbol/user. For the TD-SM system, 6 bits are carried by antenna indexes and the BPSK modulation scheme is employed to carry the other bit. For the BD-SM system, 32 beamforming patterns are used by each user, thus the index can carry 5 bits information, the other 2 bits will be carried by QPSK modulation symbols.

From this figure, we can obtain following observations. This figure indicates an excellent approximation of the theoretical derivation with simulation results for all systems under different channel configurations, especially in the high SNR range where SNR

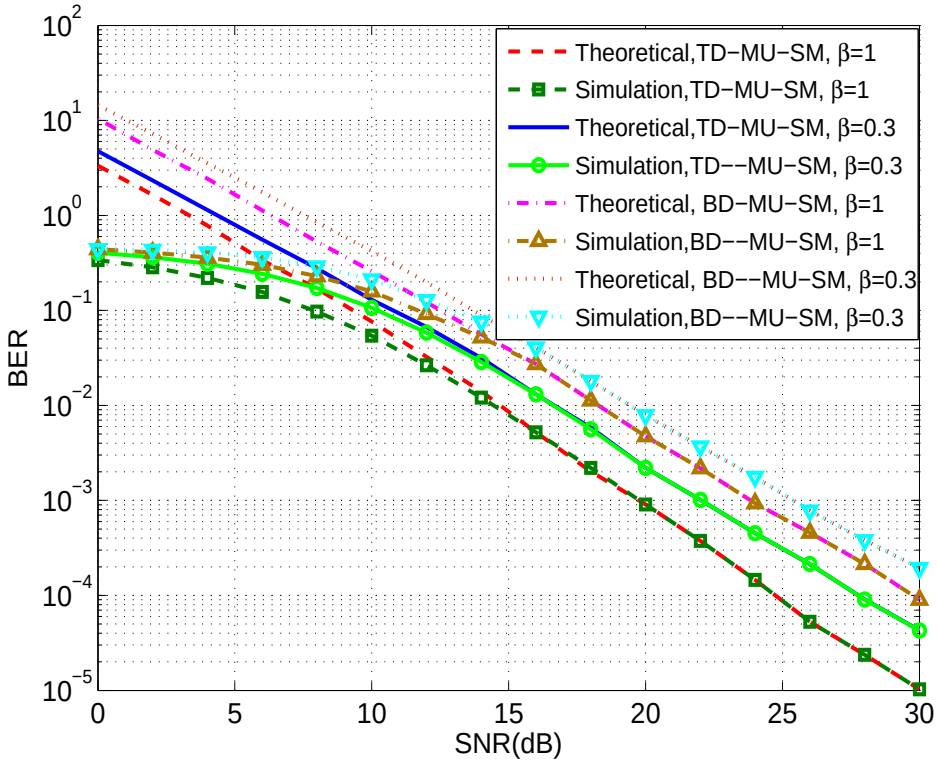

FIGURE 5.5: Theoretical and simulated BER results of SM systems under the KBSM MIMO channel model.

$\geq$ 15 dB. Based on this comparison, we can conclude that the theoretical BER upper-bound offers a reasonable accuracy, which indicates the correctness of the theoretical derivation.

5.5.2 Comparison between TD-MU-SM and DB-MU-SM in Massive MIMO Systems

Also, from Fig.5.5, it is clear that with the same data rate and using the same transit power for each user, the TD-MU-SM system can offer better performance in terms of BER than the BD-MU-SM system even when the BD system is with the CSI at the Tx side.

That is because for TD-MU-SM systems, at each time instant, only one antenna transmits signals to one user, thus the IUI can be totally avoided. While for the BD-MU-SM system, as the precoding matrix is applied to the transmitted signal, which

leads to a loss of transmit power for IUI cancellation. Consequently, the effective power for the signal transmission in BD scheme is lower.

However, it is necessary to point out that the total system data rate for the BD-MU-SM system is higher than the TD system ($K \times m$ Vs. m) with the expense of using more transmit power. Thus, for the TD scheme, in order to obtain the same data rate, it should use higher order modulation schemes.

From this analysis, we can observe that the TD scheme is suitable to light-load MU systems that require low system complexity and high accuracy, while the BD scheme is suitable for heavy-load systems that require high system capacity.

5.5.3 Impact of Scatters Evolution Factors on TD-MU-SM and DB-MU-SM Massive MIMO Systems

In Fig. 5.5, we can find that under the channel condition with the higher cluster evolution factor β, both the TD-MU-SM and BD-MU-SM systems can obtain the better BER performance compared with the case that of lower clusters evolution factors.

We can explain this phenomena from the knowledge of Section III. It has been proved by Fig. 5.3 that with the higher clusters evolution factors, the probability that different antennas observe different sets of clusters will be increased, which results in lower correlation between different sub-channels as shown in Fig. 5.4. Under the TD scheme, lower correlation between sub-channels make it easier for the Rx to correctly detect the active antennas, thus the system BER performance is better, as the TD-SM scheme can be treated as a conventional SM system. While under the BD scheme, the lower correlation between sub-channels decreases the difficulty to eliminate the IUI, which can be represented by the lower power assumption of precoding matrix, thus more power can be used to transmit effective data and the BER performance can be improved.

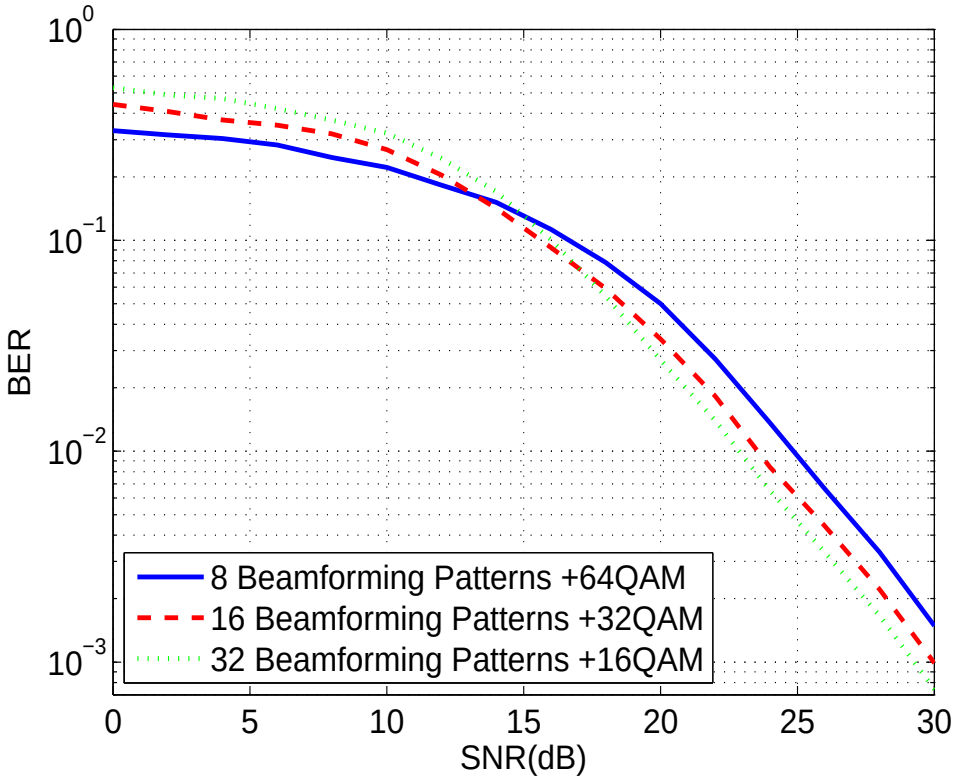

FIGURE 5.6: BER performance of BD-MU-SM systems using different systems settings, $\beta = 1$.

5.5.4 BER Performance of BD-MU-SM Systems Under Different System Settings and Scatters Evolution Factors

In Fig. 5.6 and 5.7, the BER performance of BD-MU-SM system is investigated under different system settings and different channel assumptions ($\beta = 0.3$ and 1). For the system, it is assumed that there are 8 users, and the data rate of each user is m=9 bits/symbol.

Comparing these two figures, again, we can find that the higher clusters evolution factor results in better BER performance. In Fig. 5.6, we can find that in the low SNR range, using fewer beamforming patterns to carry information results in the better BER performance. While at the high SNR range, using more beamforming patterns and lower order modulation schemes can achieve the better BER performance. And a crossing roughly at 15 dB can be found.

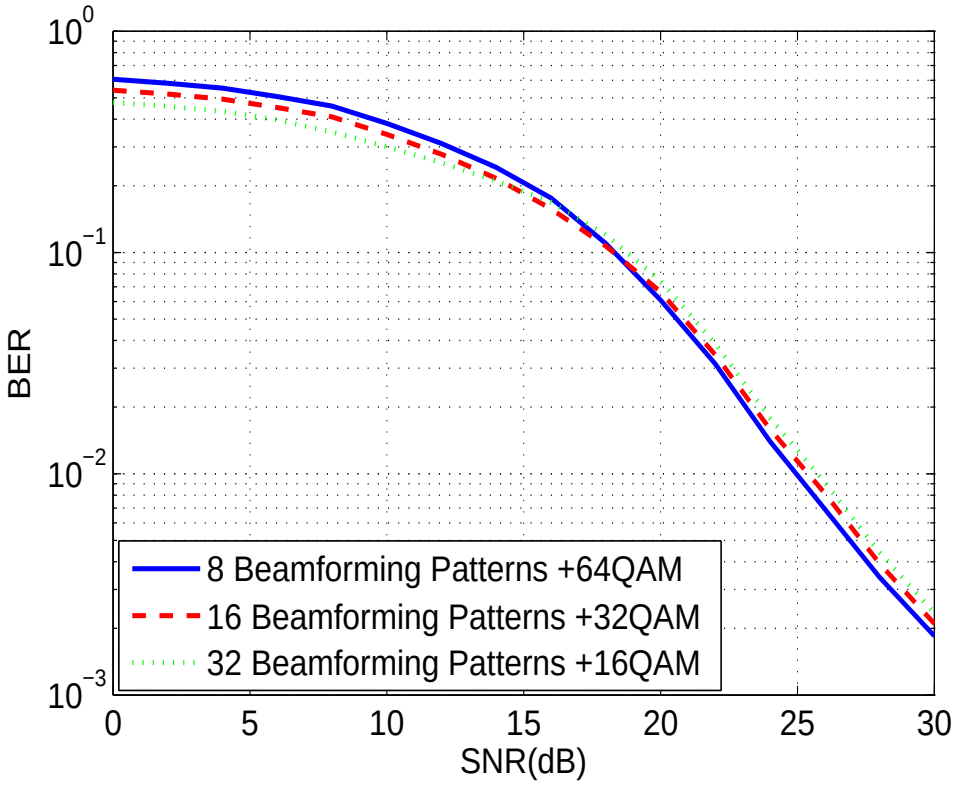

FIGURE 5.7: BER performance of BD-MU-SM systems using different systems settings, $\beta = 0.3$

Regarding these phenomena, we can give the following explanation. When using the BD scheme, smaller beamforming pattern numbers mean power is more concentrated, and as the number of patterns is small, the task of the detector will be easier which decreases the probability of error occur. Bur at the high SNR range, the benefit of lower index detection error is overstepped by the use of lower order modulation schemes. Thus, at the high SNR range, using larger numbers of beamforming patterns plus lower modulation schemes can get better perform in BER.

If we investigate Fig. 5.7, we can get the similar conclusion. However, compared with the case of higher cluster evolution factors, the difference between different system settings is not significant, and the position of the crossing point is located nearly at 20dB. The reason behind this phenomenon is the high correlation between sub-channels. Due to the high correlation, the benefit from using beamforming patterns to carry information is decreased. In this case, the system performance is mainly

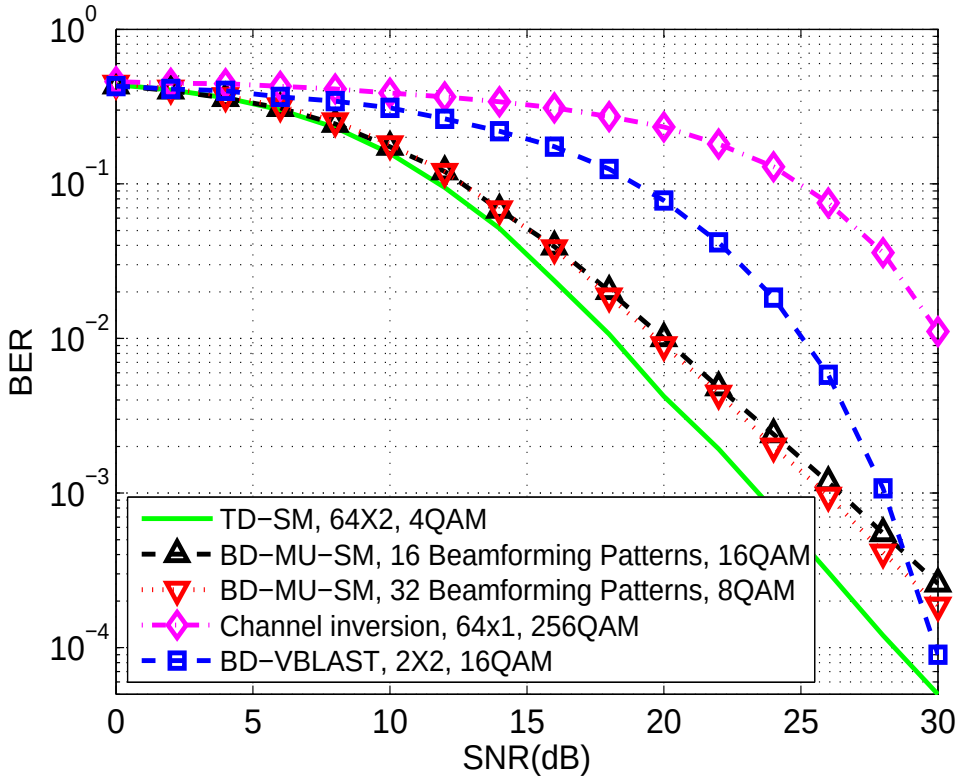

FIGURE 5.8: BER performance of different systems with 4 users, $\beta = 0.3$, data rate= 8bits /symbol/user.

determined by the SNR, thus, different system settings result in relative similar performance.

5.5.5 Comparison Between Different MU Massive MIMO Solutions

In Figs. 5.8–5.11, the BER performance of the TD-MU-SM system and the BD MU-SM system are compared with the V-BLAST technologies and the conventional channel inversion method under the massive channel model with different data rates and numbers of users. In all simulations, the evolution factor for the channel is configured as $\beta = 0.3$.

For the V-BLAST system, in order to make the comparison fair, the BD precoding scheme is also used at the Tx side to eliminate inter-user interference and the ML detector is employed as the Rx algorithm. As the V-BLAST system requires that the

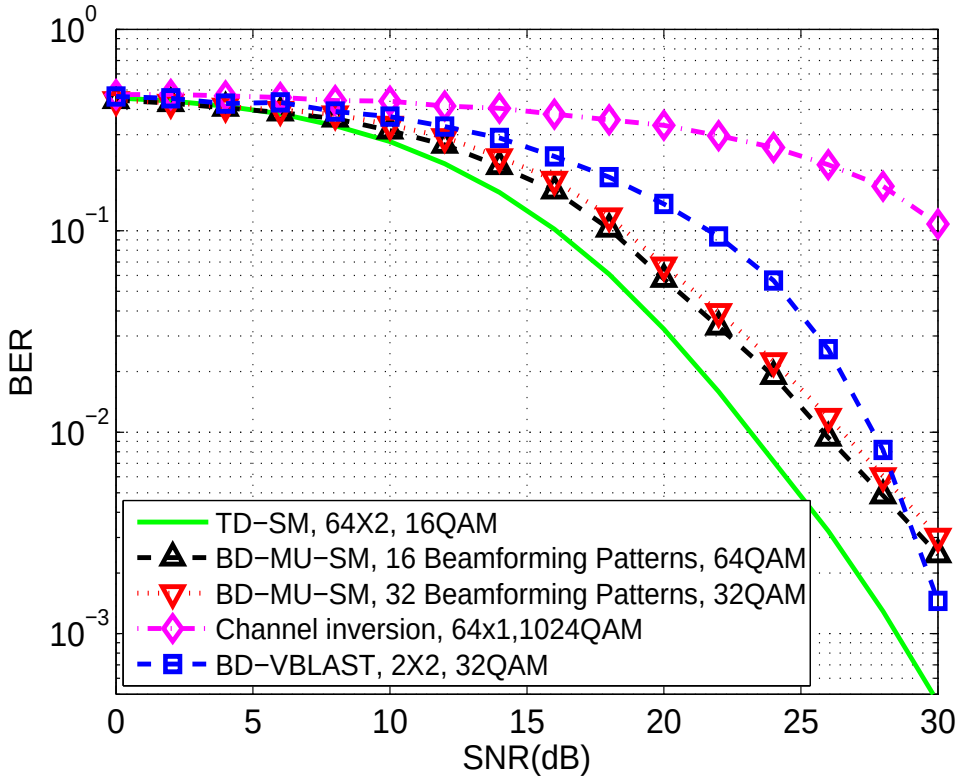

FIGURE 5.9: BER performance of different systems with 4 users, $\beta = 0.3$, data rate= 10bits /symbol/user..

receive antenna number should not be smaller than the number of layers, the number of the beamforming patterns for the V-BLAST system is configured as two for each user.

For the channel inversion method, the precoding matrix is given as the MoorePenrose pseudoinverse of the channel matrix H, which can be expressed as $W = H^H(HH^H)^{-1}$, and in this system, only single receive antenna deployed in each user.

From all figures, firstly, it is clear that for all systems, when working under lower data rates, the system performance is better as the power averaged to each bit is higher. Secondly, for both BD-SM and BD-V-BLAST systems, when the number of users increases, the system performance is worse.

The reason behind this phenomenon is with more users, the system would use more power to eliminate the inter-user-interference. As the transmit power for the system

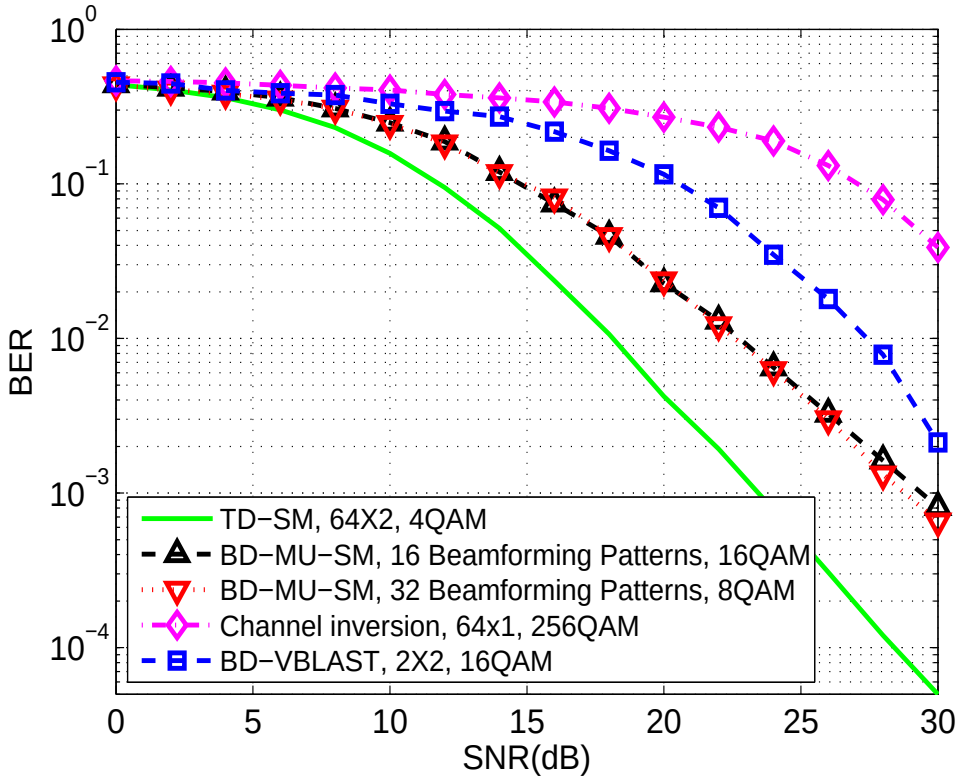

FIGURE 5.10: BER performance of different systems with 16 users, $\beta = 0.3$, data rate= 8 bits /symbol/user..

is fixed, the power for transmitting effective signals will be decreased. So the system performance will be worse.

For the TD-SM system, as there is only one user being served, its BER performance is not affected by the number of users. Compared with other two technologies, the TD-SM scheme can obtain the best performances under all cases. But for the TD-SM scheme, the system's total data rate is much lower than other systems under heavy-load scenarios as it can only serve one user at each time slot.

Compared with BD-SM systems and BD-V-BLAST systems, the BD-SM system can achieve great enhancement in BER performance at the range of SNR $<$ 28 dB. For the V-BLAST system, under the case of low date rate and small number of users, it can obtain better performance at the extremely high SNR range (SNR >28 dB), however, when under the case of high data rate with large number of users, the BD-SM system is still superior than the BD-V-BLAST system.

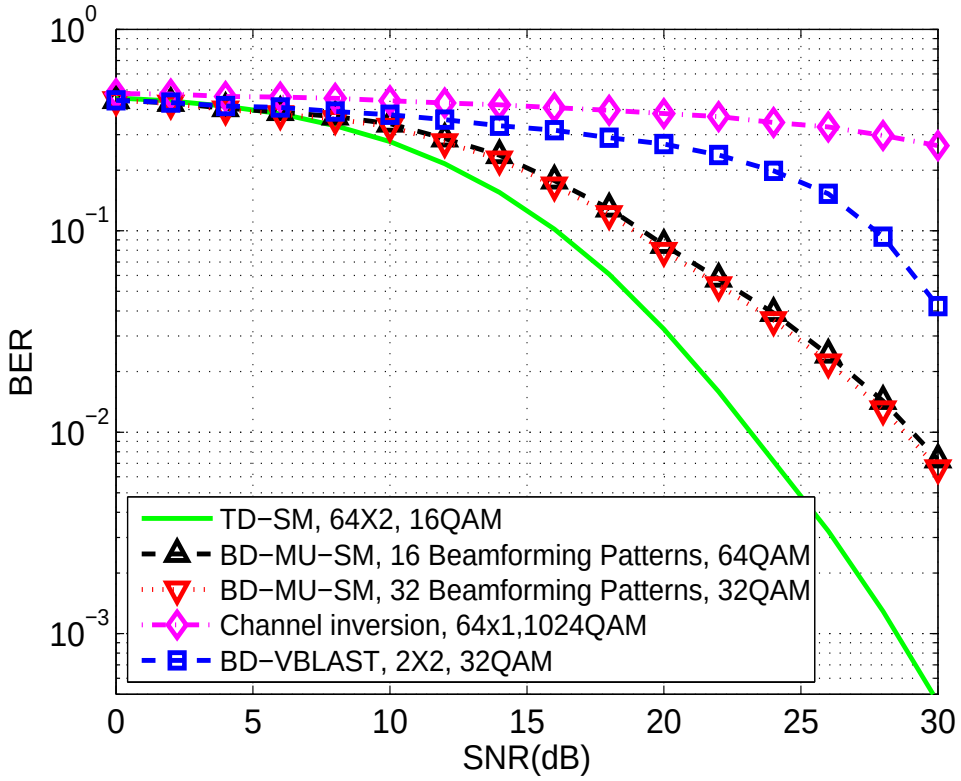

FIGURE 5.11: BER performance of different systems with 16 users, $\beta = 0.3$, data rate= 10bits /symbol/user.

Compared with the conventional channel inversion method, the advantage of the BD base precoding scheme can be announced. Benefited from supporting multiple receive antennas, the BER performance of all BD based systems is superior as the result of receive diversity gain.

5.6 Summary

In this chapter, we investigated the performance of SM systems under a KBSM massive MIMO channel model with different system settings and channel configurations. Based on our research, we can conclude that higher evolution factors values of scatters can lead to better BER performance for SM systems due to the lower correlation between sub-channels. TD-MU-SM system can obtain better BER performance with the cost of lower system data rate. The BD-MU-SM system can get better trade-off between the system data rate and the BER performance, which is a better option for

heavy loaded MU wireless communication systems. Compared with BD-V-BLAST and conventional channel inversion systems, both SM systems can obtain better BER performance considering different data rates and numbers of users under low SNR range. From all simulation results, the advantage of using SM for massive MIMO systems in terms of system performance, complexity and flexibility can be declared.

Chapter 6

Conclusions and Future Work

For this thesis, a study on the BER performance of SM under carefully selected channel models of typical 5G scenarios are presented. This work clearly reflects the trends and focus of the research on 5G wireless technologies. In this concluding chapter, all the key findings of previous chapters will be summarised, and some interesting future research directions will be suggested.

6.1 Summary of Results

In Chapter 3, the BER performance of SM is investigated under a 3D MIMO channel model of V2V scenarios. Different system settings and propagation conditions have been considered, and their influences on system performance are investigated. The theoretical ABER expression is derived through the union-bound method, and verified with simulation results to prove its accuracy. Theoretical and simulation results indicate that the lower modulation scheme can offer better BER performance due to the higher power allocated to each bit. When under the high VTD scenario, the SM system can get the better BER performance compared with that under the low VTD scenario. The higher moving speed, which is represented by the higher Doppler shift, can result in the worse BER performance due to the higher outage probability. Compared with 2D channel models, the BER performance of SM system is superior

when it is under the 3D model. That is because the extended vertical dimension which results in the lower correlations between sub-channels. Compared with other conventional MIMO technologies including the spatial multiplexing and the spatial diversity, the advantage of SM in terms of BER performance, spectral efficiency and system can be announced.

In Chapter 4, a non-stationary wideband MIMO channel for HST scenarios is used to investigate the performance of SM systems. Based on measurement results, the channel model is further configured into two sub-scenarios depending on the distance between BS and Rx. Non-ideal channel estimation is considered to make this work more realistic. Accurate theoretical ABER expressions are derived which can reflect the influence of channel model's characteristic. A novel statistical property named stationary interval in terms of the STCF is presented to accurately describe the non-stationary behaviour of the channel model. Its influence on the performance of the SM system is thoroughly investigated. From all simulation and theoretical results, it can be observed that the BER performance of SM systems shows a timing-varying behaviour due to the non-stationary characteristic of the HST channel model. Within the stationary interval, the channel can be treated as stationary and the system performance also shows stationary behaviour within this time instant. Besides, it can be observed that the BER performance of SM systems are mainly affected by the correlation between sub-channels, ISI, Doppler shift and channel estimation delay when under this HST channel model.

In Chapter 5, under a KBSM specifically designed for massive MIMO channels, the BER performance of SM system is thoroughly investigated for MU scenarios. MU-Massive MIMO systems constructed with TDMA-MU and BD-MU schemes are considered. Theoretical ABER expressions for both schemes are derived. Verified by simulation results, the reasonable accuracy of these two theoretical BER frameworks can be declared. The channel model considers the evolution factor which represents the birth-death process of clusters shared by two antennas. Based on the investigation of this influence, it can be observed that higher evolution factors can lead to the better BER performance due to the lower correlation between sub-channels. Compared with

the BD-MU-SM system, the TD-MU-SM system can get the better BER performance with the cost of the lower system data rate. The BD-MU-SM system can offer better trade-off between system data rate and BER performance, which is a better option for heavy load MU wireless communication systems. Compared with BD-VBLAST system and the conventional channel inversion method, the advantage of SM in the system performance, complexity and flexibility can be declared.

6.2 Future Research Directions

6.2.1 Investigation on SM in System Level

SM is a physical layer transmit technology, it will finally be embedded into a communications system. How this technology affects the system level performance is still an uncovered area on the research of SM. The researches on this topic is meaningful to the development of 5G systems. This study can be started by transplanting SM technologies into system level simulators such as LTE-A system simulators. Then, the investigation on the influence of using SM on different system level performance criteria, such as system throughput under different system settings and scenarios, can be carried out. The next step is to study the optimisation problem of using SM in wireless communications systems. From this research, the methodology of optimising SM technology to improve system performance can be established, which will be with the guideline meaning to the development of 5G systems.

6.2.2 Combination of Millimetre Wave Communications and SM

In recent years, as a result of the rapid growth of high-speed wireless data access, there is a serious bandwidth shortage all over the world. Nowadays, spectrum recourse allocated to cellular wireless communications are mainly within the range between 700 MHz and 2.6 GHz. It is reported that all these spectrum resource will be depleted

within few years. It is necessary to find new spectrum resources for the future wireless commutations systems. Millimetre wave communications is a promising option as it can offer large mount of available bandwidth. Besides, due to the wavelength is short, much smaller antenna element can be used, which make it easier to combine with massive MIMO technology.

In order to support the development of 5G system, it is necessary to investigate the performance of the combination of SM and millimetre wave technology. However, there are still lots of challenges for the combination. For example, due to the high frequency, the millimetre wave communications system suffers serious path loss, thus the system can only work for short range with strong LoS propagation. Under this condition, all sub-channels are highly correlated, which is harmful to SM. How to make SM work under this propagation scenario is a challenging but meaningful task.

6.2.3 SM for Wireless Body Area Networks

Wearable device is one of the most attracting research topics in recent years, and there are plenty of products available nowadays. In 5G systems, different wearable devices will be organised into networks names wireless body area networks (BANs). Wireless BANs and related device-to-device communications are key issues in the research of 5G. For BANs, the high spectral and energy efficiency are critically required. Besides, due to some devices are under a movement, it is required that communications technologies with high robustness should be used. SM is a promising technology to fulfil these requirements of body area networks. Investigation on the performance of SM in BANs will be meaningful to the research on future 5G systems.

6.2.4 Index Modulation, Beamforming Pattern Modulation, ... and X Modulation

SM was only treated as a multiple antennas technology at the beginning of its history, which uses the activated antenna index to carry extra data. As time goes by,

researches on SM indicate that not only antenna index can be used to carry extra information, there are lot of resource can be used to encode data. For example, in [148], some researchers found that in a OFDM system, some information can be mapped to the index of sub carriers, which is named as the index modulation. In our work of Chapter 6, it is also found that data can be carried by beamforming patterns rather than antenna indexes. So at this stage, we should say that SM is not only a multiple antenna technology any more. It is a methodology and a philosophy to transmit data through some unexploited resource. Here, we end this thesis with the word of X modulation. What will be the next X?

References

[1] Guglielmo Marconi. In Wikipedia. Retrieved Mar. 29, 2013, from http://http://en.wikipedia.org/wiki/Guglielmo_Marconi.

[2] V. A. Dubendorf, *Wireless Data Technologies*, Chischester, UK, John Wiley & Sons, 2003.

[3] A. F. Molisch, *Wireless communications*, 3rd Edition, Chischester, UK, John Wiley & Sons, 2010.

[4] Q. Bi, G. I. Zysman, and H. Menkes, "Wireless mobile communications at the start of the 21st century," *IEEE Commun. Mag.*, Jan. 2001, pp. 110–16.

[5] 3GPP, TR36.913, V10.0.0, "3GPP specification: Requirements for further advancements for E-UTRA (LTE Advanced) (Release 10)," Apr. 2011.

[6] S. Sesia, I. Toufik and M. Baker, *LTE: the UMTS long term evolution, from theory to practice*, Chischester, UK: John Wiley & Sons, 2009.

[7] A. Osseiran, F. B. V. Boccardi, K. Kusume, P. Marsch, M. Maternia, O. Queseth, M. Schellmann, H. Schotten, H. Taoka, H. Tullberg, M. Uusitalo, B. Timus and M. Fallgren, "Scenarios for 5G mobile and wireless communications: the vision of METIS project," *IEEE Commun. Mag.*, vol. 52, no. 5, pp. 26–35, May 2014.

[8] Ericsson, *More than 50 billion connected devices*, White Paper, February 2011, Online: http://www.ericsson.com/res/docs/whitepapers/wp-50-billions.pdf.

[9] C.-X. Wang, F. Haider, X. Gao, X.-H. You, Y. Yang, D. Yuan, H. Aggoune, H. Haas, S. Fletcher, and E. Hepsaydir, "Cellular architecture and key technologies for 5G wireless communication networks," *IEEE Commun. Mag.*, vol. 52, no. 2, pp. 122–130, Feb. 2014.

[10] S. Mumtaz, K. M. S. Huq, and J. Rodriguez, "Direct mobile-to-mobile communication: Paradigm for 5G," *IEEE Wireless Commun.*, vol. 21, no. 5, pp. 14–23, Oct. 2014.

[11] J. G. Andrews, S. Buzzi, W. Choi, S. Hanly, A. Lozano, A. C. Soong, and J. C. Zhang, "What will 5G be?," *IEEE J. Sel. Areas Commun.*, vol. 32, no. 6, pp. 1065–1082, 2014.

[12] Website: UK-China Science Bridges R&D on (B)4G Wireless Mobile Communications, http://www.ukchinab4g.ac.uk/.

[13] FP7 European Project 317669 METIS (Mobile and Wireless Communications Enablers for the Twenty-Twenty Information Society) 2012, https://www.metis2020.com/.

[14] FP7 European Project 318555 5G NOW (5th Generation NonOrthogonal Waveforms for Asynchronous Signalling) 2012, http://www.5gnow.eu/.

[15] F. Boccardi, R.W. Heath, A. Lozano, T.L. Marzetta, "Five disruptive technology directions for 5G," *IEEE Commun. Mag.*, vol. 52, no. 2, pp. 74–80, Feb. 2014.

[16] N. Bhushan, J. Li, D. Malladi, R. Gilmore, D. Brenner, A. Damnjanovic, R. T. Sukhavasi, C. Patel, and S. Geirhofer, "Network densification: the dominant theme for wireless evolution into 5G," *IEEE Commun. Mag.*, vol. 52, no. 2, pp. 82–89, Feb. 2014.

[17] B. Bangerter, S. Talwar, R. Arefi, and K. Stewart, "Networks and Devices for the 5G Era," *IEEE Commun. Mag.*, vol. 52, no. 2, pp. 90–96, Feb. 2014.

[18] Chih-Lin I, C. Rowell, S. Han, Z. Xu, G. Li and Z. Pan, "Towards Green and Soft: A 5G perspective," *IEEE Commun. Mag.*, vol. 52, no. 2, pp. 66–73, Feb. 2014.

[19] W. H. Chin, Z. Fan, and R. Haines,"Emerging technologies and research challenges for 5G wireless networks," *IEEE Wireless Commun.*, vol. 21, no. 2, pp. 106–112, Apr. 2014.

[20] P. Demestichas, A. Georgakopoulos, D. Karvounas, K. Tsagkaris, V. Stavroulaki, Jianmin Lu, Chunshan Xiong and Jing Yao,"5G on the Horizon: Key challenges for the radio-access network," *IEEE Veh. Tech. Mag.*, vol. 8, no. 3, pp. 47–53, Sept. 2013.

[21] M. D. Renzo, H. Haas and P. Grant, "Spatial modulation for multiple-antenna wireless systems: a survey," *IEEE Commu. Mag.* , vol. 49, no. 12, pp.182–191, Dec. 2011.

[22] R. Mesleh, H. Haas, S. Sinanovic, C. W. Ahn, and S. Yun, "Spatial modulation," *IEEE Trans. Veh. Technol.*, vol. 57, no. 4, pp. 2228–2241, July. 2008.

[23] M. Di Renzo, H. Haas, A. Ghrayeb, S. Sugiura, and L. Hanzo, "Spatial modulation for generalized MlMO: Challenges, opportunities, and implementation,.

[24] J. Jeganathan, A. Ghrayeb, and L. Szczecinski, "Spatial modulation: optimal detection and performance analysis," *IEEE Commun. Lett.,* vol. 12, no. 8, pp. 545–547, Aug. 2008.

[25] J. Jeganathan, A. Ghrayeb, L. Szczecinski, and A. Ceron, "Space shift keying modulation for MIMO channels," *IEEE Trans. Wireless Commun.*, vol. 8, no. 7, pp. 3692–3703, July. 2009.

[26] M. Di. Renzo and H. Haas, "Bit error probability of SM-MIMO over generalized fading channels," *IEEE Trans. Veh. Technol.*, vol. 61, no. 3, pp. 1124–1144, Mar. 2012.

[27] M. Di Renzo and H. Haas, "Space shift keying (SSK-) MIMO over correlated Rician fading channels: Performance analysis and a new method for transmit-diversity," *IEEE Trans. Commun* , vol. 59, no. 1, pp. 116–129, Jan. 2011.

[28] M. Di Renzo and H. Haas, "A general framework for performance analysis of space shift keying (SSK) modulation for MISO correlated Nakagami-m fading channels," *IEEE Trans. Commun* , vol. 58, no. 9, pp. 2950–2603, Sept. 2010.

[29] C.-X. Wang, X. Hong, X. Ge, X. Cheng, G. Zhang, and J. S. Thompson, "Cooperative MIMO channel models: a survey," *IEEE Commun. Mag.*, vol. 48, no. 2, pp. 80–87, Feb. 2010.

[30] E. Telatar, "Capacity of multi-antenna Gaussian channels," *European Transaction Telecommunication*, vol. 10, no. 6, pp. 558–595,November/December 1999.

[31] J. Mietzner, R. Schober, L. Lampe, W. H. Gerstacker, and P. A. Hoeher, "Multiple-antenna techniques for wireless communications-A comprehensive literature survey," IEEE Commun. Surv. Tut., vol. 11, no. 2, pp. 87–105, 2nd Quart. 2009.

[32] P. Wolniansky, G. Foschini, G. Golden, and R. Valenzuela, " V-BLAST: an architecture for realizing very high data rates over the richscattering wireless channel," in *Proc. URSI ISSSE*, Pisa, Italy, Sep. 29-Oct. 2, 1998, pp. 295–300.

[33] S. Alamouti, "A simple transmit diversity technique for wireless communications," *IEEE J. Sel. Areas Commun.* , vol. 16, no. 8, pp. 1451–1458, Oct. 1998.

[34] A. Goldsmith, S. Jafar, N. Jindal, and S. Vishwanath, "Capacity limits of MIMO channels," *IEEE J. Sel. Areas Commun.*, vol. 21, no. 5, pp. 684–702, Jun. 2003.

[35] Y. Chau and S.-H. Yu, "Space modulation on wireless fading channels," in *Proc. IEEE VTC'01-Fall*, Atlantic City, USA, 07-11 Oct. 2001, pp. 1668–1671.

[36] S. Song, Y. L. Yang, Q. Xiong, K. Xie, B.-J. Jeong, and B. L. Jiao, "A channel hopping technique I: Theoretical studies on band efficiency and capacity," in *Proc. IEEE ICCAS'04*, Chengdu, China, 27-29 Jun. 2004, pp. 229–233.

[37] R. Y. Mesleh, H. Haas, C. W. Ahn, and S. Yun, Interchannel interference avoidance in MIMO transmission by exploiting spatial information, in *Proc. IEEE Int. Symp. Pers. Indoor Mobile Radio Commun.*, Berlin, Germany, 11-14 Sept. 2005, pp. 141–145.

[38] R. Y. Mesleh, H. Haas, C. W. Ahn, and S. Yun, "Spatial modulation-OFDM," in *Proc. Int. OFDM Workshop*, Hamburg, Germany, Aug. 2006, pp. 288–292.

[39] S. Ganesan, R. Y. Mesleh, H. Haas, C. W. Ahn, and S. Yun, "On the performance of spatial modulation OFDM," in /em Proc. Asilomar Conf. Signals Syst. Comput., Pacific Grove, USA, Oct. 2006, pp. 1825–1829.

[40] R. Y. Mesleh, H. Haas, C. W. Ahn, and S. Yun, "Spatial modulation-a new low complexity spectral efficiency enhancing technique," in *Proc. IEEE Int. Conf. Commun. Netw. China*, Beijing, China, 25-27 Oct. 2006.

[41] R. Y. Mesleh, S. Ganesan, and H. Haas, "Impact of channel imperfections on spatial modulation OFDM," in *Proc. IEEE PIMRC07*, Athens Greece, 3–7 Sep. 2007.

[42] S. Sugiura, S. Chen, and L. Hanzo, "A universal space-time architecture for multiple-antenna aided systems," *IEEE Commun. Surv. Tut.*, vol. 14, no. 2, pp. 401–420, 2nd Quart. 2012.

[43] A. Younis, W. Thompson, M. Di Renzo, C.-X. Wang, M. A. Beach, H. Haas, and P. M. Grant, "Performance of spatial modulation over measured real-world channel," in *Proc. IEEE VTC13-Fall*, Las Vegas, USA, Sept. 2013.

[44] N. Serafimovski, A. Younis, R. Y. Mesleh, P. Chambers, M. D. Renzo, C.-X. Wang, P. M. Grant, M. A. Beach, and H. Haas, "Practical implementation of spatial modulation," *IEEE Trans. Vehi. Technol.*, vol. 62, no. 9, pp. 4511–4523, Nov. 2013.

[45] R. Y. Mesleh, S. Engelken, S. Sinanovic, and H. Haas, "Analytical SER calculation of spatial modulation", in *Proc. IEEE Int. Symp. Spread Spectrum Technol. Appl.*, Bologna, Italy, 25-29 Aug. 2008, pp. 272–276.

[46] T. Handte, A. Muller, and J. Speidel, "BER analysis and optimization of generalized spatial modulation in correlated fading channels," in *Proc. IEEE VTC'09-Fall*, Anchorage, USA, 20-23 Sep. 2009, pp. 1–5.

[47] Alshamali and B. Quza, "Spatial modulation: Performance evaluation in Nakagami fading channels," in *Proc. IEEE GCC Conf. Exhibit.*, Kuwait City, 17-19 Mar. 2009, pp, 1–4.

[48] Alshamali and B. Quza, "Performance of spatial modulation in correlated and uncorrelated Nakagami fading channel," *J. Commun.*, vol. 4, no. 3, pp. 170–174, Apr. 2009.

[49] M. Di Renzo and H. Haas, "On the performance of space shift keying MIMO systems over correlated Rician fading channels," in *Proc. ITG Int. Workshop Smart Antennas*, Bremen, Germany, Feb. 2010, pp. 72–79.

[50] M. Di Renzo and H. Haas, "Performance comparison of different spatial modulation schemes in correlated fading channels," in *Proc. IEEE ICC'10*, Cape Town, South Africa, 23-27 May 2010.

[51] M. Di Renzo and H. Haas, "On the performance of SSK modulation over correlated Nakagami-phm fading channels," in *Proc. IEEE ICC'10*, Cape Town, South Africa, 23-27 May 2010.

[52] M. Di Renzo and H. Haas, "Performance analysis of spatial modulation (SM) over Nakagami-m fading channels," in *Proc. Int. Conf. Commun. Netw.* China, Aug. 2010, pp.1–6.

[53] M. Di Renzo and H. Haas, "Bit error probability of space modulation over Nakagami-m fading: Asymptotic analysis," *IEEE Commun. Lett.*, vol. 15, no. 10, pp. 1026–1028, Oct. 2011.

[54] M. Koca and H. Sari, Performance analysis of spatial modulation over correlated fading channels, in *Proc. IEEE VTC'12- Fall*,Quebec City, Canada, Sep. 2012.

[55] R. Mesleh, M. Di Renzo, H. Haas, and P. M. Grant, "Trellis coded spatial modulation," *IEEE Trans. Wireless Commun.*, vol. 9, no. 7, pp. 2349–2361, July 2010.

[56] E. Basar, U. Aygolu, E. Panayirci, and H. V. Poor, "New trellis code design for spatial modulation," *IEEE Trans. Wireless Commun.*, vol. 10, no. 8, pp. 2670–2680, Aug. 2011.

[57] R. Zhang, L. L. Yang, and L. Hanzo, "Generalised pre-coding aided spatial modulation," *IEEE Trans. Wireless Commun.*, vol. 12, no. 11, pp. 5434–5443, Nov. 2013.

[58] A. Younis, N. Serafimovski, R. Mesleh, and H. Haas, "Generalised spatial modulation," in *Proc. ASILOMAR'11*, Pacific Grove, USA, Nov. 2010, pp. 1498–1502.

[59] J. L. Fu, C. P. Hou, W. Xiang, L. Yan and Y. H. Hou "Generalised spatial modulation with multiple active transmit antennas," in *Proc. GLOBECOM'10*, Miami, USA, Dec. 2010, pp. 839–844.

[60] J. T. Wang, S. Y. Jia, and J. Song, "Generalised spatial modulation system with multiple active transmit antennas and low complexity detection scheme," *IEEE Trans. Wireless Commun.*, vol. 11, no. 4, pp. 1605–1615, Apr. 2009.

[61] E. Basar, U. Aygolu, E.Panayirci, and H. V. Poor, "Space-time block coded spatial modulation," *IEEE Trans. Commun.*, vol. 59, no. 3, pp. 823–832, Mar. 2011.

[62] N. Serafimovski, M. Di Renzo, S. Sinanovic, R. Y. Mesleh, and H. Haas, "Fractional bit encoded spatial modulation (FBE-SM)," *IEEE Commun. Lett.*, vol. 14, no. 5, pp. 429–431, May 2010.

[63] Y. Yang and S. Aissa, "Bit-padding information guided channel hopping," *IEEE Commun. Lett.*, vol. 15, no. 2, pp. 163–165, Feb. 2011.

[64] A. Stavridis, S. Sinanovic, M. Di Renzo, H. Haas, and P. M. Grant, "An energy saving base station employing spatial modulation," in *Proc. IEEE Int. Workshop Comput.-Aided Model. Anal. Design Commun. Links Netw.*, Barcelona, Spain, 17-19 Sep. 2012, pp. 231–235.

[65] X. Wu, S. Sinanovic, M. Di Renzo, and H. Haas, "Base station energy consumption for transmission optimized spatial modulation (TOSM) in correlated channels," in *Proc. IEEE Int. Workshop Comput.-Aided Model. Anal. Design Commun. Links Netw.*, Barcelona, Spain, 17-19 Sep., pp. 261–265.

[66] Website: Europe project Energy Aware Radio and neTwork technologies (EARTH), https://www.ict-earth.eu/.

[67] R. Y. Chang, S.-J. Lin, and W.-H. Chung, "Energy efficient transmission over space shift keying modulated MIMO channels," *IEEE Trans. Commun.*, vol. 60, no. 10, pp. 2950–2959, Oct. 2012.

[68] N. Serafimovski, S. Sinanovic, M. Di Renzo, and H. Haas,"Dual-hop spatial modulation (Dh-SM)," in *Proc. IEEE VTC11-Spring*, Yokohama, Japan, 15-18 May 2011, pp. 1–5.

[69] R. Y. Mesleh, S. S. Ikki, E.-H. M. Aggoune, and A. Mansour, "Performance analysis of space shift keying (SSK) modulation with multiple cooperative relays," *EURASIP J. Adv. Signal Process.*, vol. 201, 2012.

[70] R. Y. Mesleh and S. S. Ikki, "Space shift keying with amplify-and-forward MIMO relaying," *Trans. Emerging Telecommun. Technol.*, Jan. 2013.

[71] S. Sugiura, S. Chen, H. Haas, P. M. Grant, and L. Hanzo, "Coherent versus non-coherent decode-and-forward relaying aided cooperative space-time shift keying," *IEEE Trans. Commun.*, vol. 59, no. 6, pp. 1707–1719, Jun. 2011.

[72] M. I. Kadir, L. Li, S. Chen, and L. Hanzo, "Successive-relaying-aided decode-and-forward coherent versus noncoherent cooperative multicarrier space-time shift keying," *IEEE Trans. Veh. Technol.*, vol. 62, no. 6, pp. 2544–2557, Jul. 2013.

[73] Y. Yang and S. Aissa, "Information-guided transmission in decode-and-forward relaying systems: Spatial exploitation and throughput enhancement," *IEEE Trans. Wireless Commun.*, vol. 10, no. 7, pp. 2341–351, Jul. 2011.

[74] S. Narayanan, M. Di Renzo, F. Graziosi, and H. Haas, "Distributed space shift keying for the uplink of relay-aided cellular networks," in *Proc. IEEE Int. Workshop Comput.-Aided Model. Anal. Design Commun. Links Netw.*, Barcelona, Spain, 17-19 Sep. 2012, pp. 130–134.

[75] S. Narayanan, M. Di Renzo, F. Graziosi, and H. Haas, "Distributed spatial modulation for relay networks," in *Proc. IEEE VTC13-Fall*, Las Vegas, USA, Sept. 2013, pp. 1–5.

[76] R. Mesleh, H. Elgala, and H. Haas, "Optical Spatial Modulation," *IEEE/OSA J. Optical Commun. Net.*, vol. 3, no. 3, pp. 234–244, Mar. 2011.

[77] R. Mesleh, H. Elgala, and H. Haas, "Performance of optical spatial modulation with transmitters-receivers alignment," *IEEE Commun. Lett.*, vol. 15, no. 1, pp. 79–81, Jan. 2011.

[78] W. Popoola, E. Poves, and H. Haas, "Spatial pulse position modulation for optical communications," *J. Lightw. Technol.*, vol. 30, no. 18, pp. 948–954, Sep. 2012.

[79] T. Fath and H. Haas, Performance comparison of MIMO techniques for optical wireless communications in indoor environments," *IEEE Trans. Commun.*, vol. 61, no. 2, pp. 733–742, Feb. 2013.

[80] M. Patzold, *Mobile Fading Channels*,Chischester, UK, John Wiley & Sons, 2002.

[81] A. S. Akki and F. Haber, "A statistical model for mobile-to-mobile land communication channels," *IEEE Trans. Veh. Technol.,* vol. 35, no. 1, pp. 2–10, Feb. 1986.

[82] E. T. Michailidis, P. Theofilakos, and A. G. Kanatas, "Three-dimensional modeling and simulation of MIMO Mobile-to-Mobile via stratospheric relay fading channels," *IEEE Trans. Veh. Technol.*, vol. 62, no. 5, pp. 2014–2030, June 2013.

[83] C. S. Patel, G. L. Stuber, and T. G. Pratt, "Simulation of Rayleigh faded mobile-to-mobile communication channels," *IEEE Trans. Commun.*, vol. 53, no. 11, pp. 1876–1884, Nov. 2005.

[84] X. Cheng, C.-X. Wang, D. I. Laurenson, S. Salous, and A. V. Vasilakos, "An adaptive geometry-based stochastic model for non-isotropic MIMO mobile-to-mobile channels," *IEEE Trans. Wireless Commun.*, vol. 8, no. 9, pp. 4824–4835, Sept. 2009.

[85] X. Cheng, Q. Yao, C.-X. Wang, B. Ai, G. L. Stuber, D. Yuan, and B. Jiao, "An improved parameter computation method for a MIMO V2V Rayleigh fading channel simulator under non-isotropic scattering environments," *IEEE Commun. Lett.*, vol. 17, no. 2, pp. 265–268, Feb. 2013.

[86] X. Cheng, C.-X. Wang, D. I. Laurenson, S. Salous, and A. V. Vasilakos, "New deterministic and stochastic simulation models for non-isotropic scattering Mobile-to-mobile Rayleigh fading channels," *Wireless Commun. Mobile Computing*, John Wiley & Sons, vol. 11, no. 7, pp. 829–842, July 2011.

[87] Y. Yuan, C.-X. Wang, X. Cheng, B. Ai, and D. I. Laurenson, "Novel 3D geometry-based stochastic models for non-isotropic MIMO vehicle-to-vehicle channels," *IEEE Trans. Wireless Commun.*, vol. 13, no. 1, pp. 298–309, Jan. 2014.

[88] C. Briso-Rodriguez, J. M. Cruz, and J. I. Alonso, "Measurements and modeling of distributed antenna systems in railway tunnels," *IEEE Trans. Veh. Technol.*, vol. 56, no. 5, pp. 2870–2879, Sept. 2007.

[89] K. Guan, Z. Zhong, B. Ai, and T. Kurner, "Propagation measurements and analysis for train stations of high-speed railway at 930 MHz," *IEEE Trans. Veh. Technol.*, vol. 63, no. 2, pp. 1–16, Feb. 2014.

[90] L. Liu, C, Tao, J, Qiu, H. Chen, L. Yu, W. Dong, and Y. Yuan, "Position-based modeling for wireless channel on high-speed railway under a viaduct at 2.35 GHz," *IEEE J. Sel. Areas Commun.*, vol. 30, no. 4, pp. 834–845, May 2012.

[91] 3GPP, TS36.104, V11.3.1, "3GPP; Technical Specification Group Radio Access Network; E-UTRA; Base Station radio transmission and reception (Release 11)," Jan. 2013.

[92] P. Kyosti, et al., "WINNER II channel models," IST-4-027756, WINNER II D1.1.2, v1.2, Apr. 2008.

[93] B. Chen, Z. Zhong, and B. Ai, "Stationarity intervals of time-variant channel in high speed railway scenario," *J. China Commun.*, vol. 9, no. 8, pp. 64–70, Aug. 2012.

[94] R. Parviainen, P. Kyosti, Y. Hsieh, P. Ting, and J. Chiou, "Results of high speed train channel measurements," in *COST 2100 TD'08*, Lille, France, Oct. 2008.

[95] A. Ghazal, C.-X. Wang, H. Haas, M. A. Beach, X. Lu, and D. Yuan, "A non-stationary MIMO channel model for high speed train communication systems," in *Proc. IEEE VTC'12-Spring*, Yokohama, Japan, May. 2012, pp. 1–5.

[96] A. Ghazal, C.-X. Wang, H. Haas, M. Beach, R. Mesleh, D. Yuan, X. Ge, and M. K. Chahine, "A non-stationary geometry-based stochastic model for MIMO high-speed train channels," invited paper, in *Proc. ITST'12*, Taipei, Taiwan, Nov. 2012, pp. 7–11.

[97] A. Ghazal, C.-X. Wang, B. Ai, D. Yuan, and H. Haas, "A non-stationary wideband MIMO channel model for high-mobility intelligent transportation systems," *IEEE Trans. Intelligent Transportation Systems*, vol. 16, no. 1, pp. 1–13, Feb. 2015.

[98] E. G. Larsson, F. Tufvesson, O. Edfors, and T. L. Marzetta, "Massive MIMO for next generation wireless systems," *IEEE Commun. Mag.*, vol. 52, no. 2, pp. 186–195, Feb. 2014.

[99] F. Rusek et al., "Scaling up MIMO: Opportunities and challenges with very large arrays," *IEEE Signal Process. Mag.*, vol. 30, no. 1, pp. 40–60, Jan. 2012.

[100] J. Mietzner, R. Schober, L. Lampe,W. Gerstacker and P. Hoeher, "Multiple-antenna techniques for wireless communications-a comprehensive literature survey," *IEEE Communications Surveys and Tutorials*, vol. 11, no. 2, pp. 87–105, 2009.

[101] L. Lu, G. Y. Li, A. L. Swindlehurst, A. Ashikhmin and R. Zhang, "An overview of massive MIMO:benefits and challenges," *IEEE J. Sel. Topics Signal Process*, vol. 8, no. 5, pp.742–758, Oct. 2014.

[102] S. K. Mohammed and E. G. Larsson, "Per-antenna constant envelope precoding for large multi-user MIMO systems," *IEEE Trans. Commun.*, vol. 61, no. 3, pp. 1059-1071, Feb. 2013.

[103] J. Zhang, X. Yuan and L. Ping, "Hermitian precoding for distributed MIMO systems with individual channel state information," *IEEE J. Sel. Areas Commun.*, vol. 31, no. 2, pp. 241–250, Feb. 2013.

[104] S. Noh, M. D. Zoltowski and D. J. Love, "Pilot beam pattern design for channel estimation in massive MIMO systems," *IEEE J. Sel. Topics in Signal Processing.*, vol. 8, no. 5, pp. 787–801, May 2014.

[105] R. Couillet, M. Debbah and J. W. Silverstein, "A deterministic equivalent for the analysis of correlated MIMO multiple access channels," *IEEE Trans. Inf. Theory.*, vol. 57, no. 6, pp. 787–801, June 2011.

[106] J. Chen and V. K. N. Lau, "Two-Tier precoding for FDD multi-Cell massive MIMO time-varying interference networks," *IEEE J. Sel. Areas Commun.*, vol. 32, no. 6, pp. 1230–1238, May 2014.

[107] S. Payami and F. Tufvesson, "Channel measurements and analysis for very large array systems at 2.6GHz," in *Proc. of the 6th European Conference on Antennas and Propagation*, Prague, Czech Republic, Mar. 2012, pp. 433–37.

[108] X. Gao, F. Tufvesson, O. Edfors, and F. Rusek, "Measured propagation characteristics for very-large MIMO at 2.6 GHz," in *Proc. of the 46th Annual Asilomar Conference on Signals, Systems, and Computers*, Pacific Grove, California, USA, Nov. 2012, pp. 295–99.

[109] S. Wu, C.-X. Wang, H. Aggoune, M. M. Alwakeel and Y. He, "A non-stationary 3D wideband twin-cluster model for 5G massive MIMO channels," *IEEE J. Sel. Areas Commun.*, vol. 32, no. 6, pp. 1207–1218, June 2014.

[110] S. Wu, C.-X. Wang, H. Haas, H. Aggoune, M. M. Alwakeel and B. Ai, "A non-stationary wideband channel model for massive MIMO communication systems", *IEEE Trans. Wireless Commun.*, accepted for publication.

[111] S. Wu, C.-X. Wang, H. M. Aggoune and M. M. Alwakeel, "A novel kronecker-based stochastic model for massive MIMO channels," in *Proc. of IEEE/CIC International Conference on Communications* , Shenzhen, China, 2-4 Nov. 2015.

[112] C.-X. Wang, X. Cheng, and D. I. Laurenson, "Vehicle-to-vehicle channel modeling and measurements: recent advances and future challenges," *IEEE Commun. Mag.*, vol. 47, no. 11, pp. 96–103, Nov. 2009.

[113] A. Younis, M. Di Renzo, R. Mesleh, and H. Haas, "Sphere decoding for spatial modulation," in *Proc. IEEE ICC'11*, Kyoto, Japan, June 2011, pp. 1–6.

[114] Y. Fu, C.-X. Wang, R. M. Mesleh, X. Cheng, H. Haas, and Y. He,"A performance study of spatial modulation technology under vehicle-to-vehicle channel models," in *Proc. IEEE VTC'14-Spring*, Seoul, South Korea, May 2013.

[115] M. K. Simon and M.-S. Alouini, *Digital Communication over Fading Channels*, 2nd edition, John Wiley & Sons, 2005.

[116] A. Hedayat, H. Shah, and A. Nosratinia, "Analysis of space-time coding in correlated fading channels," *IEEE Trans. Wireless Commun.*, vol. 4, no. 6, pp. 2882–2891, Nov. 2005.

[117] M.-S. Alouini and A. J. Goldsmith, "A unified approach for calculating the error rates of linearly modulated signals over generalized fading channels," *IEEE Trans. Commun.* , vol. 47, no. 9, pp. 1324–1334, Sept. 1999.

[118] A. Forenza, D. J. Love, and R. W. Heath,"A low complexity algorithm to simulate the spatial covariance matrix for clustered MIMO channel models,", in *Proc. VTC'04*, Miami, USA, May. 2004, vol.2, pp. 889–893.

[119] G. Acosta and M. A. Ingram, "Six time- and frequency-selective empirical channel models for vehicular wireless LANs," *IEEE Veh. Technol. Mag.*, vol. 2, no. 4, pp. 4–11, Dec. 2007.

[120] D. Xin. (2010) Record-breaking train on track. [Online]. Available: http://www.chinadaily.com.cn/china/2010-12/04/content-11651930.htm.

[121] D. T. Fokum and V. S. Frost, "A survey on methods for broadband internet access on trains," *IEEE Commun. Surveys & Tutotials*, vol. 12, no. 2, pp. 171–185, 2nd Quarter 2010.

[122] Y. Zhou, Z. Pan, J. Hu, J. Shi, and X. Mo, "Broadband wireless communications on high speed trains," in *Proc. IEEE WOCC'11*, New Jersey, USA, Apr. 2011.

[123] J. Wang, H. Zhu, and N. J. Gomes, "Distributed antenna systems for mobile communications in high speed trains," *IEEE J. Sel. Areas Commun.*, vol. 30, no. 4, pp. 675–683, May 2012.

[124] C. Yang, L. Lu, C. Di, and X. Fang, "An on-vehicle dual-antenna handover scheme for high-speed railway distributed antenna system," in *Proc. IEEE WiCOM'10*, Chengdu, China, Sept. 2010, pp. 1–4.

[125] L. Tian, J. Li, Y. Huang, J. Shi, and J. Zhou, "Seamless dual-link handover scheme in broadband wireless communication systems for high-speed rail," *IEEE J. Sel. Areas Commun.*, vol. 30, no. 4, pp. 708–718, May 2012.

[126] O. B. Karimi, L. J. Liu, and C. Wang, "Seamless wireless connectivity for multimedia services in high speed trains," *IEEE J. Sel. Areas Commun.*, vol. 30, no. 4, pp. 729–739, May 2012.

[127] F. Haider, C.-X. Wang, H. Haas, D. Yuan, H. Wang, X. Gao, X.-H. You, and E. Hepsaydir, "Spectral efficiency analysis of mobile femtocell based cellular systems," in *Proc. IEEE ICCT'11*, Jinan, China, Sept. 2011, pp. 347–351.

[128] E. Basar, U. Aygolu, E. Panayirci, and H. V. Poor, "Performance of spatial modulation in the presence of channel estimation errors," *IEEE Commun. Lett.*, vol. 16, no. 2, pp. 176–179, Feb. 2012.

[129] R. Mesleh and S. S. Ikki, "On the effect of Gaussian imperfect channel estimations on the performance of space modulation techniques," in *Proc. IEEE VTC'12-Spring*, Yokohama, Japan, May 2012, pp. 1–5.

[130] S. Sesia, I. Toufik, and M. Baker, *LTE - The UMTS Long Term Evolution: From Theory to Practice*, John Wiley & Sons, 2009.

[131] D. Gesbert, M. Shafi, D. Shiu, P. J. Smith, and A. Naguib, "From theory to practice: An overview of MIMO space-time coded wireless systems," *IEEE J. Sel. Areas Commun.*, vol. 21, no. 3, pp. 281–302, Apr. 2003.

[132] G. J. Foschini, "Layered space-time architecture for wireless communication in a fading environment when using multielement antennas," *Bell Labs Tech. J.* , vol. 1, no. 2, pp. 41–59, 1996.

[133] B. L. Zhou, L. G. Jiang, S. J. Zhao and C. He, "BER analysis of TDD downlink multiuser MIMO systems with imperfect channel state information," *EURASIP J. Adv. Signal Process.*, pp. 104–104, 2011.

[134] H. Q. Ngo, E. G. Larsson, and T. L. Marzetta,"Massive MU-MIMO downlink TDD systems with linear precoding and downlink pilots," in *Proc. of 51st Annual Allerton Conference on Communication, Control, and Computing*, Illinois, USA, Oct. 2013, pp.293-298.

[135] Q. Spencer, C. Peel, A. Swindlehurst and M. Haardt,"An introduction to the multi-user MIMO downlink," *IEEE Commun. Mag.*, vol. 42, no. 10, pp. 60–67, 2004.

[136] M. Joham, W. Utschick and J. A. Nossek, "Linear transmit processing in MIMO communications systems," *IEEE Trans. Signal Process.*, vol. 53, no. 8, pp. 2700–2712, Aug. 2005.

[137] C. B. Peel, B. M. Hochwald, and A. L. Swindlehurst, "A vector-perturbation technique for near-capacity multiantenna multiuser communicationpart I: channel inversion and regularization," *IEEE Trans. Commun.*, vol. 53, no. 1, pp. 195–202, Jan. 2005.

[138] S. Narayanan, M. J. Chaudhry, A. Stavridis, M. Di Renzo, F. Graziosi, H. Haas, "Multi-user spatial modulation MIMO," in *Proc. of IEEE Wireless Communications and Networking Conference*, Istanbul, Turkey, 6-9 April 2014, pp.671–676.

[139] Q. H. Spencer, A. L. Swindlehurst, and M. Haardt, "Zero-forcing methods for downlink spatial multiplexing in multiuser MIMO channels," *IEEE Trans. Signal Process.*, vol. 52, no. 2, pp. 461–471, Feb. 2004.

[140] F. Haider, C.-X. Wang, H. Haas and E. Hepsaydir, "Spectral-energy efficiency trade-off for multi-user spatial modulation in massive MIMO networks," to be submitted.

[141] J. L. Zhang, Y. Wang, L. Q. Ding and N. T. Zhang, "Bit error probability of spatial modulation over measured indoor channels," *IEEE Trans. Wireless Commun.* , vol. 13, no. 3, pp. 1380–1387, Mar. 2014.

[142] M. Di Renzo and H. Haas, "Bit error probability of space shift keying MIMO over multiple-access independent fading channels," *IEEE Trans. Veh. Technol.*, vol. 60, no. 8, pp. 3694–3711, Oct. 2011.

[143] M. I. Kadir, S. Sugiura, J. Zhang, S. Chen and L. Hanzo, "OFDMA/SCFDMA aided space-time shift keying for dispersive multi-user scenarios," *IEEE Trans. Veh. Technol.*, vol. 62, no. 1, pp. 408–414, Jan. 2013.

[144] K. M. Humadi, A. I. Sulyman and A. Alsanie, "Spatial modulation concept for massive multiuser MIMO systems," em International Journal of Antennas and Propagation, Article ID 563273, 9 pages, 2014.

[145] L. L. Yang, "Signal detection in antenna-hopping space-division multiple-access systems with space shift keying modulation," *IEEE Trans. Sig. Process.*, vol. 60, no. 1, pp. 351-366, Jan. 2012.

[146] J. Wang, Y. Xiao, S.Q. Li, L. Li and J. Zhang, "Performance evaluation of precoding in spatial modulation OFDM on a LTE channel," in *Proc. of IEEE 14th International Conference on Communication Technology* , Chengdu, China, 9-11 Nov. 2012, pp.1188–1192.

[147] Q. H. Spencer, C. B. Peel, A. L. Swindlehurst and M. Li. Haardt, "An introduction to the multi-user MIMO downlink," *IEEE Commun. Mag.* , vol. 42, no. 10, pp. 60-67, Oct. 2004.

[148] E. Basar, U. Aygolu, E. Panayirci, and H. V. Poor, , "Orthogonal frequency division multiplexing with index modulation," *IEEE Trans. Signal Process.*, vol. 61, no. 22, pp. 5536–5549, Nov. 2013.